Wilbur L Mitchell

TECH LIBRARY KAFB, NM
0144557

1181

8008

WLMITCHELL

NATIONAL ADVISORY COMMITTEE FOR AERONAUTICS

TECHNICAL NOTE

No. 1181

WING PRESSURE-DISTRIBUTION MEASUREMENTS UP TO 0.866 MACH NUMBER IN FLIGHT ON A JET-PROPELLED AIRPLANE

By Harvey E. Brown and Lawrence A. Clousing

Ames Aeronautical Laboratory
Moffett Field, Calif.

Washington
March 1947

AFMDC
TECHNICAL LIBRARY
AFL 2811

TECH LIBRARY KAFB, NM

0144557

NATIONAL ADVISORY COMMITTEE FOR AERONAUTICS

TECHNICAL NOTE No. 1181

WING PRESSURE-DISTRIBUTION MEASUREMENTS UP TO 0.866 MACH NUMBER IN FLIGHT ON A JET-PROPELLED AIRPLANE

By Harvey B. Brown and Lawrence A. Clousing

SUMMARY

Flight tests were conducted to determine scale and compressibility effects on the pressure distributions over a wing having an NACA low-drag profile. The jet-propelled airplane used permitted tests to be conducted to a Mach number of 0.866.

For lift coefficients ranging from 0 to 0.60, for which data are presented, no appreciable compressibility effects on spanwise wing loading were noted below 0.75 Mach number. Above this Mach number an inboard lateral shift of load occurred which is attributed principally to upfloating of the ailerons.

The tests showed a more negative value of section pitching-moment coefficient as Mach number increased up to about 0.78. From this peak negative value the pitching-moment coefficient rapidly shifted to much less negative values as the Mach number was increased especially for low lift coefficients. The variation of pitching-moment coefficient with lift coefficient became stabilizing at Mach numbers of 0.82 to 0.84.

Above 0.75 Mach number the ailerons floated up, and the pressure-distribution measurements showed that extremely large aileron hinge moments were present due presumably to flow separation on the upper surface of the wing. The aileron flutter which occurred above 0.83 Mach number was considered to be interrelated with the occurrence of these large hinge moments.

INTRODUCTION

In continuance of a program for obtaining research information at high speeds from flight tests, pressure-distribution measurements have

been made over the left wing of a jet-propelled airplane possessing a wing with an NACA low-drag airfoil section.

The primary purpose of this investigation was to determine the effect of compressibility on fundamental aerodynamic characteristics as far into the supercritical speed range as practicable. It was intended thus to supplement previous work done on an airplane having conventional airfoil sections (reference 1) at somewhat lower speeds.

SYMBOLS

The following symbols are used throughout the report:

A_Z airplane normal acceleration factor (Z/W)

$b/2$ wing semispan, feet

c wing section chord, feet

c_h section hinge-moment coefficient

$$\left[16 \int_{0.75}^{1.00} \left(P_U - P_L\right)\left(\frac{x}{c} - 0.75\right) d\left(\frac{x}{c}\right) \right]$$

$C_{b.m._{w.s.62}}$ wing bending-moment coefficient

$$\left[\frac{b}{2S} \int_{0.265}^{1.00} c_n c \left(\frac{y}{b/2} - 0.265\right) d\left(\frac{y}{b/2}\right) \right]$$

C_L airplane lift coefficient $\left(\frac{A_Z W}{qS} \text{ as used in this report}\right)$

c_n section normal-force coefficient

$$\left[\int_0^{1.0} \left(P_L - P_U\right) d\left(\frac{x}{c}\right) \right]$$

$C'_{N_{w.s.62}}$ wing normal-force coefficient

$$\left[\frac{b}{2S} \int_{0.265}^{1.00} c_n c \; d\left(\frac{y}{b/2}\right) \right]$$

$c_{m_{c/4}}$ section pitching-moment coefficient about quarter chord

$$\left[\int_0^{1.0} \left(P_L - P_U\right)\left(\frac{x}{c} - 0.25\right) d\left(\frac{x}{c}\right)\right]$$

g acceleration due to gravity, 32.2 feet per second per second

H total pressure, pounds per square foot

h_p pressure altitude, feet

M Mach number, ratio of airspeed to speed of sound

P pressure coefficient $[(p-p_o)/q]$

P_U pressure coefficient on upper surface

P_L pressure coefficient on lower surface

p static orifice pressure, pounds per square foot

p_o free-stream static pressure, pounds per square foot

$p_{S.L.}$ standard barometric pressure at sea level, pounds per square foot

q dynamic pressure $\left(\frac{1}{2}\rho V^2\right)$, pounds per square foot

R Reynolds number (based on section chord except where noted)

S wing area, square feet

V airspeed, miles per hour

V_i correct indicated airspeed, miles per hour

$$V_i = 1703\left[\left(\frac{H-p_o}{p_{S.L.}}+1\right)^{0.286}-1\right]^{\frac{1}{2}}$$

x chordwise location from leading edge, feet

y spanwise location from plane of symmetry, feet

W	airplane gross weight, pounds
Z	aerodynamic normal-force on airplane, pounds
δ_a	aileron control-surface deflection, degrees

Subscripts

w.s.	wing station

DESCRIPTION OF THE AIRPLANE

The tests reported herein were conducted on a jet-propelled airplane, photographs of which are presented in figures 1 and 2. A three-view drawing of the airplane showing the spanwise locations of the wing-static-pressure orifices is given in figure 3. The dimensions of the airplane pertinent to this report are:

Wing

Airfoil section	NACA 65_1-213(a= 0.5)
Area, sq ft	237
Span, ft	38.9
Aspect ratio	6.4
Root chord, in	110
Tip chord, in	40
Taper ratio	0.363
Mean aerodynamic chord, in.	80.6
Incidence (with respect to fuselage reference line)	
Root chord, deg	1.0
Tip chord, deg	-0.5
Dihedral (at trailing edge on wing reference plane), deg	3.83

The wing has a constant airfoil section along the span with the 52-percent-chord point of all sections lying in a plane perpendicular to the fuselage reference line.

The ailerons are attached by a piano-type hinge to the upper wing surface at the 75-percent-chord line. They are statically and dynamically mass-balanced, but have no aerodynamic balance. The piano-type hinge effectively gives a sealed condition. The inboard end of the aileron is at wing station 127 and the outboard end at wing station 216.

The locations of the flush orifices on the wing are listed in table I. Approximately 40 orifices are located at each of the four principal stations tested and additional orifices are located at intermediate stations.

The ordinates of the NACA 65_1-213 (a=0.5) airfoil are presented in table II and a comparison with the actual wing contour is presented in figure 4. This figure presents the difference between the actual and theoretical ordinates; positive values for the upper and lower surface refer to "bumps" or elevations outside the theoretical contour, and negative values refer to depressions below the theoretical contour. One of the primary sources of contour irregularities is the wing spars which are located at 20, 52, and 70 percent of the chord.

INSTRUMENTATION

All quantities presented herein were obtained by the use of standard NACA photographically recording instruments synchronized by the use of a timer. Manometers were used to record the pressure difference between the wing orifices and the fuselage nose compartment in which the manometers were housed. (See fig. 5.) A sensitive pressure cell was used to determine the pressure difference between the nose compartment and the static pressure at the airspeed head.[1]

METHOD OF TESTING

The following flight technique was employed by the pilot. After stabilizing in a steady straight run the airplane was rolled into a progressively tightening turn, maintaining as constant an airspeed as possible up to either the stall or as high an acceleration factor as the pilot deemed safe.

The aileron movement during this maneuver proved to be a serious drawback to this technique. At high speeds the aileron deflections

[1]The airspeed head was located 1.26 chord lengths ahead of the wing leading edge on a boom attached to the wing-tip tank shackles. (See fig. 6.)

necessary to roll were small and could be considered negligible but, at low speeds, aileron angles of 3° to 4° were not uncommon. It appears that better flight results in the low-speed range would be obtained with a flight technique utilizing either straight pull-ups or steady turns.

The data presented herein for the higher Mach numbers ($M = 0.78$ to $M = 0.866$) were obtained during entry into and recovery from shallow dives.

REDUCTION OF DATA – ACCURACY

The results of the pressure-distribution tests are presented in the form of graphs showing the chordwise variation of pressure coefficient P. This coefficient is based on the static pressure at the airspeed head, corrected for position error as determined from a low-altitude flight calibration. This flight calibration was made by flying the airplane past an object of known height to obtain the pressure difference between the airplane static pressure and the barometric pressure. An attempt to determine this difference at a higher altitude proved inconclusive. In addition the error in static pressure inherent in the airspeed head itself was determined up to $M = 0.85$ by calibrating it in the Ames 16-foot high-speed wind tunnel. The airspeed and altimeter readings were also corrected for these errors.

All the pressure lines of the airspeed system were balanced to provide equal rates of flow during rapid changes in altitude. In order to avoid the use of an excessively long impact pressure line to provide equal rates of flow, two separate sources of static pressure were provided, one for the airspeed recorder and one for the altitude recorder. All lines were 3/16-inch inside diameter and about 7 feet long, for which length the lag was considered to be negligible. (See reference 2.)

The airspeed instrument, altimeter, and all pressure cells were calibrated at several temperatures to determine the correction due to temperature. This correction was a function of the instrument temperature, a somewhat difficult quantity to determine in flight, and therefore the instrument temperatures were estimated from the ambient-air temperature and the rate of cooling of the instrument. For the airspeed instrument and altimeter the error was quite small and for the orifice-pressure manometers the temperature correction showed a wide variation between cells. For the average cell the error introduced by temperature change was the principal error involved.

The estimated accuracy with which the various quantities were evaluated is given as follows:

V_i	±0.7 miles per hour
M	±0.005
h_p	±50 feet
P	$\pm 10/q$
δ_a	$\pm 0.25^\circ$

In general, the accuracy of the results was considered satisfactory above a Mach number of 0.50 and above a Reynolds number of 10×10^6. Below these values the errors involved in measuring pressure coefficient P produced inconclusive results.

All values of section-force coefficients and section-moment coefficients were obtained by mechanical integration of the chordwise variation of the pressure coefficients.

RESULTS

The range of Mach and Reynolds numbers covered during the tests is illustrated in figure 7.

In general, results are presented as a function of Mach and Reynolds numbers with emphasis being placed on the effect resulting from variations in Mach number. A typical comparison of pressure distributions obtained at substantially constant Mach number but with varying Reynolds number is illustrated in figure 8.

Typical chordwise pressure distributions measured in straight unaccelerated flight between M = 0.69 and M = 0.79 are presented in figures 9 and 10. Similar data taken during dives in which a maximum Mach number of 0.866 was reached are presented in figure 11. Included with the data presented in figures 9, 10, and 11 for wing station 65 is a comparison of pressure distributions obtained on a 1/3-scale model of the airplane tested in the Ames 16-foot high-speed wind tunnel. Although the wind-tunnel data presented were measured at wing station 78, this station was considered close enough to the airplane test section (wing station 65) to permit valid comparison.

A summary of the data pertinent to each pressure distribution presented is shown in table III. Owing to an instrument failure the pressure coefficients for the flight data plotted in figures 9(e) to 9(l) are based on the nose-compartment static pressure and not the free-stream static pressure; thus all values of P are subject to a slight undetermined constant correction.

From the chordwise pressure distributions at various spanwise stations the spanwise lift distribution outboard of station 65 was determined. These data have been broken down to show the effect of Mach number on the basic lift distribution ($C_L = 0$, fig. 12) and on the total lift distribution (fig. 13). From the data of figure 12 the variations with Mach number of normal-force coefficient C'_N the wing bending-moment coefficient $C_{b,m.}$ and the lateral center of pressure of the wing panel outboard of station 62 (26.5 percent semispan) were calculated for several values of airplane lift coefficient and are presented in figures 14, 15, and 16, respectively.

From the chordwise-pressure-distribution data the section pitching-moment coefficients about the section quarter-chord points were determined. These data are presented in figure 17 as functions of Mach number and section normal-force coefficient. The spanwise variation of section pitching-moment coefficient with airplane lift coefficient and Mach number is shown in figure 18.

In the determination of the spanwise lift distribution it was noted that the aileron floated up, during the dives, at the higher speeds. Therefore, the upfloat of the aileron with airplane lift coefficient at Mach numbers up to 0.86 was determined and is presented in figure 19. To investigate the reasons for this upfloat a measurement of the aerodynamic hinge moment was obtained from the chordwise pressure distribution over the aileron. (See fig. 20.) The variation of pressure over the aft portion of the wing was determined (fig. 21), and the variation of section hinge-moment coefficient with Mach number for several values of normal-force coefficient was calculated. (See figs. 22 and 23.)

DISCUSSION

Chordwise Pressure Distribution

Relative importance of Mach and Reynolds numbers.- Above a Mach number of 0.5 (the range in which the data are accurate enough to permit comparison) the effect of the Reynolds number variations shown in figure 7 were well within experimental error. This is demonstrated by a typical plot in figure 8 in which a comparison is made between pressure distributions at approximately the same Mach number but at different Reynolds numbers. The location of the shock was the same in both cases and the small differences between the two curves could be reasonably attributed to a slight difference in Mach number.

Furthermore, in plotting the various parameters c_n, $c_{m_{c/4}}$, spanwise loads, and so forth, as a function of Mach number, no consistent

variations with altitude were apparent. As a consequence, it was considered justifiable to neglect the effect of Reynolds number and to present the results as a function solely of Mach number.

Comparison with high-speed wind-tunnel data.- In general the comparison between the flight-test results and the wind-tunnel model tests shown in figures 9, 10, and 11 indicated very good agreement. The principal source of difference was the manufacturing irregularities in the wing of the test airplane.

The wind-tunnel model as is customary had a smooth and accurately finished wing surface as contrasted with the actual airplane and therefore did not experience the irregularities in pressure distribution present in the flight data. In spite of the exceptionally smooth wing contour of the test airplane there are sufficient irregularities, principally due to wing spars, to produce quite considerable peaks in the pressure distributions. These peaks become increasingly apparent at speeds above the critical and constitute a considerable dissimilarity when comparison is made with the wind-tunnel results.

Nevertheless, the shock wave on the upper surface generally had a chordwise location in flight which was only slightly aft of the location given by the tunnel data. The static pressures at the trailing edge were not always in agreement.

Among the secondary sources of differences, that due to the pressure field of the model supporting struts is considered to be most important. The velocity profile due to the support struts is indicated in reference 3 for 5-percent-thick struts. The model as tested has 12-percent-thick struts, and it is estimated that the Mach number varied about 0.03 along the chord of the model at the test station at $M = 0.80$.

No consistent differences are observable between the tunnel and flight pressure distributions which can definitely be attributed to Reynolds number. Examination of the comparisons afforded by figures 9, 10, and 11 show no greater discrepancies existing when the Reynolds number difference is as large as 7.4×10^6 to 34.3×10^6 (fig. 9(a)) than when the difference is reduced to 7.6×10^6 to 15.9×10^6 (fig. 10(m)).

Section Pitching-Moment Coefficient

Figure 17 indicates a peak negative value of $c_{m_{c/4}} = -0.068$ at $M = 0.78$. With further increase in speed, $c_{m_{c/4}}$ rapidly becomes less

negative for low values of c_n. For higher values of c_n this trend is small and the diving moment increases with further increase in Mach number. The indication therefore is that above about $M = 0.82$ the wing itself becomes stable with respect to normal-force coefficient (dc_m/dc_n is negative) and that this stability increases rapidly as the Mach number is increased to 0.86. Similar results were obtained in tests on a model wing in the Langley 8-foot high-speed wind tunnel.

In viewing the results shown for wing stations 152 and 207 it should be borne in mind that these stations are over the aileron and that the aileron was floating up.

Spanwise Load Variation

The data of figures 12 and 13, which show the variation of spanwise loading over a Mach number range of 0.60 to 0.86, indicate a substantial unloading of the wing outboard of station 62 at speeds above $M = 0.75$. This can be largely explained by the upfloat of the ailerons and a shift in the zero-lift angle of the wing. Aileron deflections of from 2° to 4° up for Mach numbers above 0.80 (fig. 19) should unload the outboard section of the wing. The positive shift in the zero-lift angle of the wing at speeds above its critical would serve to increase the amount of lift to be furnished by the fuselage.

Figures 14, 15, and 16 indicate an inward shift of load with Mach number above $M = 0.70$ and a decrease in the wing load above $M = 0.78$. To determine if perhaps some of the lateral shift of load could be attributed to twisting of the wing under load, the torsional deflection of the wing at a $C_L = 0.70$ at $M = 0.78$ was calculated, using values of torsional stiffness furnished by the manufacturer of the test airplane. Under this loading the calculated angular deflection of the tip with respect to wing station 62 was 0.16°. This was considered too small to be an appreciable factor in the load distribution.

From the foregoing it may be concluded that below $M = 0.75$ the effect of compressibility on the span load distribution is of a minor nature. The determination of this effect at higher Mach numbers was prevented at this time by the lack of data on the effect of the upfloat of the aileron.

Aileron Characteristics and Trailing-Edge Loads

On the last two flights made, large changes in aileron angle were noted for the highest speeds attained in straight dives and pull-outs.

Unfortunately only one aileron position recorder had been installed and that one was on the push-pull tube of the right aileron. The aileron position as a function of C_L and Mach number is shown in figure 19.

It has been assumed that the left aileron was behaving in a similar manner since the data were obtained during straight dives and pull-outs. This supposition is further supported by the linearity of the variation of c_{hq} with the aileron deflection as shown in figure 20. The scatter in the results may be attributed partly to effect of temperature on the control-system rigidity and partly to errors in determination of c_h.

To determine the effect of the aileron deflection on hinge moments, the pressure distributions over the aft 25-percent chord at wing stations 65 and 105.25 were integrated as well as those over the aileron. This procedure gives results corresponding to zero aileron deflections and allows comparison with the results obtained with the aileron deflected.

Figure 23 shows the hinge-moment characteristics based on the pressure distributions over the aft 25-percent chord at wing station 65. From this it may be seen that $\partial c_h/\partial c_n$ underwent a considerable change at about M = 0.75. This would indicate a substantial change in aileron control forces in this range (M = 0.75 to 0.85). Between M = 0.85 and M = 0.86 a reversal of the slope indicates a sudden change in the aileron characteristics. This decrease in hinge moments at the higher values of c_n is thought to be caused by the rearward chordwise location of the peak pressures and shock wave location on the lower surface as well as flow separation on the lower surface.

It appears logical that a large-scale separation on the upper surface with the accompanying loss in pressure recovery produces the large hinge moments obtained. This condition may be readily observed in the pressure distributions of figure 11.

Figure 21 shows a typical variation with Mach number of the pressure coefficients for orifices near the trailing edge both at stations over the aileron and inboard of the aileron compared on the basis of constant section normal-force coefficients. The sudden decrease in the coefficients of upper-surface pressures at about M = 0.80 is interpreted as being a result of the flow separation.

Comparing these curves of pressure coefficients for the trailing-edge orifices for the various stations, it may be noted that the flow at wing station 152 separates at a much lower Mach number than at any of the other stations, an effect caused possibly by the relatively large bumps on the nose. (See fig. 4.) In addition, the separation at stations over the ailerons occurs at a lower Mach number than that over the inboard wing stations. This is attributed to the fact that comparison

between stations is made on the basis of equal values of sectional normal-force coefficients c_n, which means that due to the upfloating aileron a higher section angle of attack will be necessitated at the stations over the aileron. It is this higher angle of attack which is believed to be the cause of separation at a lower Mach number.

Although the aileron deflection produces sizable changes in the appearance of the pressure distributions over both the upper and lower surface, the change in hinge moments due to the deflection is small compared to the large change in hinge moments occurring at Mach numbers above 0.80. This is demonstrated in figure 22 in which a c_h of 0.13 at M = 0.85 was obtained. It appears that the curves may have begun to level off at about this value and that values of −0.16 to −0.20 would not be exceeded. Separation on the lower surface would have the effect of relieving these large hinge moments. Since this lower-surface separation at least for low lift coefficients may be expected to occur at a Mach number not greatly above those already reached (0.866), these large hinge moments are probably a characteristic of a rather narrow range of Mach number.

It might be noted that the aileron flutter observed at about M = 0.83 on this airplane could possibly be explained by a coupling of the shock and separation induced on the lower surface with the up-deflection of the aileron, the flow remaining virtually unchanged on the upper surface due to the thick boundary layer.

Inspection of the pressure distributions above M = 0.80 to 0.86 in figure 11 indicates that the aileron loading is uniform along the chord. The most rearward pressure orifices installed on the wing were at approximately 95-percent-chord location. In this report the practice has been to fair the pressure diagrams in the proximity of the trailing edge. There is a possibility that a pressure discontinuity exists at the trailing edge; in which case the aileron hinge moments would be slightly higher than stated herein.

On the basis of the results obtained to date it is recommended that for the aileron and aft 30 percent of the wing chord a uniform chordwise loading of 0.40q in the Mach number range of 0.80 to 0.866 be used for design purposes. This corresponds to a c_h = −0.20.

CONCLUSIONS

The following conclusions were formed as a result of high-speed flight tests on an airplane having an NACA low-drag airfoil.

The results were considered accurate over a Raynolds number range from 10×10^6 to 30×10^6 and over a Mach number range from 0.50 to 0.86. Airplane lift coefficients varied from 0 to 0.60 for the lower Mach numbers and from 0 to 0.40 for the higher Mach numbers. Whereas a few of the results are applicable only to the specific airplane tested, most of the conclusions may be applied to any aircraft with this type of wing profile in the high-speed range.

1. No significant effect due to Reynolds number was noticeable on the chordwise pressure distributions or spanwise loading.

2. Chordwise pressure distributions made in the Ames 16-foot high-speed wind tunnel agree well with the flight-test results except for disturbances caused by manufacturing irregularities in the airplane wing surface. Although the test airplane has an exceptionally smooth wing surface, the irregularities present have a definite effect on pressure distributions.

3. A peak negative value of $c_{m_{c/4}}$ occurs at $M = 0.78$. Above this Mach number $c_{m_{c/4}}$ rapidly becomes less negative for low values of c_n. For the higher values of c_n this trend is reversed. This leads to a change of $dc_{m_{c/4}}/dc_n$ from positive to negative (stable) at Mach numbers of 0.82 to 0.84.

4. No large changes in spanwise loadings or wing bending moments due to Mach number were obtained below $M = 0.75$. Above $M = 0.75$ an unloading of the outer portion of the wing with an inboard shift of the lateral center of pressure took place. The principal cause of this was considered to be the upfloat of the ailerons with a shift in the zero lift angle of the wing also having an effect.

5. The ailerons were found to have a large upfloating deflection during dives above a Mach number of 0.80. This was caused by a sudden increase in hinge moments when the Mach number was increased above $M = 0.78$. The high hinge moments were attributed to large-scale separation causing a loss in pressure recovery on the aft portion of the upper surface.

6. It is recommended that for design purposes the aft 30 percent of the wing chord and the ailerons should be designed to withstand a uniform chordwise loading of 0.40q at supercritical Mach numbers.

Ames Aeronautical Laboratory,
National Advisory Committee for Aeronautics,
Moffett Field, Calif., August 1946.

REFERENCES

1. Clousing, Lawrence A., Turner, William N., and Rolls, L. Stewart: Measurements in Flight of the Pressure Distribution on the Right Wing of a P-39N-1 Airplane at Several Values of Mach Number. NACA ARR No. 4K09, 1945.

2. Turner, Howard L., and Rathert, George A.: Pressure Lag in Tubing Used in Flight Research. NACA RB No. 5F15, 1945.

3. Nissen, James M., Gadeberg, Burnett L., and Hamilton, William T.: Correlation of the Drag Characteristics of a P-51B Airplane Obtained from High-Speed Wind-Tunnel and Flight Tests. ACR No. 4K02, 1945.

TABLE I.- ORIFICE LOCATIONS ON WINGS OF THE TEST AIRPLANE
[Given in percent of chord]

Left wing

Upper surface								Lower surface							
Orifice No.	Spanwise station, in. from center line of airplane							Orifice No.	Spanwise station, in. from center line of airplane						
	65	87.5	105.25	131	152	180	207		65	87.5	105.25	131	152	180	207
1	0.68	----	0.72	---	0.32	---	0.36	1	0.69	----	0.69	---	0.39	---	0.25
2	1.47	----	1.55	---	.95	---	1.43	2	1.48	----	1.47	---	1.05	---	1.12
3	2.79	----	2.69	---	2.20	---	2.61	3	2.87	----	2.81	---	2.17	---	2.23
4	5.31	----	5.25	---	4.62	---	5.09	4	5.26	----	5.34	---	4.60	---	4.86
5	10.32	10	10.25	10	9.65	10	10.02	5	10.20	10	10.34	10	9.57	10	11.43
6	16.24	----	16.62	---	15.49	---	16.02	6	16.30	----	16.23	---	15.49	---	16.69
7	22.58	----	23.32	---	22.73	---	23.10	7	23.07	----	23.68	---	22.59	---	23.43
8	26.12	----	25.84	---	25.93	---	26.13	8	26.19	----	25.95	---	25.88	---	26.31
9	33.23	----	33.97	---	34.33	---	34.19	9	33.54	----	33.87	---	34.19	---	34.28
10	41.16	----	42.09	---	40.62	---	41.73	10	41.40	----	41.84	---	41.33	---	41.78
11	45.78	----	46.53	---	48.70	---	48.78	11	45.93	----	46.50	---	48.24	---	47.89
12	54.13	----	55.96	---	53.76	---	55.23	12	56.13	----	54.97	---	53.76	---	55.10
13	59.18	----	59.89	---	58.78	---	60.12	13	59.59	----	59.99	---	58.88	---	60.03
14	64.14	----	64.60	---	63.96	---	64.96	14	64.23	----	65.02	---	63.56	---	65.16
15	69.12	----	69.56	---	68.68	---	75.61	15	69.51	----	72.59	---	67.63	---	-----
16	73.38	----	76.88	---	78.41	---	80.18	16	71.87	----	76.47	---	78.59	---	79.94
17	79.11	----	79.83	---	83.30	---	85.14	17	79.09	----	79.96	---	83.51	---	85.02
18	83.03	----	84.58	---	89.93	---	90.27	18	82.90	----	85.12	---	90.14	---	93.04
19	89.14	----	88.93	---	93.24	---	95.25	19	89.15	----	88.76	---	93.16	---	-----
20	94.19	----	94.39	---	-----	---	-----	20	94.09	----	95.06	---	-----	---	-----
Section chord, feet	7.46	6.92	6.40	5.83	5.18	4.46	3.73	Section chord, feet	7.46	6.92	6.40	5.83	5.18	4.46	3.73

Right wing

At spanwise station 105, orifices located at 23, 26, 34, and 42 percent chord.
Upper and lower surfaces

TABLE II.- ORDINATES OF NACA 65_1-213 (a = 0.5) AIRFOIL
[All stations and ordinates in percent chord]

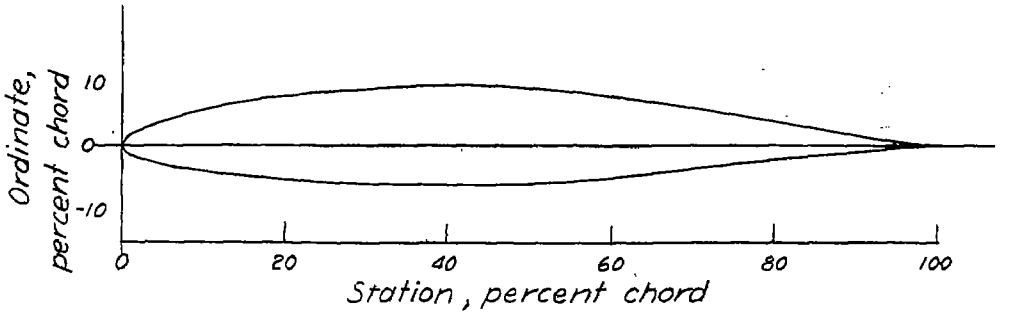

Upper surface		Lower surface	
Station	Ordinate	Station	Ordinate
0	0	0	0
.38	1.06	.62	-.92
.62	1.29	.88	-1.10
1.10	1.64	1.40	-1.35
2.34	2.28	2.66	-1.76
4.81	3.26	5.19	-2.38
7.31	4.02	7.69	-2.84
9.80	4.67	10.20	-3.22
14.81	5.71	15.19	-3.82
19.83	6.51	20.17	-4.26
24.86	7.12	25.14	-4.59
29.89	7.56	30.11	-4.82
34.92	7.85	35.08	-4.96
39.96	7.98	40.04	-5.01
45.01	7.94	44.99	-4.95
50.07	7.71	49.93	-4.77
55.11	7.26	54.89	-4.47
60.13	6.63	59.87	-4.07
65.14	5.89	64.86	-3.60
70.13	5.04	69.87	-3.06
75.11	4.14	74.89	-2.49
80.09	3.19	79.91	-1.88
85.06	2.24	84.94	-1.29
90.04	1.33	89.97	-.72
95.01	.53	94.99	-.24
100.00	0	100.00	0

L. E. radius: 1.174. Slope of radius through L. E.: 0.084

TABLE III.- SUMMARY OF PRESSURE-DISTRIBUTION PLOTS PRESENTED IN FIGURES 9, 10, AND 11.

Mach number, M	Pressure altitude, h_p (ft)	Airplane Reynolds number, R (x 10^{-6})	C_L	Wing station 65		Wing station 105.25		Wing station 152		Wing station 207	
				c_n	Figure number	c_n	Figure number	c_n	Figure number	c_n	Figure number
0.699	4,200	32.3	0.065	0.118	*9(a)	0.119	9(b)	0.059	9(c)	-0.006	9(d)
.706	10,000	25.0	.082	.114	9(e)	.135	9(f)	.084	9(g)	.010	9(h)
.688	20,200	17.8	.134	.182	[1]9(i)	.183	9(j)	.109	9(k)	.045	9(l)
.704	29,300	13.3	.190	.241	[1]9(m)	.267	9(n)	.164	9(o)	.102	9(p)
.754	3,400	32.3	.053	.116	[1]10(a)	.092	10(b)	.031	10(c)	-.012	10(d)
.758	8,300	31.1	.065	.103	[1]10(e)	.107	10(f)	.074	10(g)	-.015	10(h)
.755	20,400	18.8	.104	.136	[1]10(i)	.151	10(j)	.104	10(k)	.061	10(l)
.790	30,300	14.7	.110	.171	[1]10(m)	.142	10(n)	.063	10(o)	-.002	10(p)
.807	20,500	19.9	.016	.102	[1]11(a)	.056	11(b)	-.034	11(c)	-.074	11(d)
.829	18,200	22.4	.200	.24	11(e)	.20	11(f)	.106	11(g)	.039	11(h)
.866	27,400	17.7	.411	.43	11(i)	.38	11(j)	.20	11(k)	.29	11(l)
.808	17,400	22.6	.482	.58	[1]11(m)	.55	11(n)	.375	11(o)	.44	11(p)

[1]Indicates comparison made with high-speed wind-tunnel results.

Figure 1.- Three-quarter side view, test airplane.

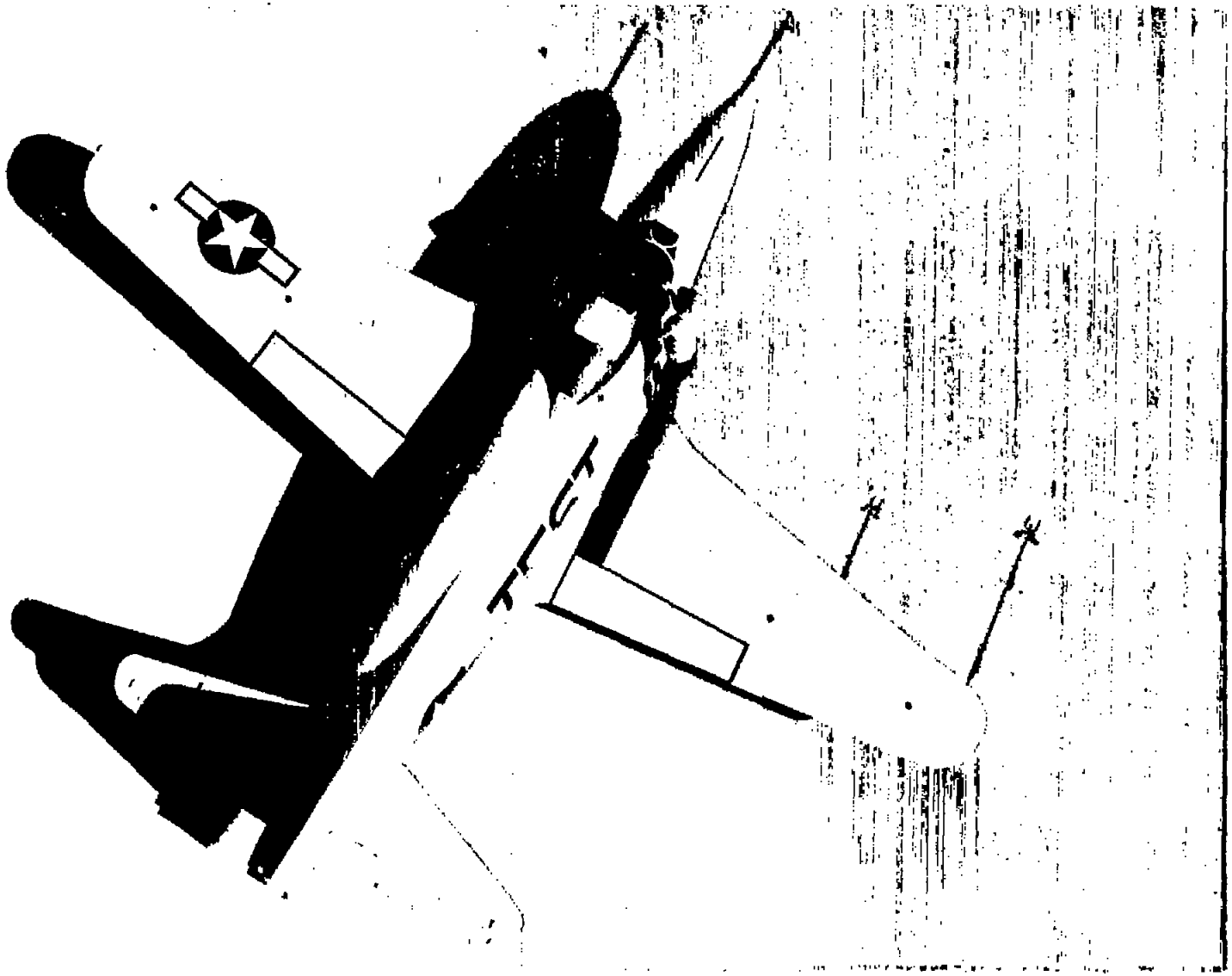

Figure 2.- Plan view of the test airplane.

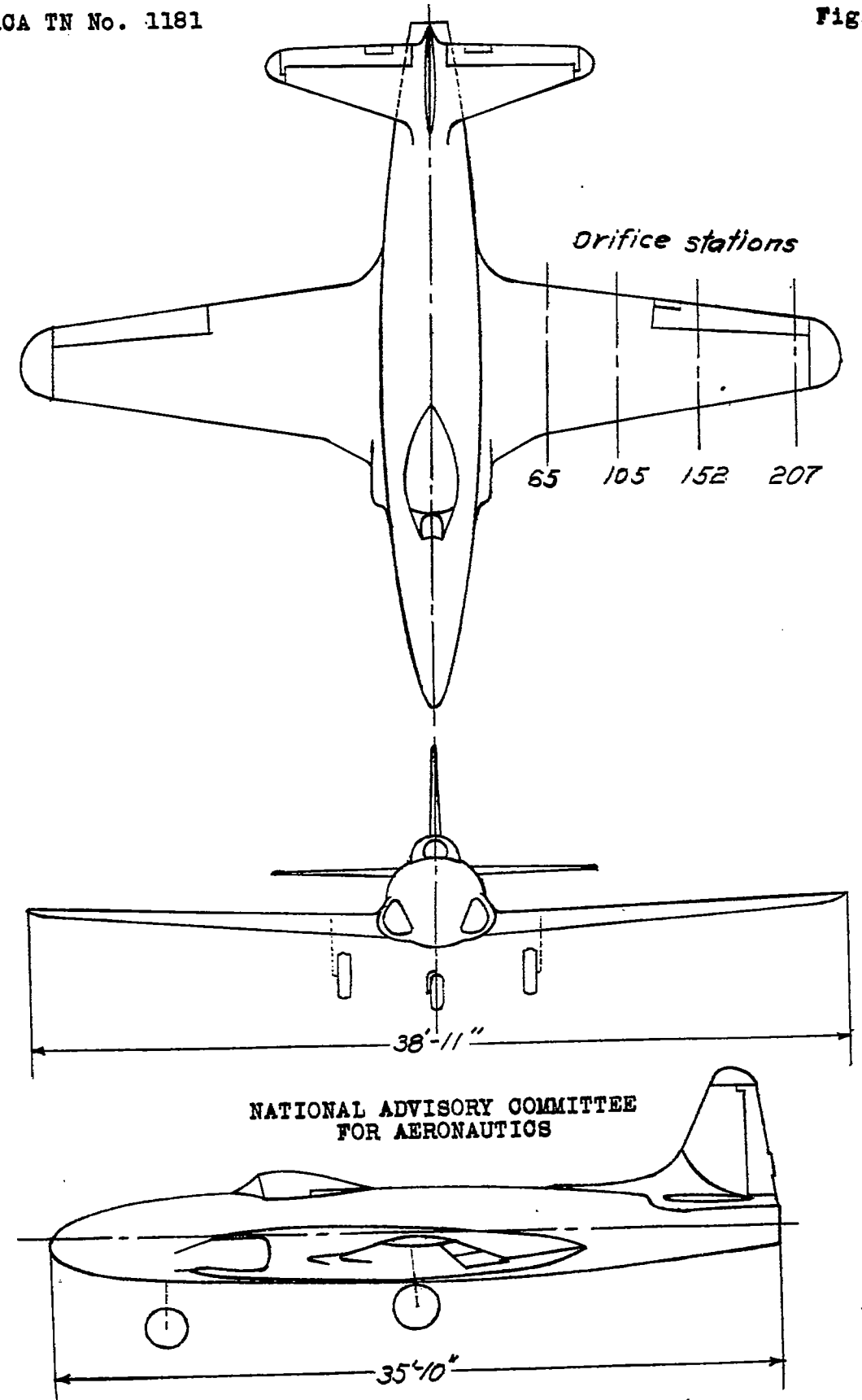

Figure 3.- Three-view drawing of the test airplane

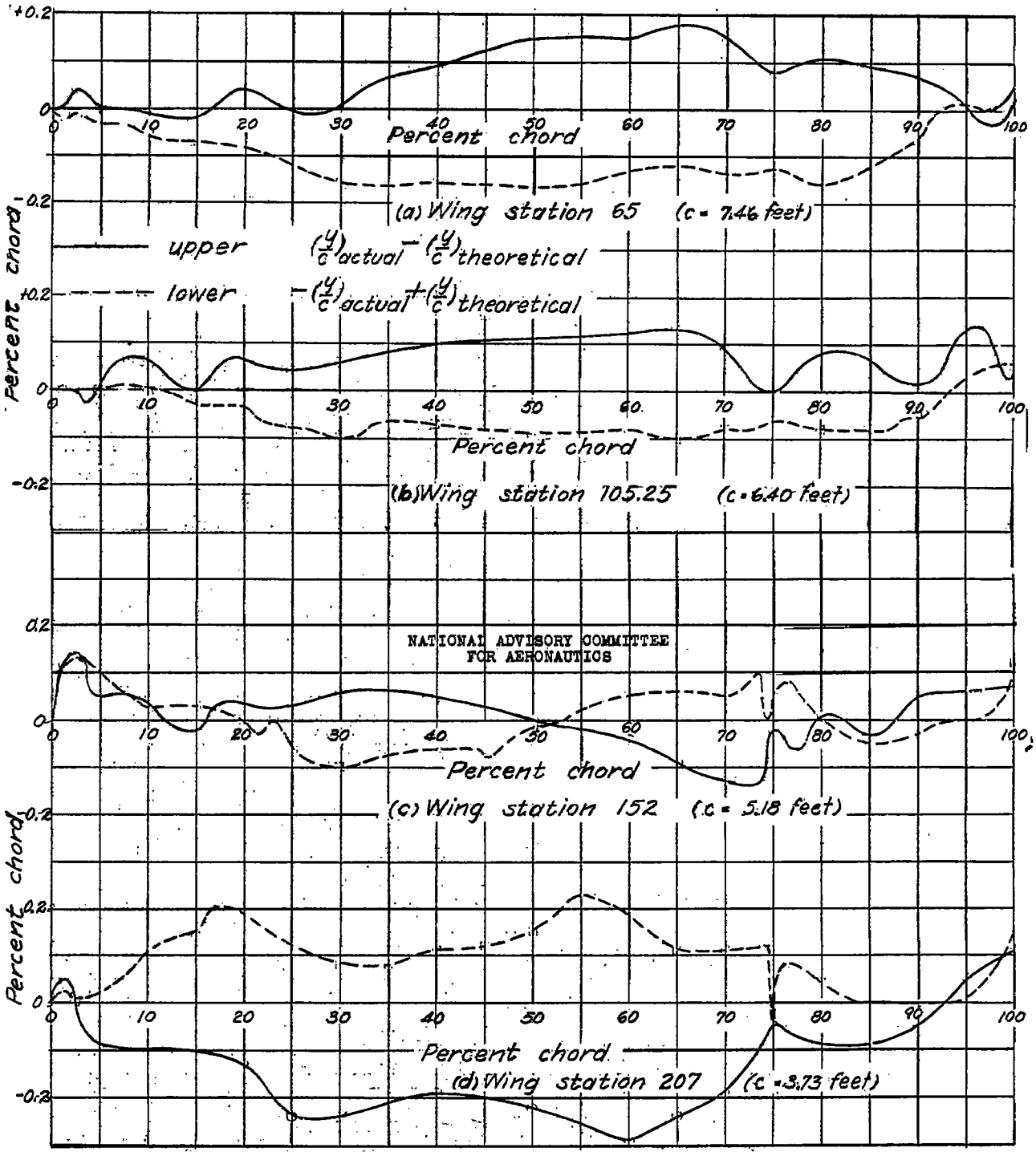

Figure 4.—Deviation in percent chord of actual wing contour from the theoretical airfoil at various spanwise locations.

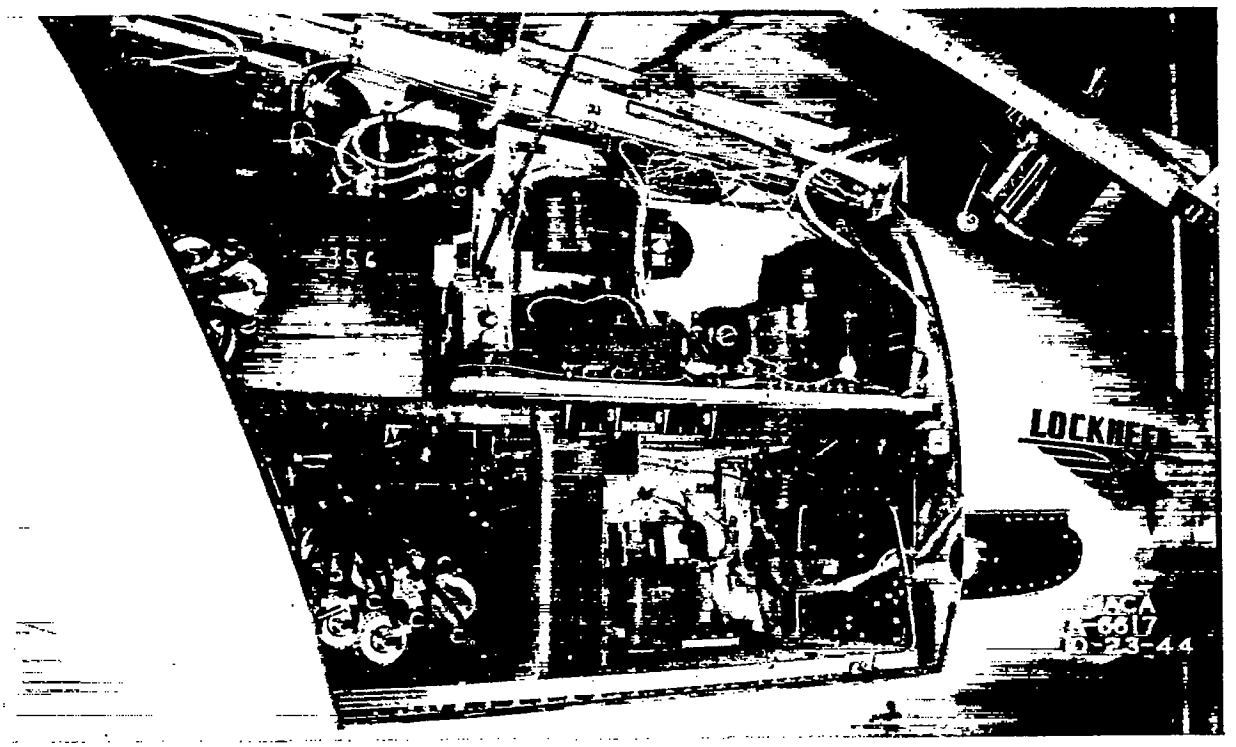

(a) Right-hand side.

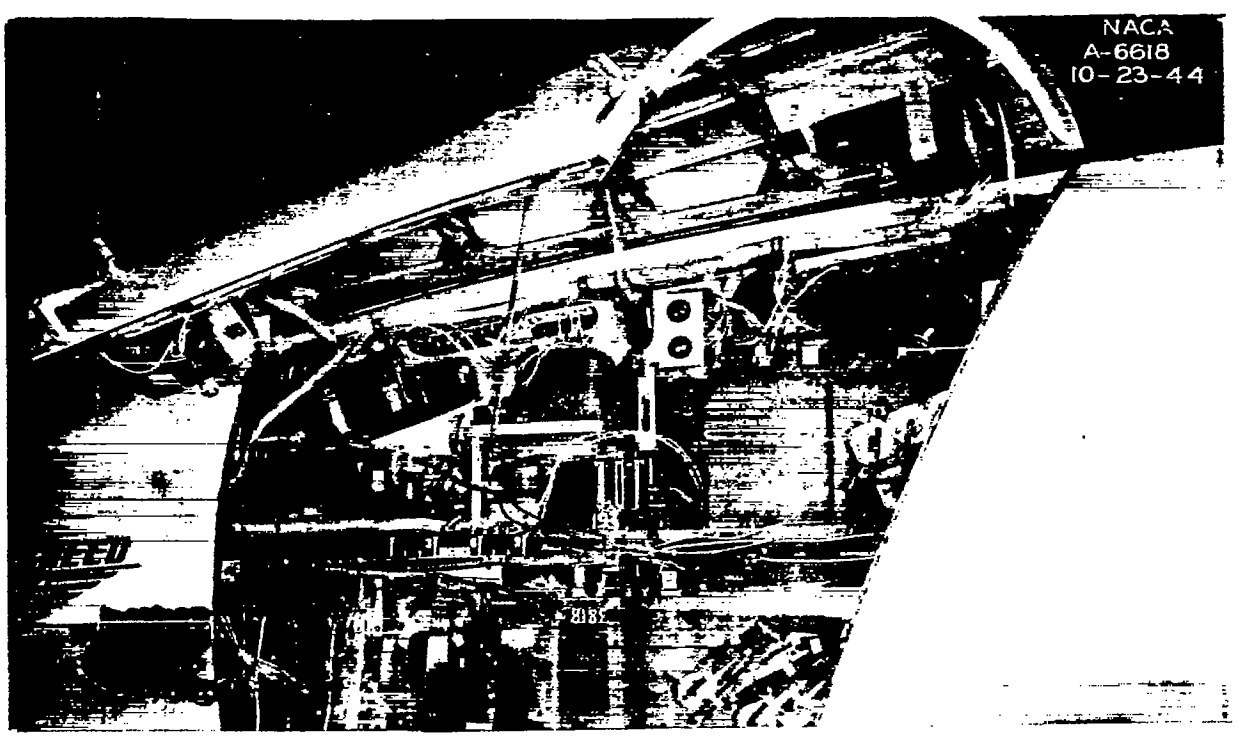

(b) Left-hand side.

Figure 5.- Nose compartment instrumentation in the test airplane.

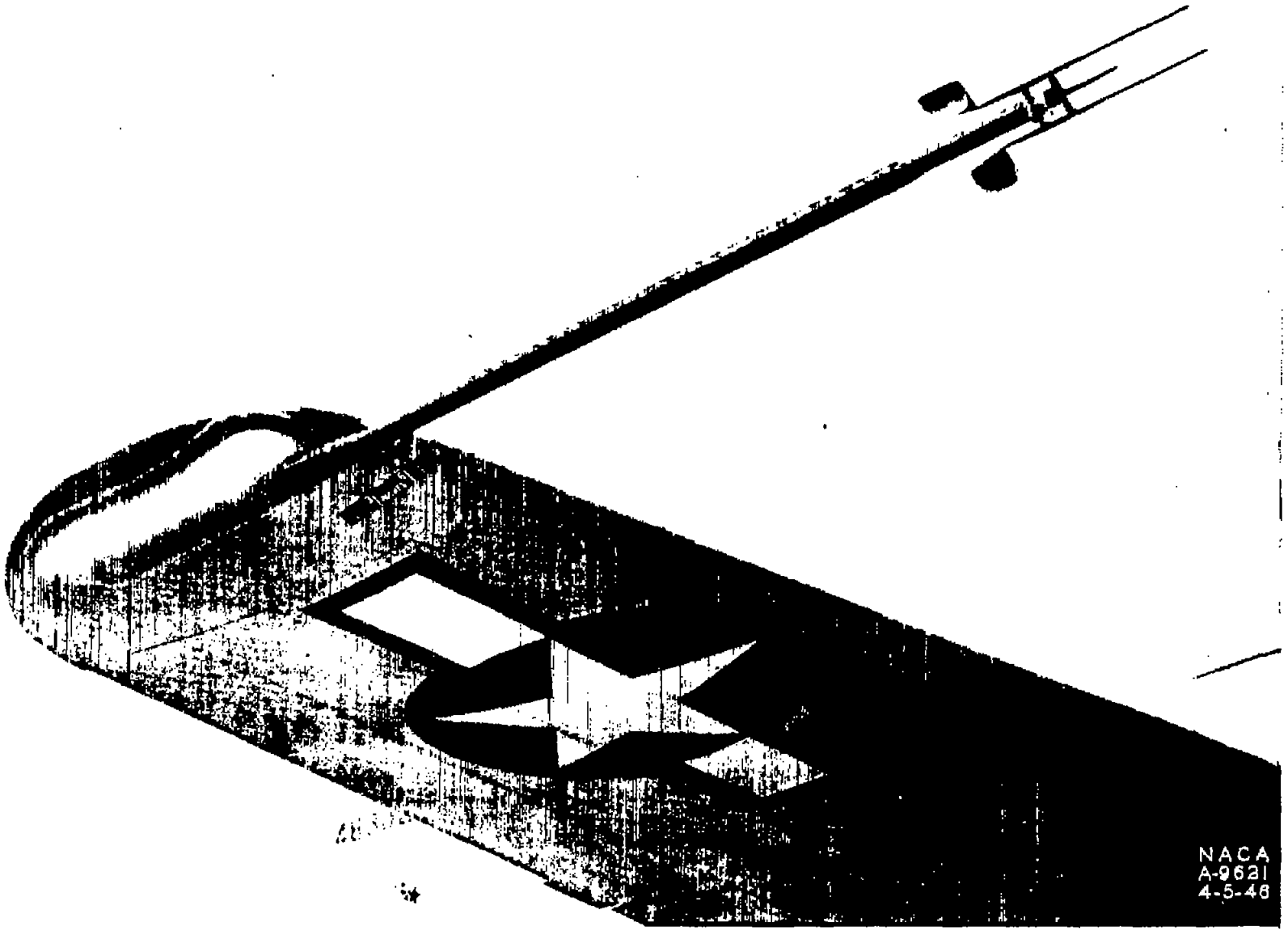

Figure 6.- Airspeed-boom installation on the test airplane.

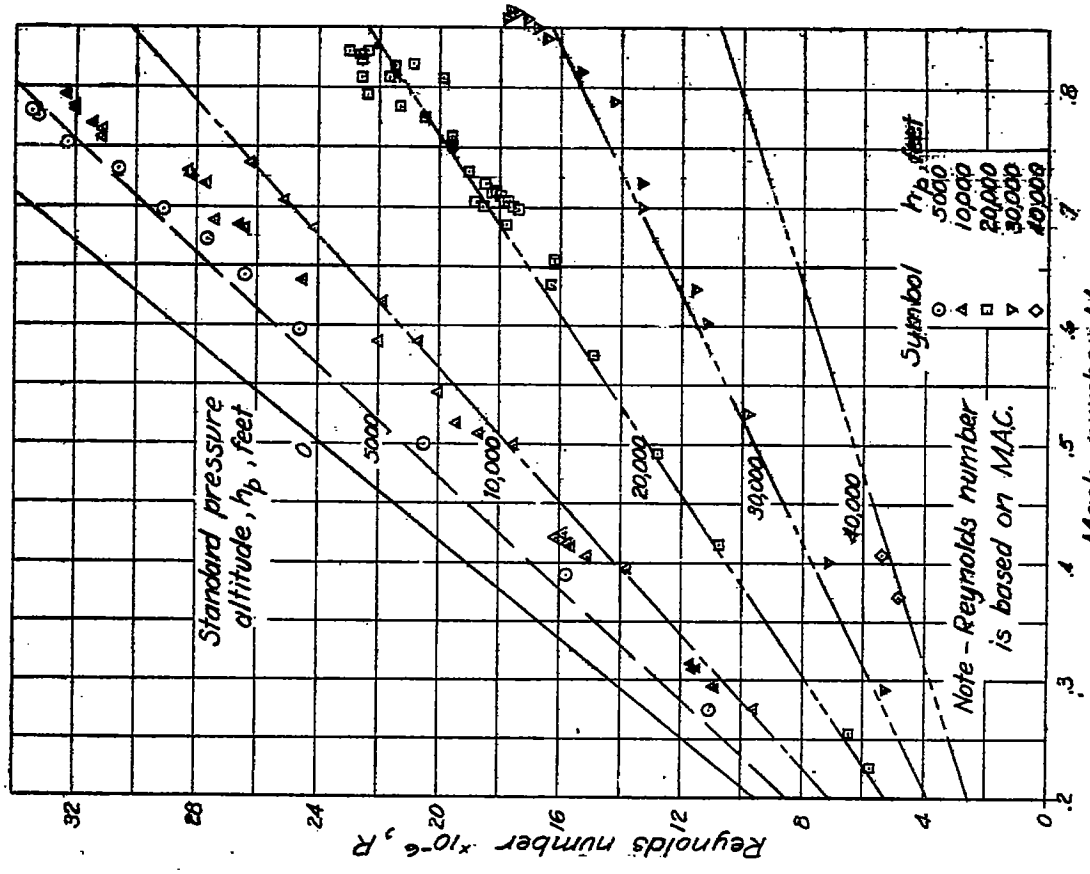

Figure 7.— Range of Mach number and Reynolds number for flight-test data obtained.

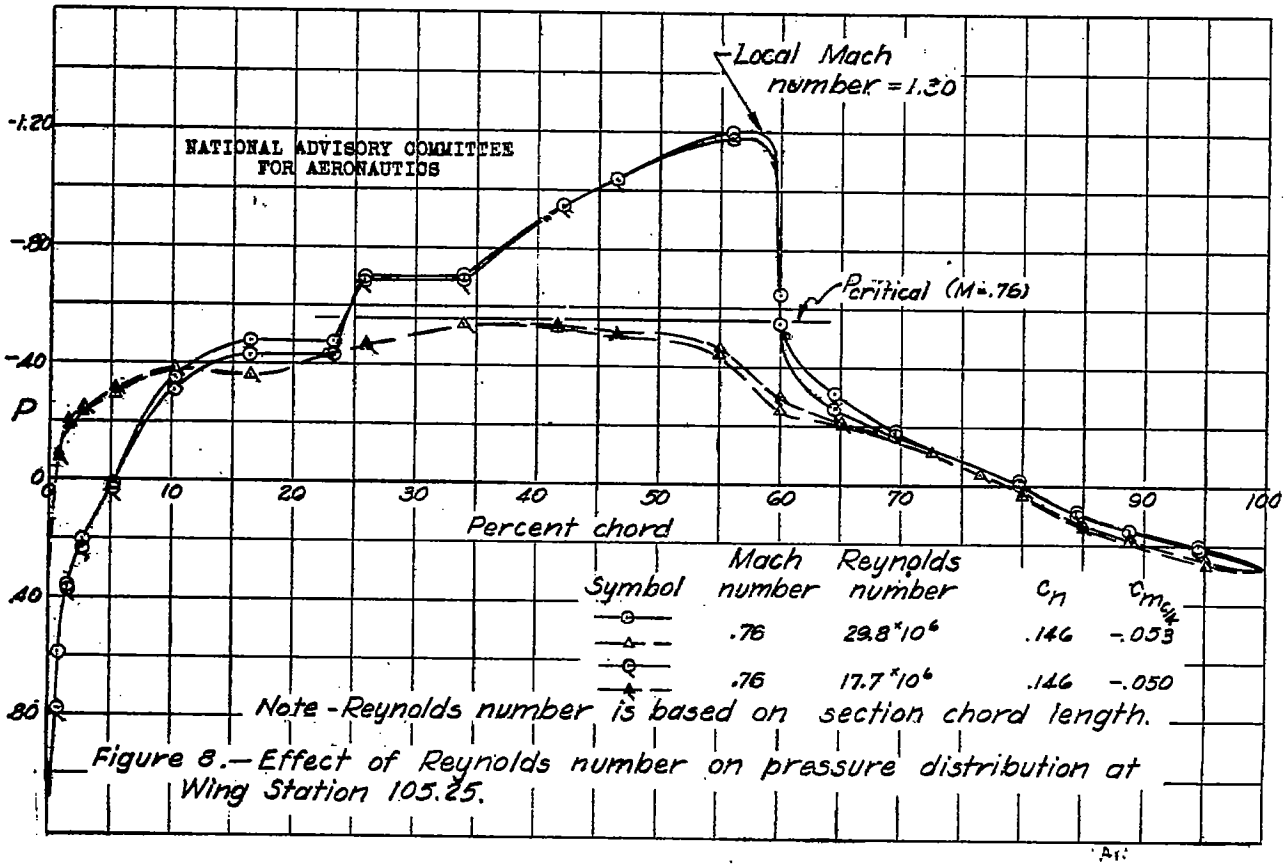

Figure 8.— Effect of Reynolds number on pressure distribution at Wing Station 105.25.

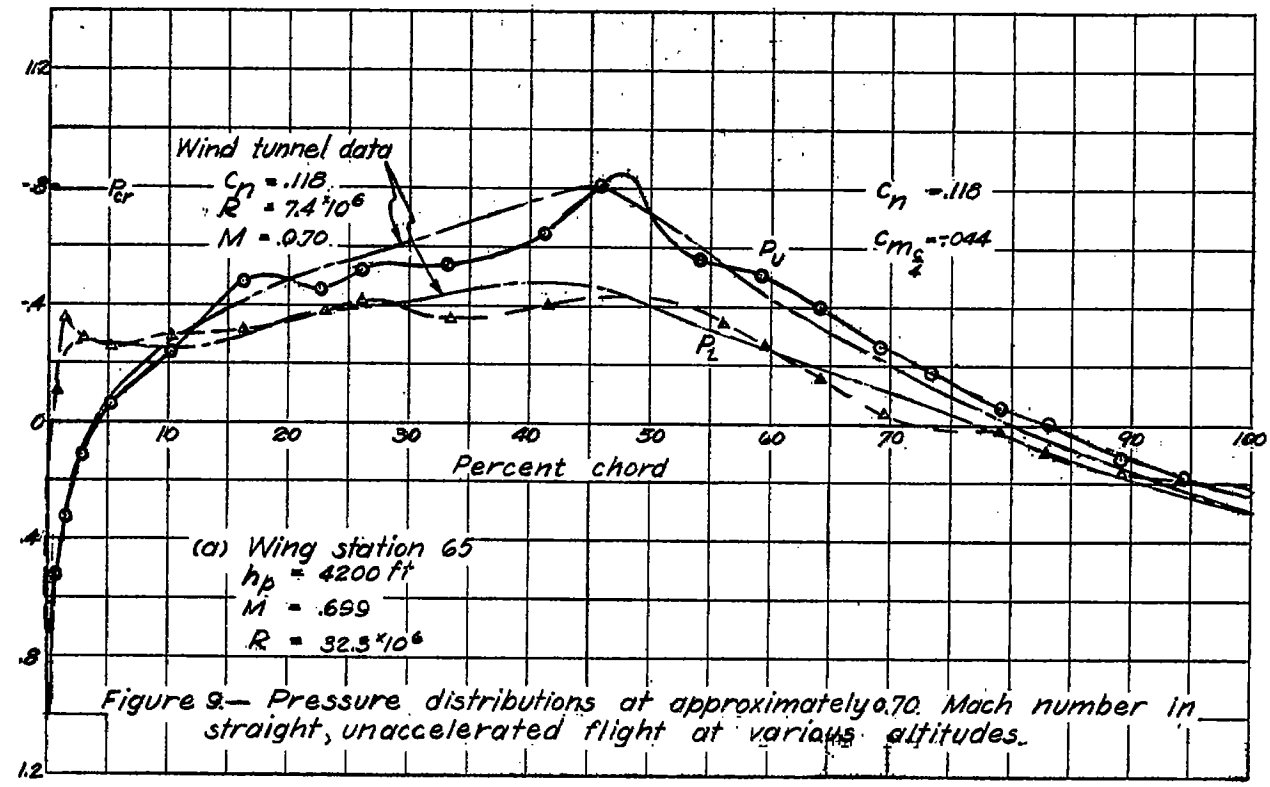

Figure 9.— Pressure distributions at approximately 0.70 Mach number in straight, unaccelerated flight at various altitudes.

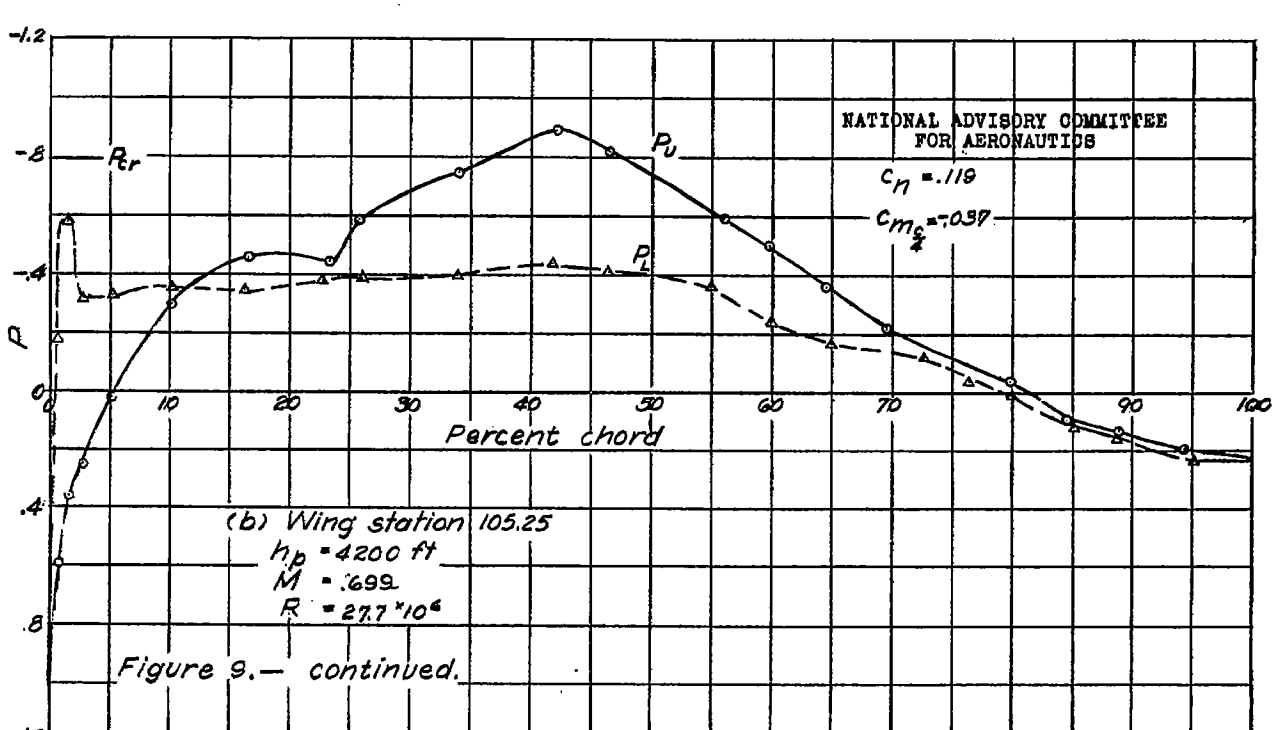

Figure 9.— continued.

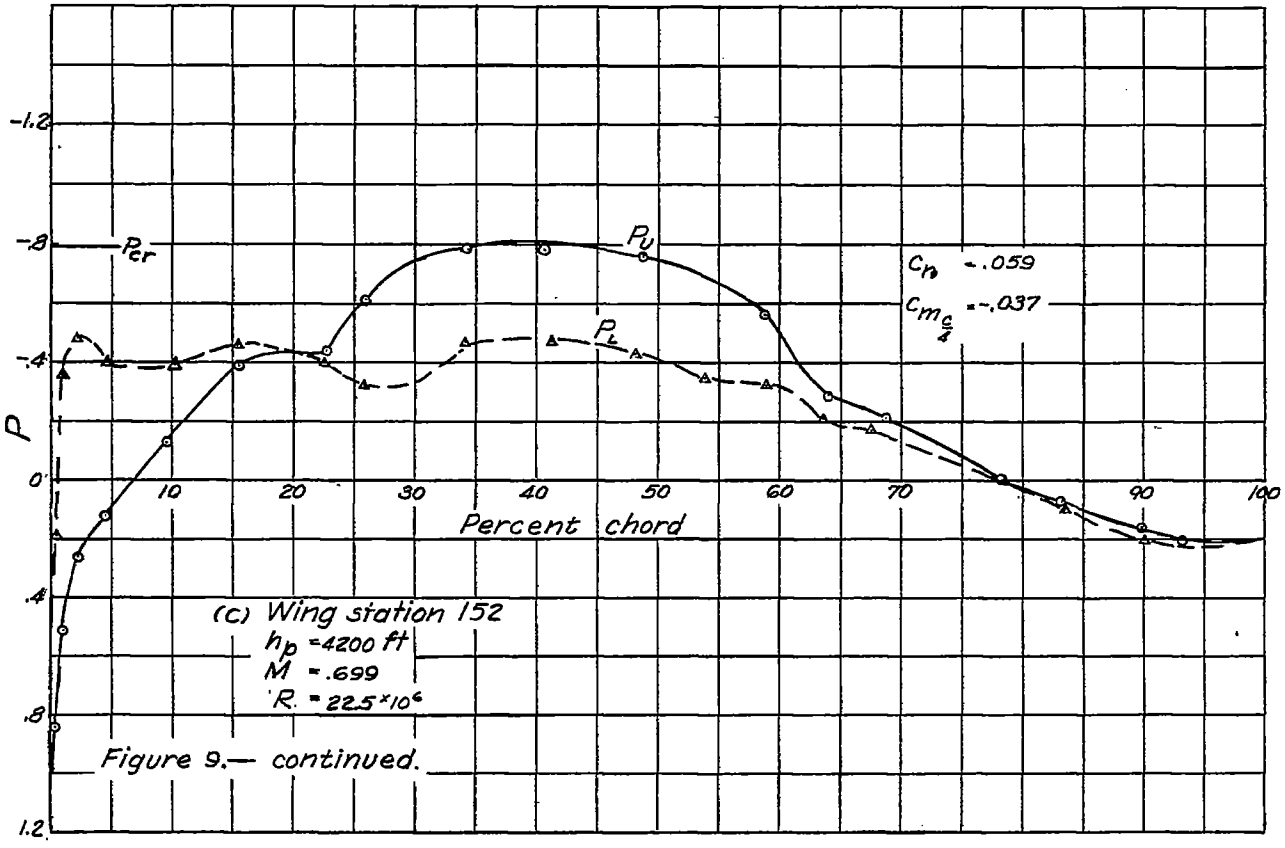

Figure 9.— continued.

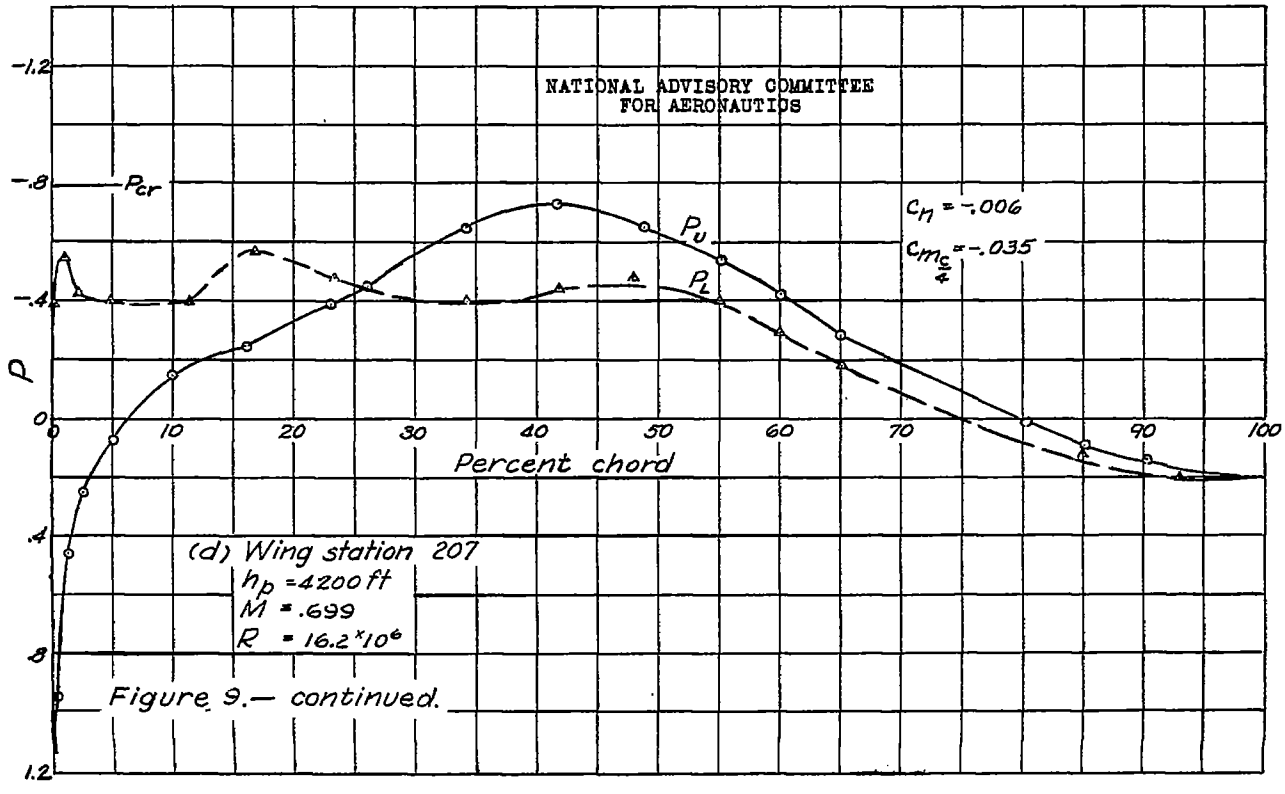

Figure 9.— continued.

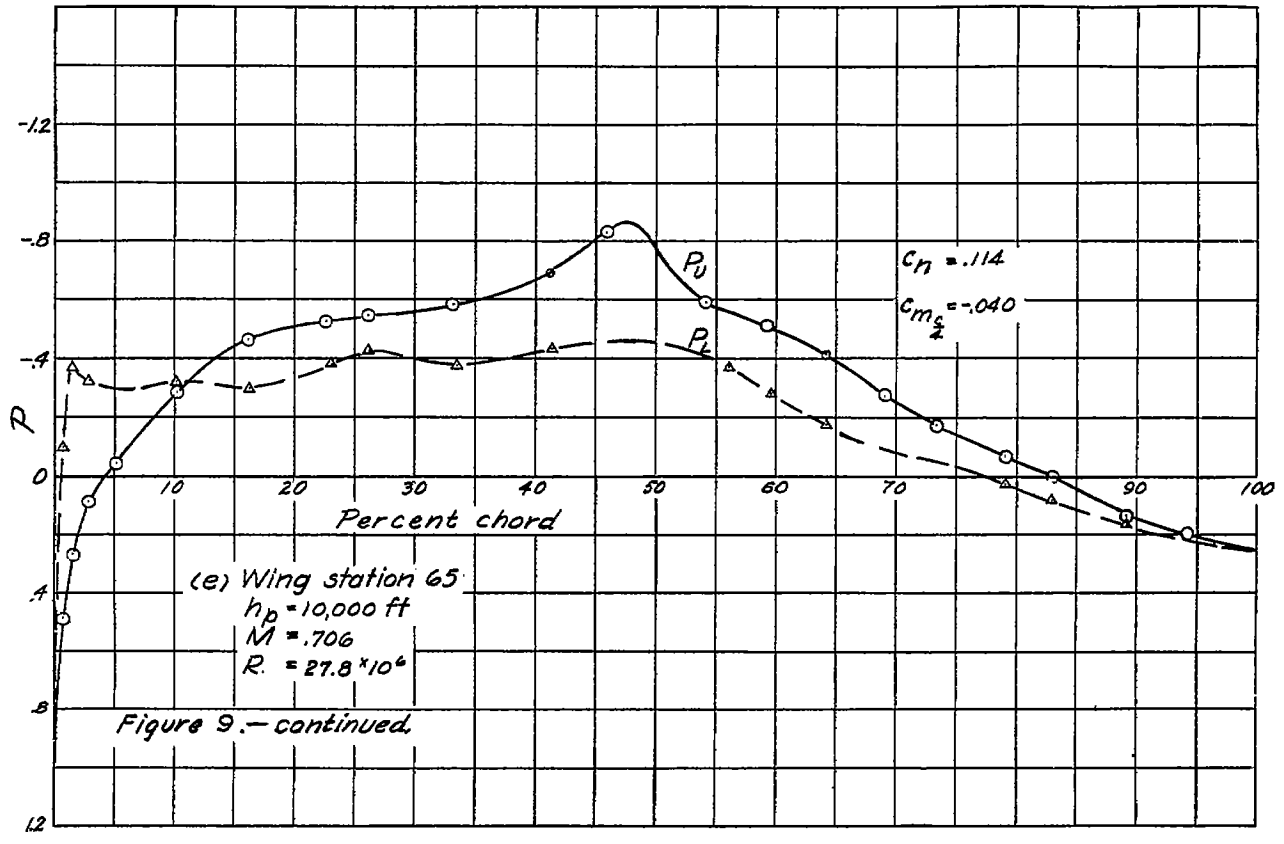

Figure 9.— continued.

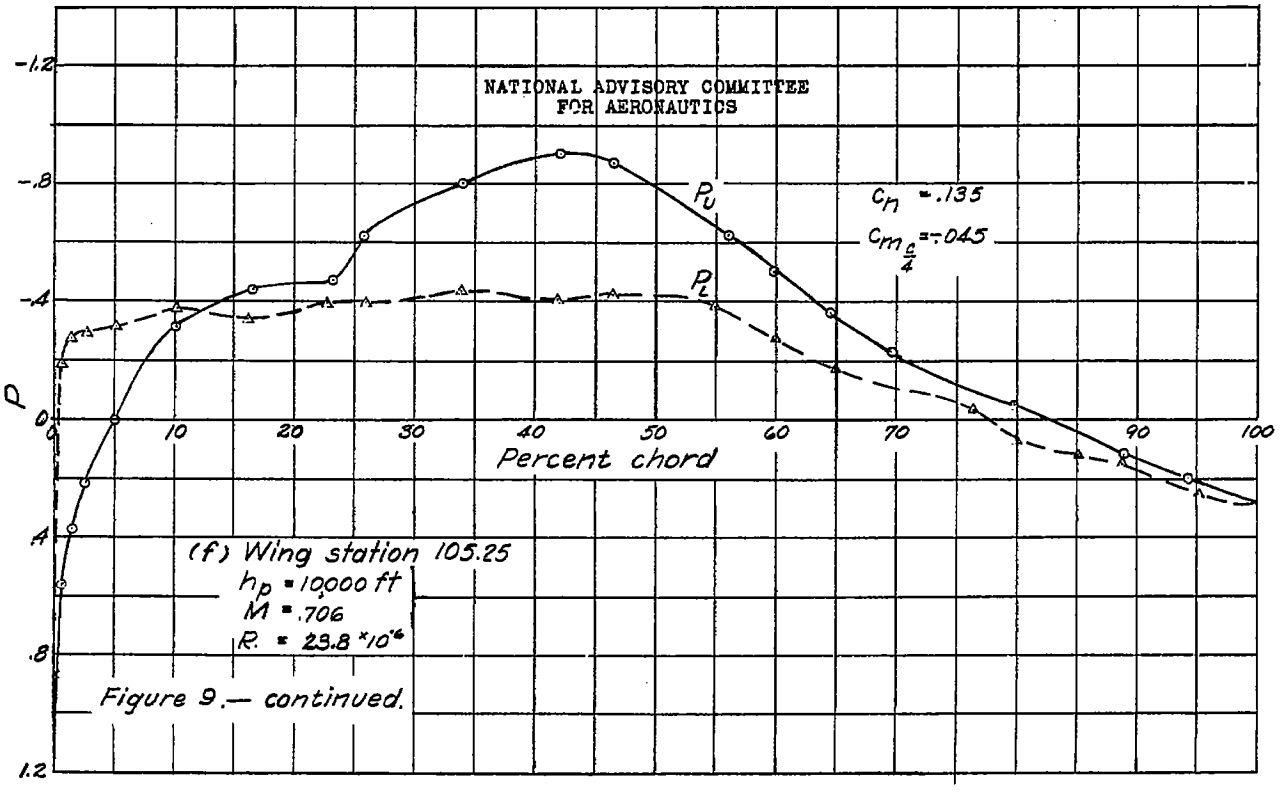

NATIONAL ADVISORY COMMITTEE FOR AERONAUTICS

Figure 9.— continued.

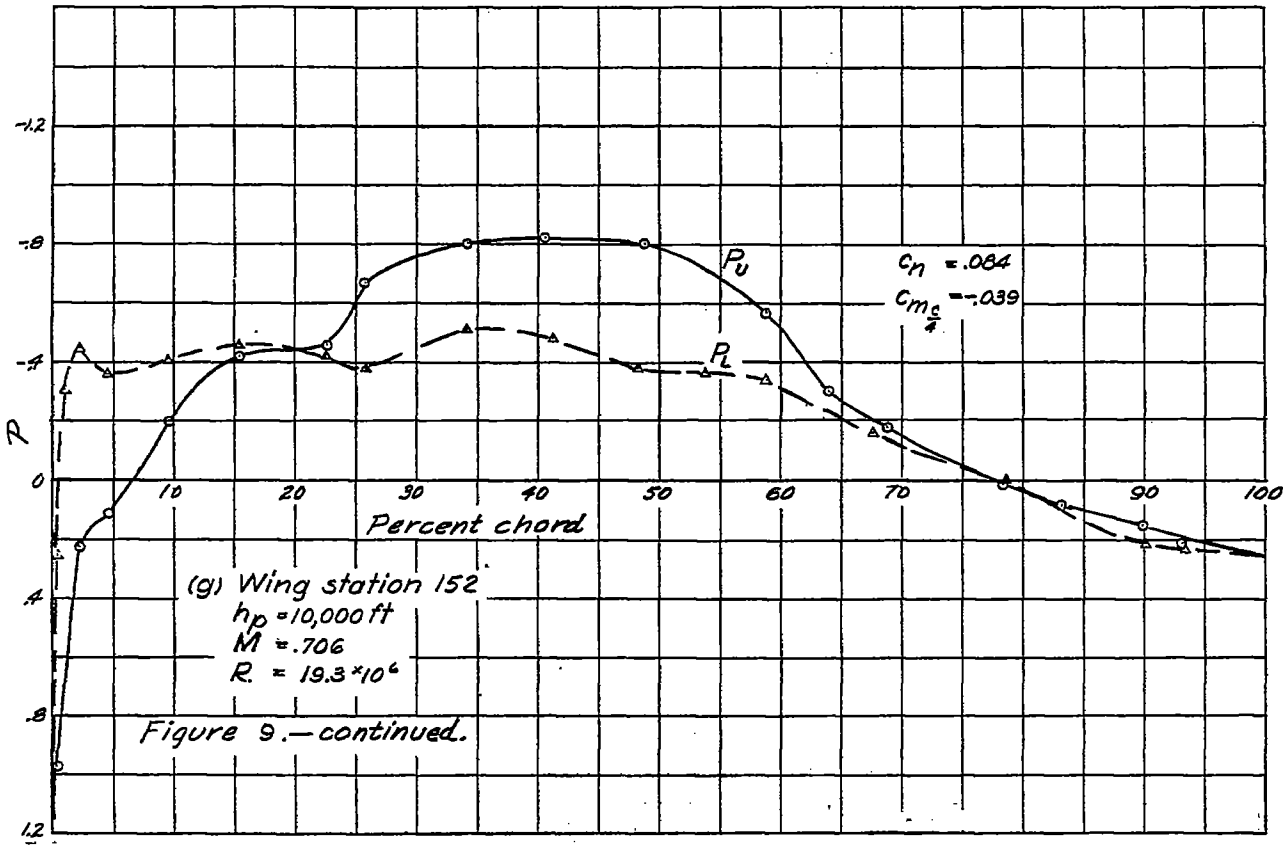

Figure 9.—continued.

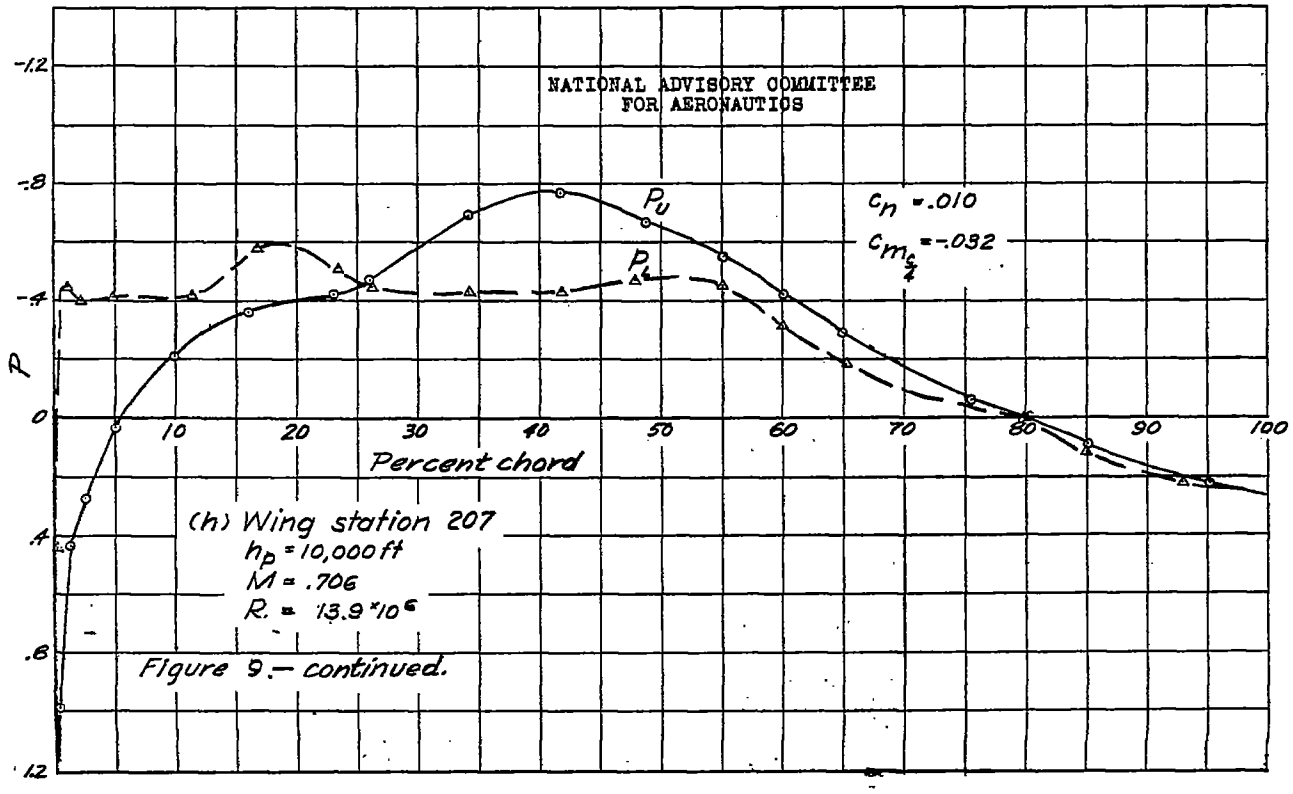

Figure 9.— continued.

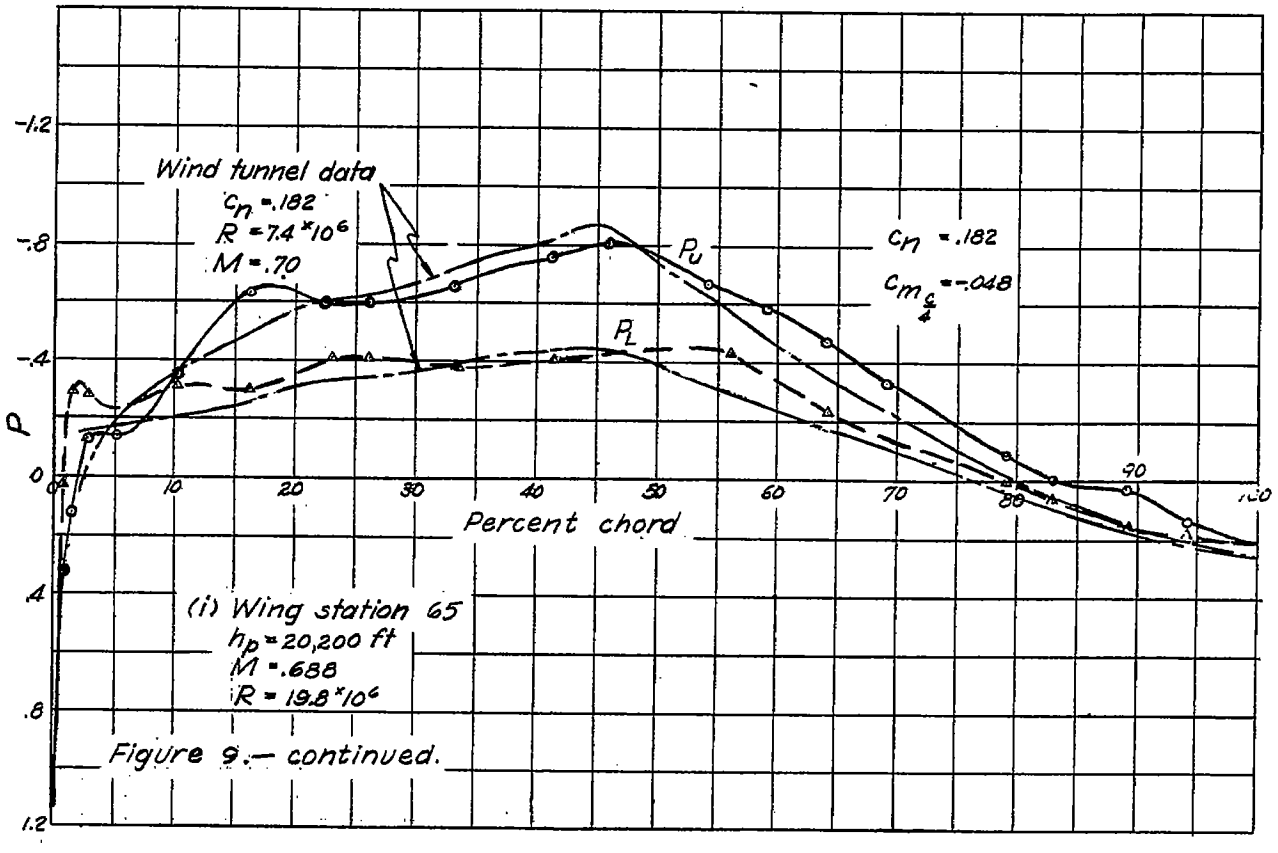

Figure 9.— continued.

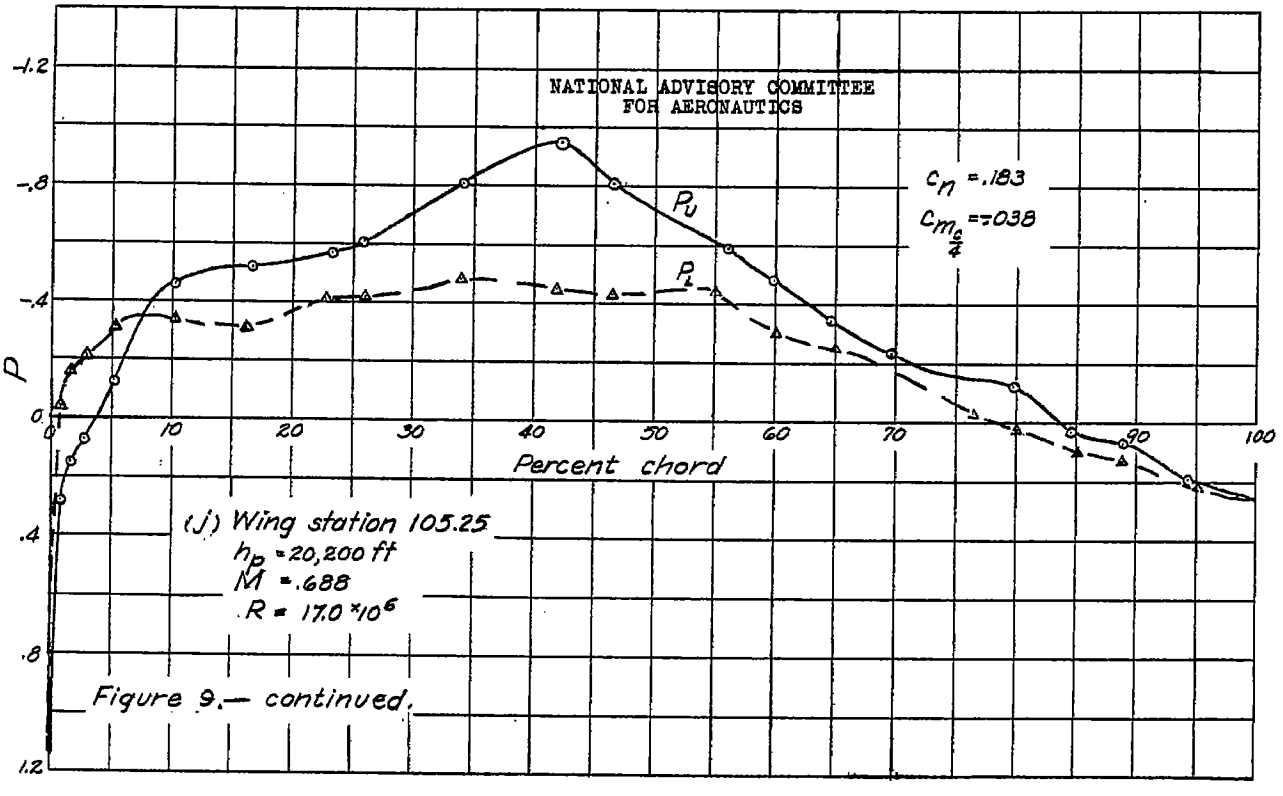

Figure 9.— continued.

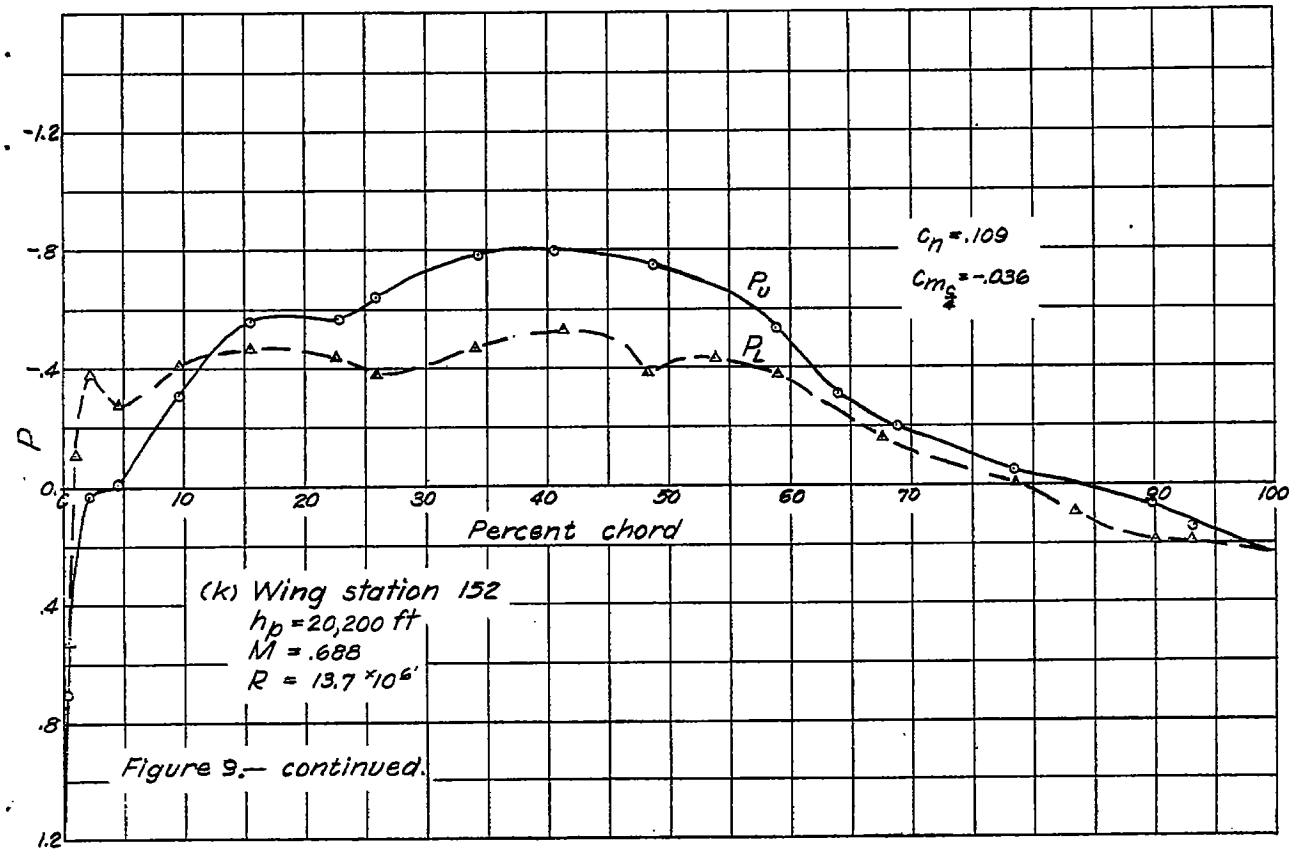

Figure 9.— continued.

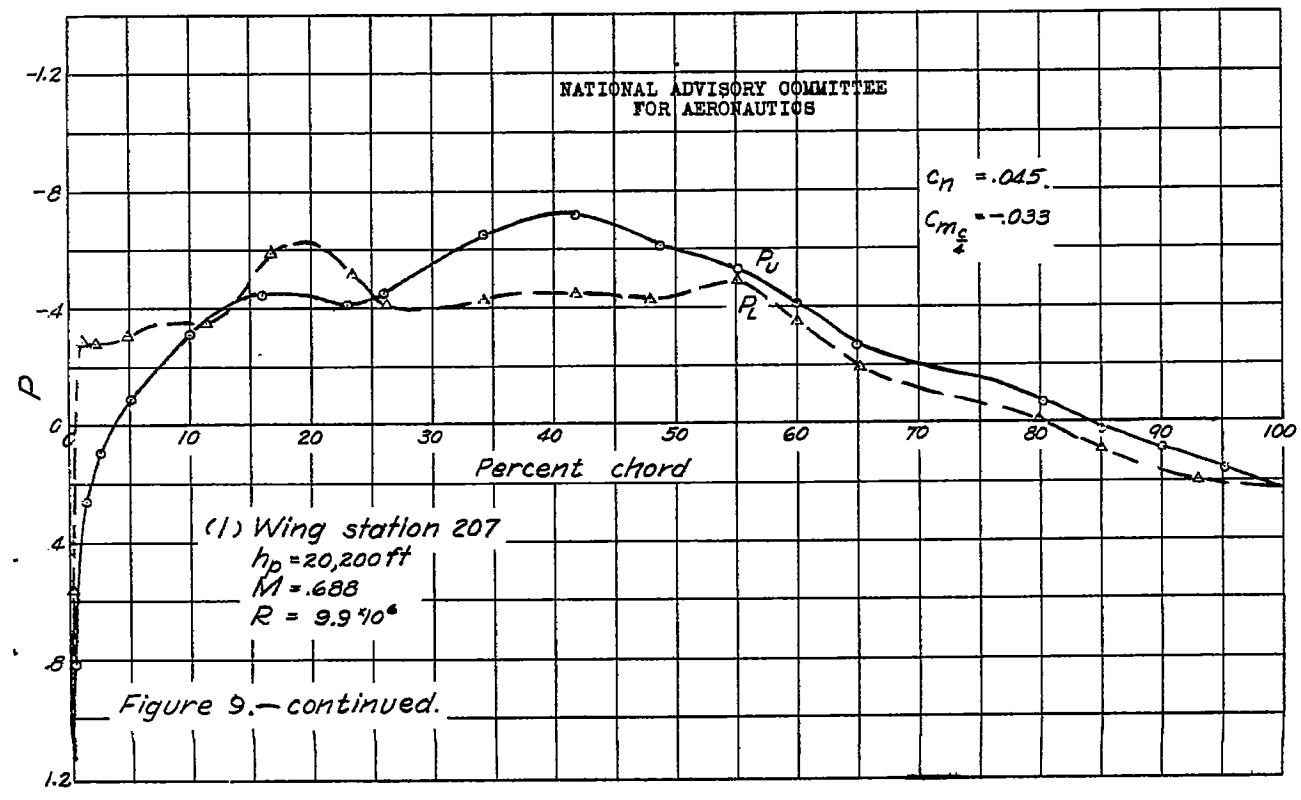

Figure 9.— continued.

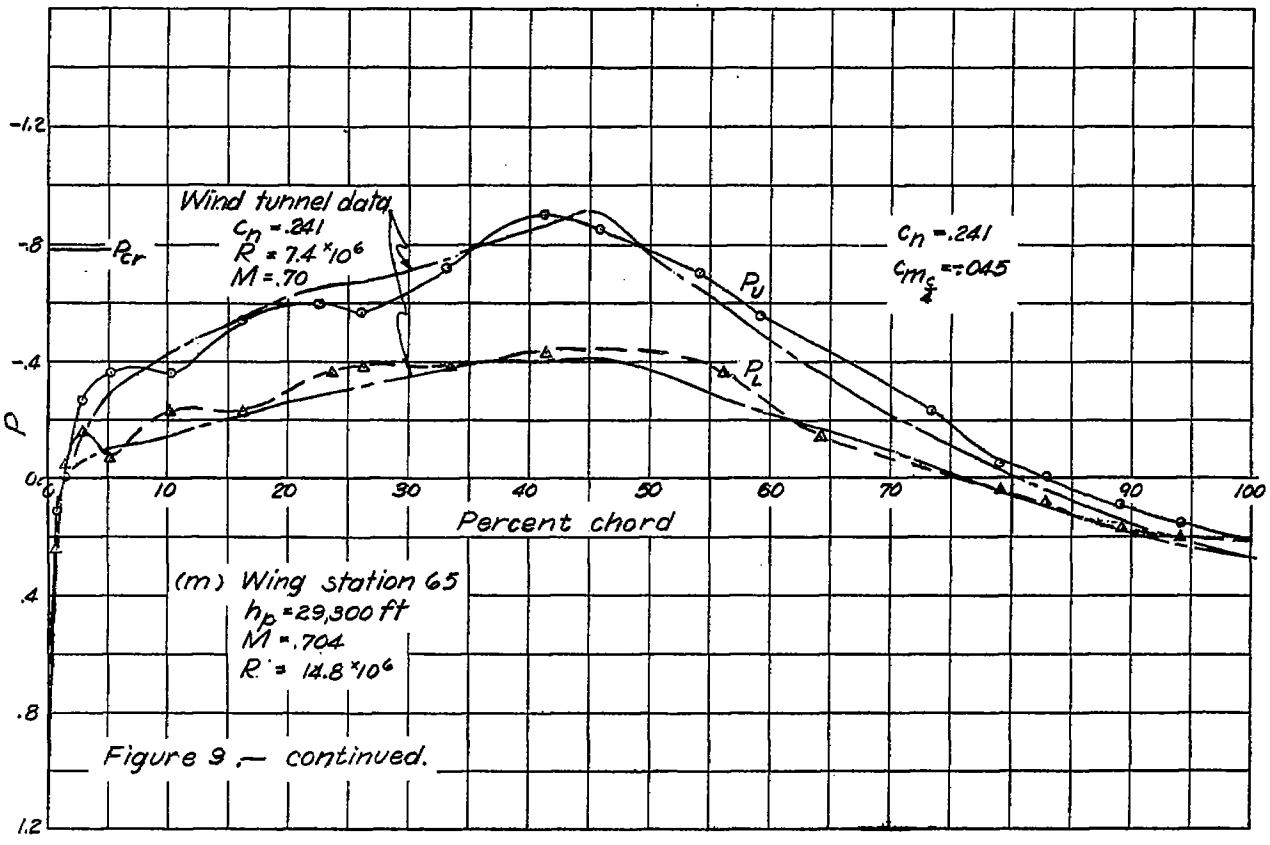

Figure 9.— continued.

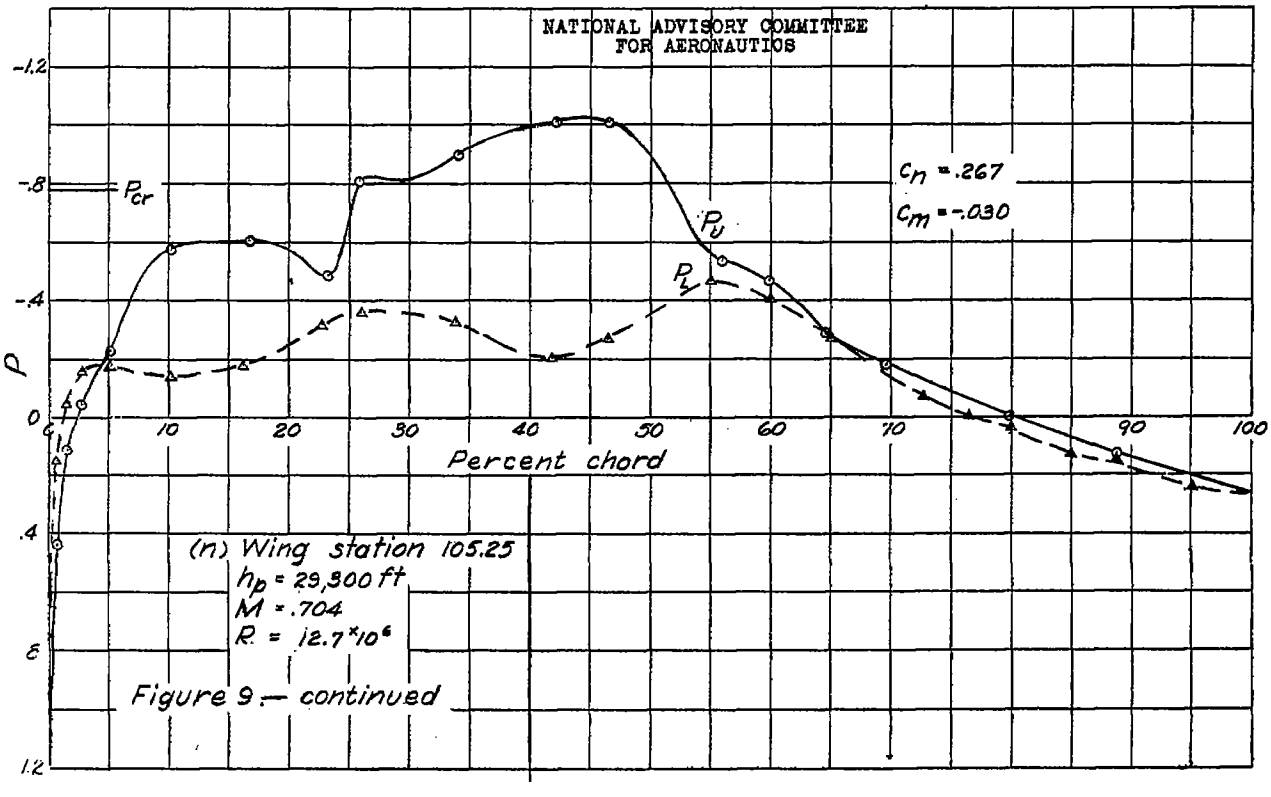

Figure 9.— continued

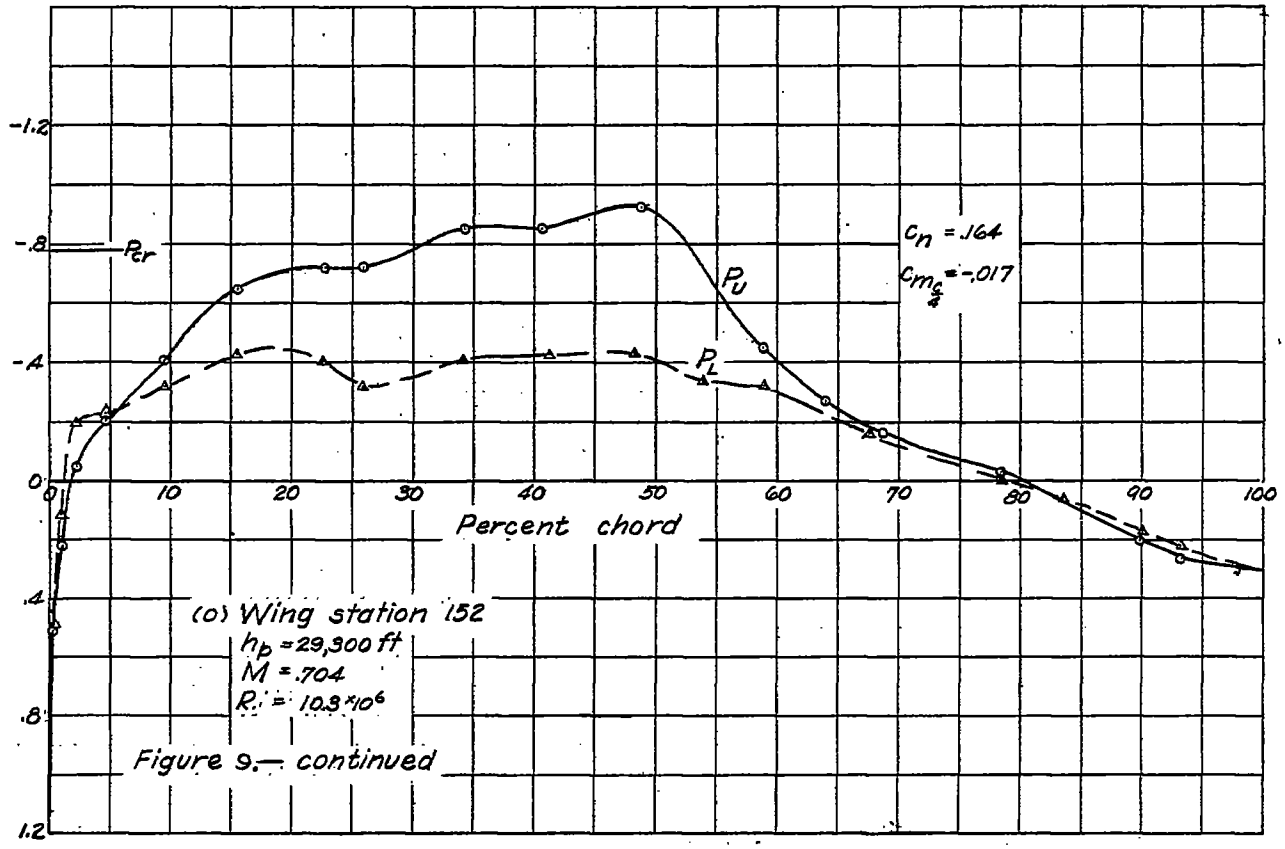

Figure 9.— continued

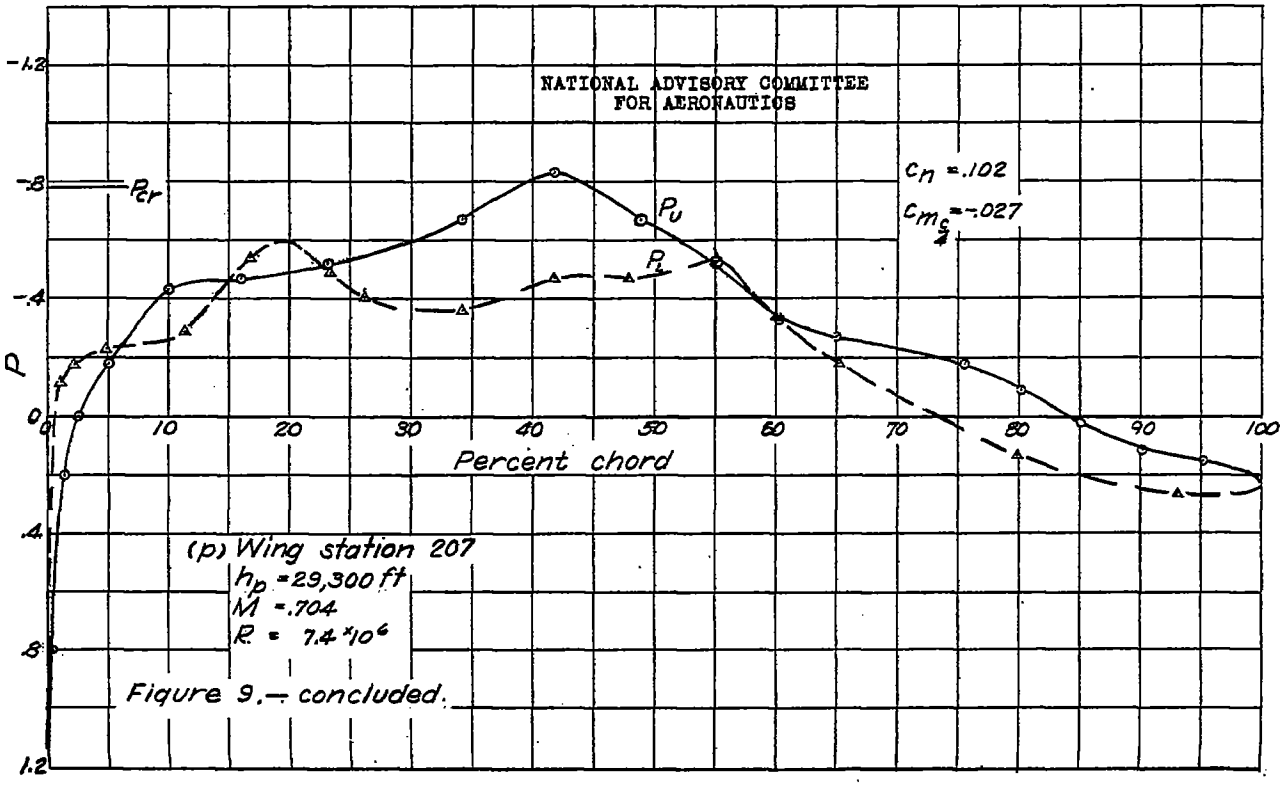

Figure 9.— concluded.

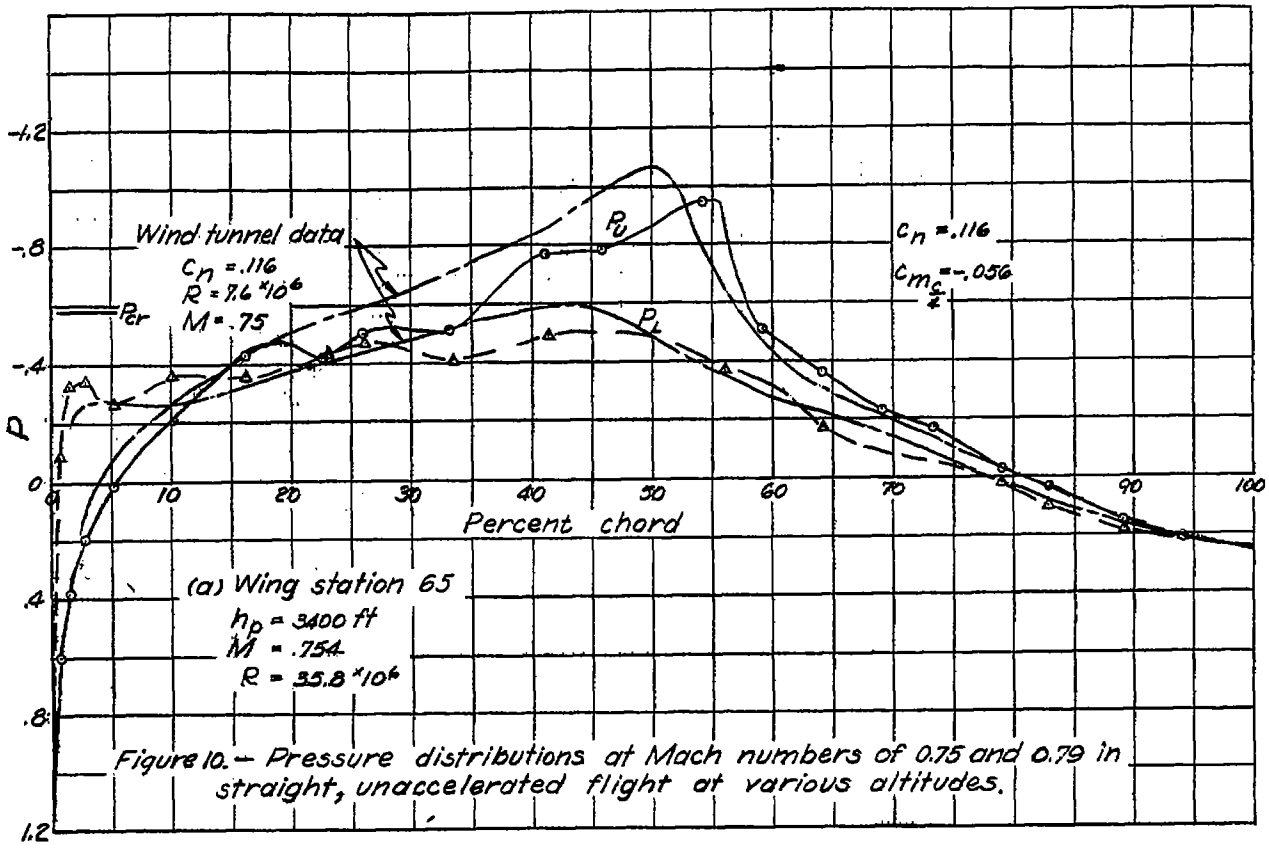

Figure 10.— Pressure distributions at Mach numbers of 0.75 and 0.79 in straight, unaccelerated flight at various altitudes.

NATIONAL ADVISORY COMMITTEE FOR AERONAUTICS

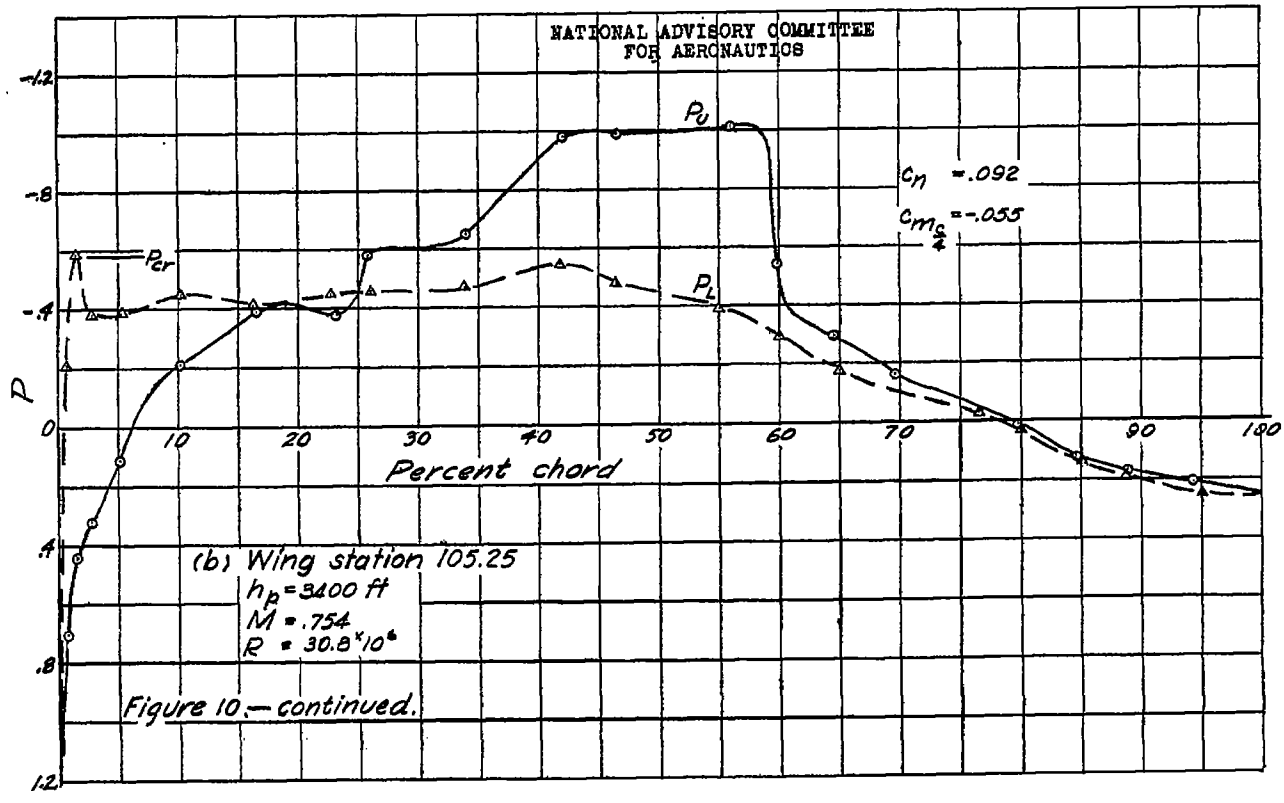

Figure 10.— continued.

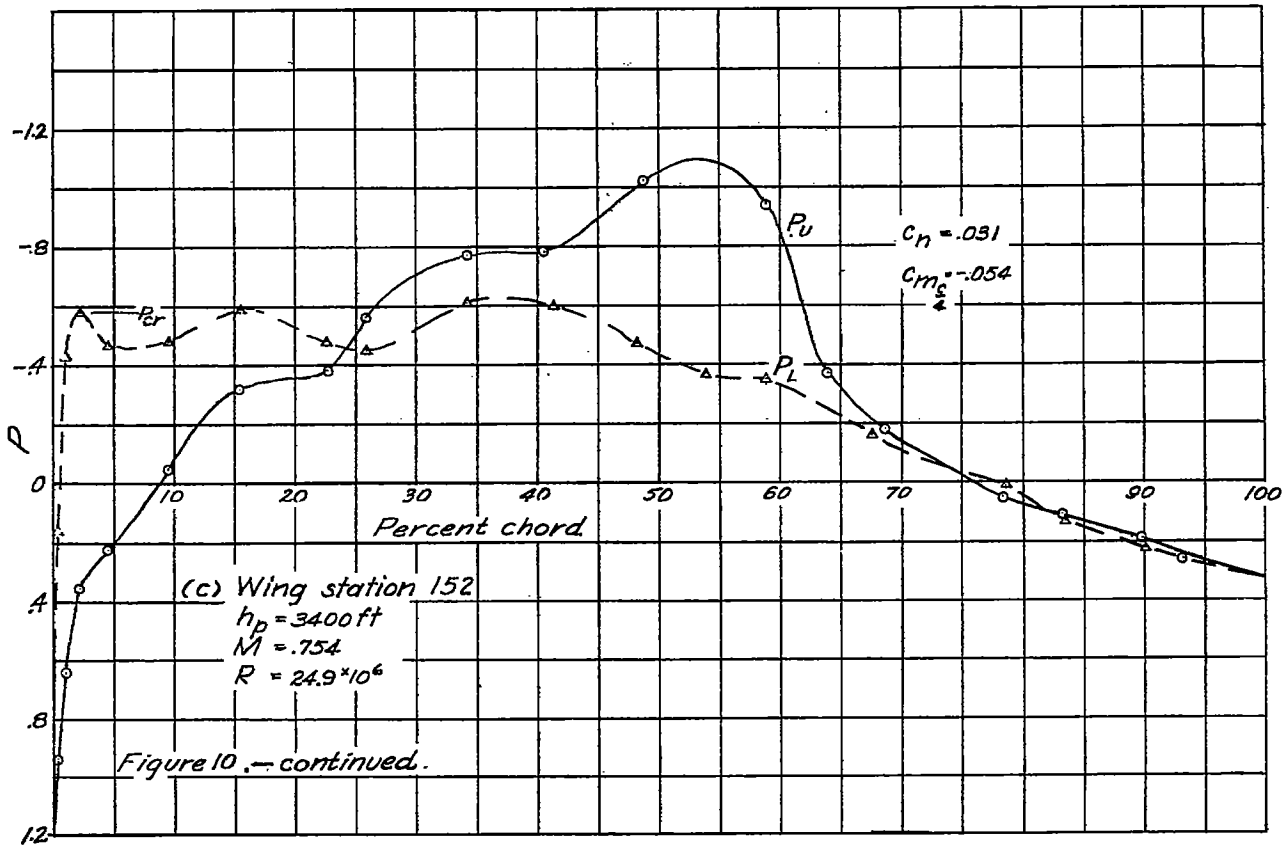

Figure 10.— continued.

NATIONAL ADVISORY COMMITTEE
FOR AERONAUTICS

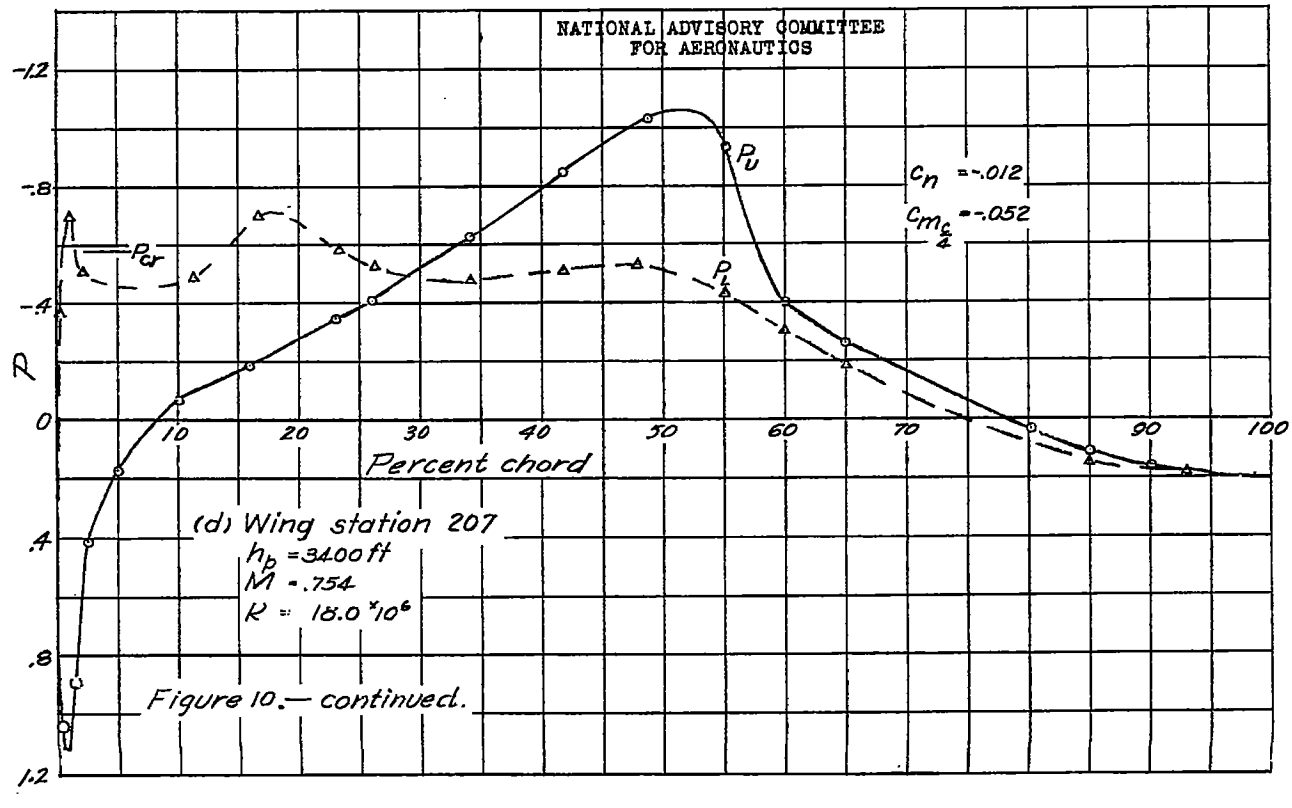

Figure 10.— continued.

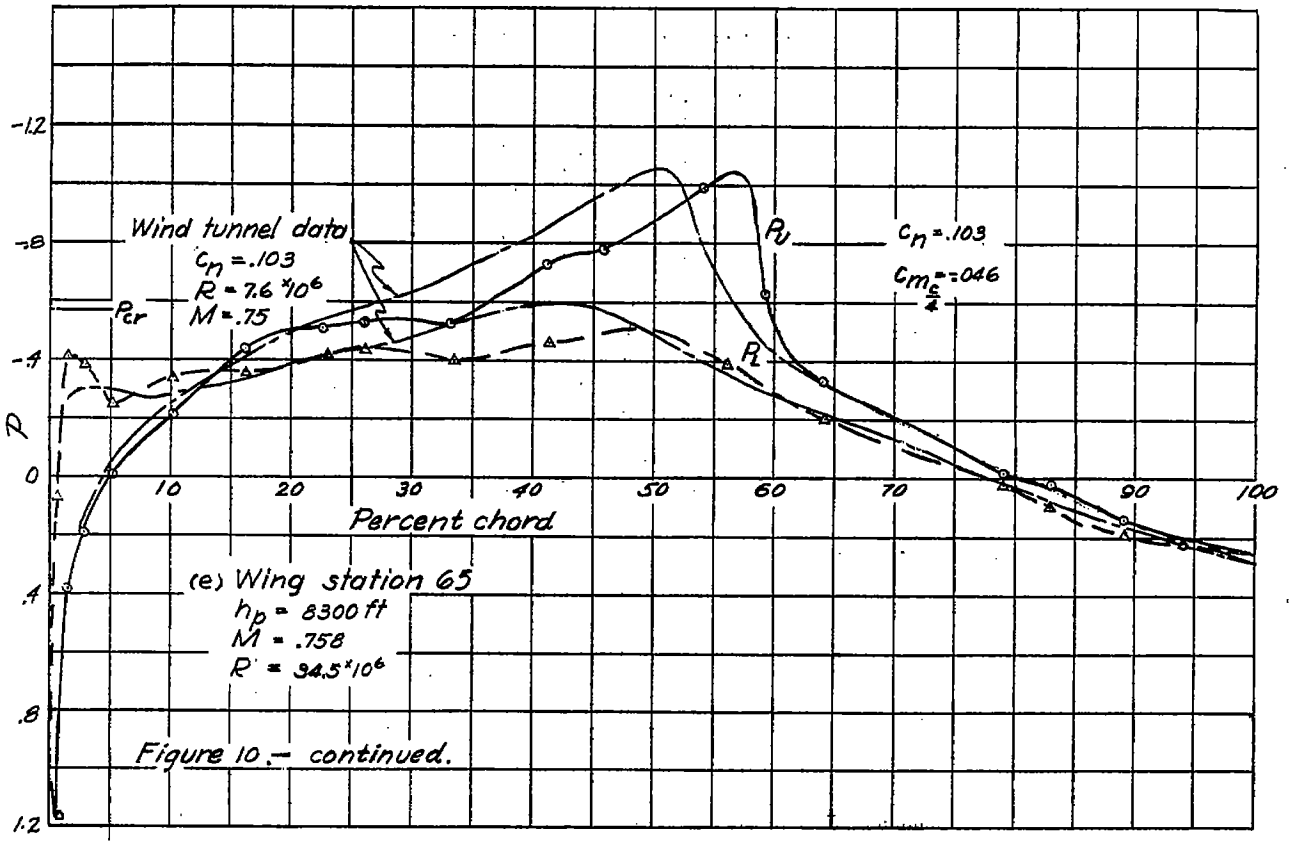

Figure 10.- continued.

NATIONAL ADVISORY COMMITTEE
FOR AERONAUTICS

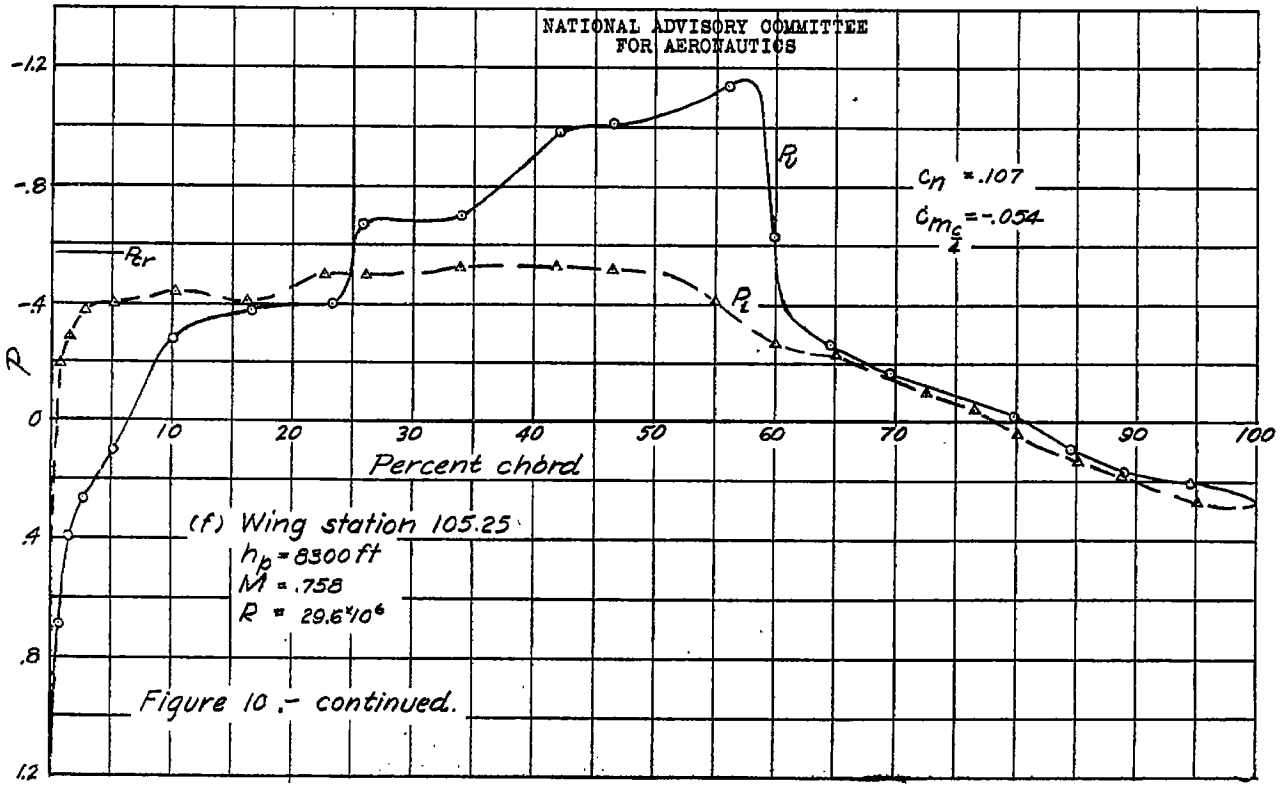

Figure 10.- continued.

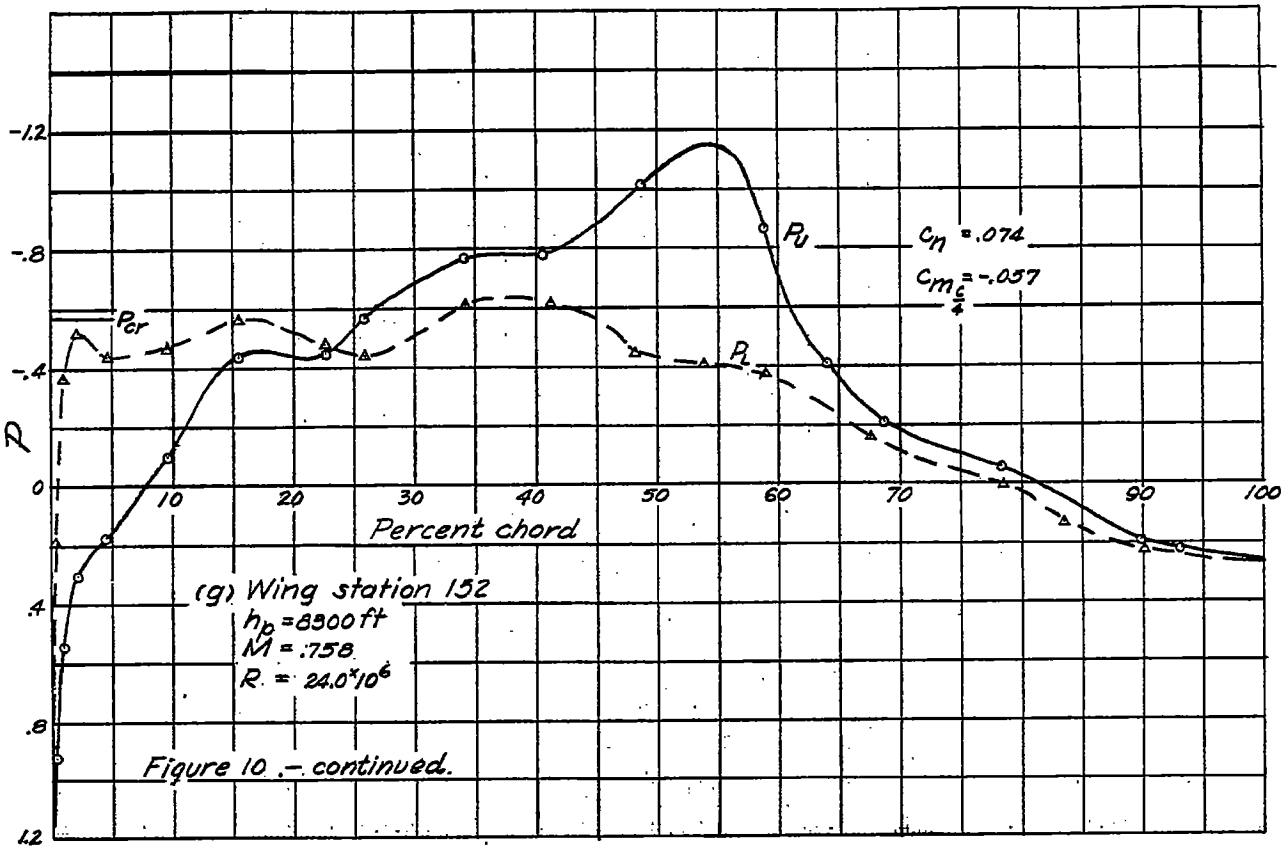

Figure 10.- continued.

NATIONAL ADVISORY COMMITTEE
FOR AERONAUTICS

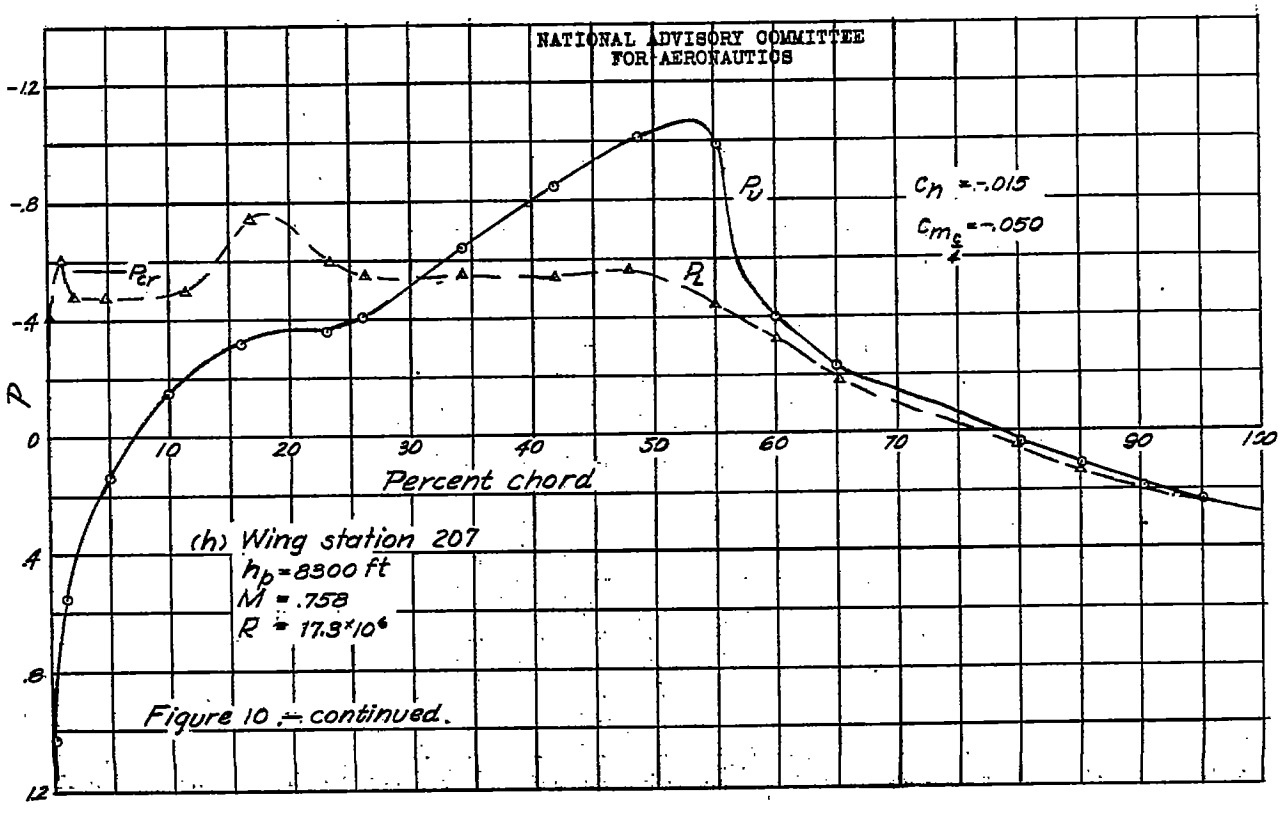

Figure 10.- continued.

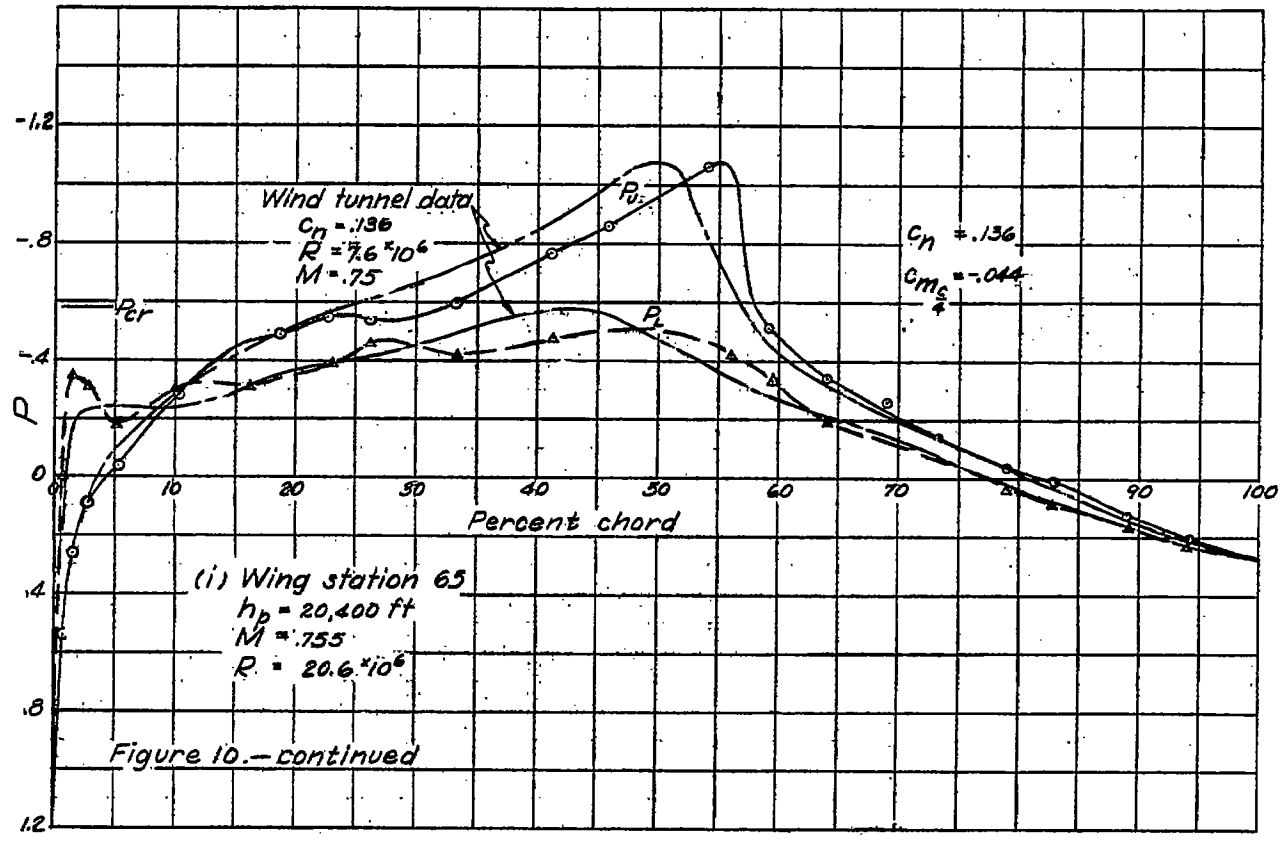

Figure 10.— continued

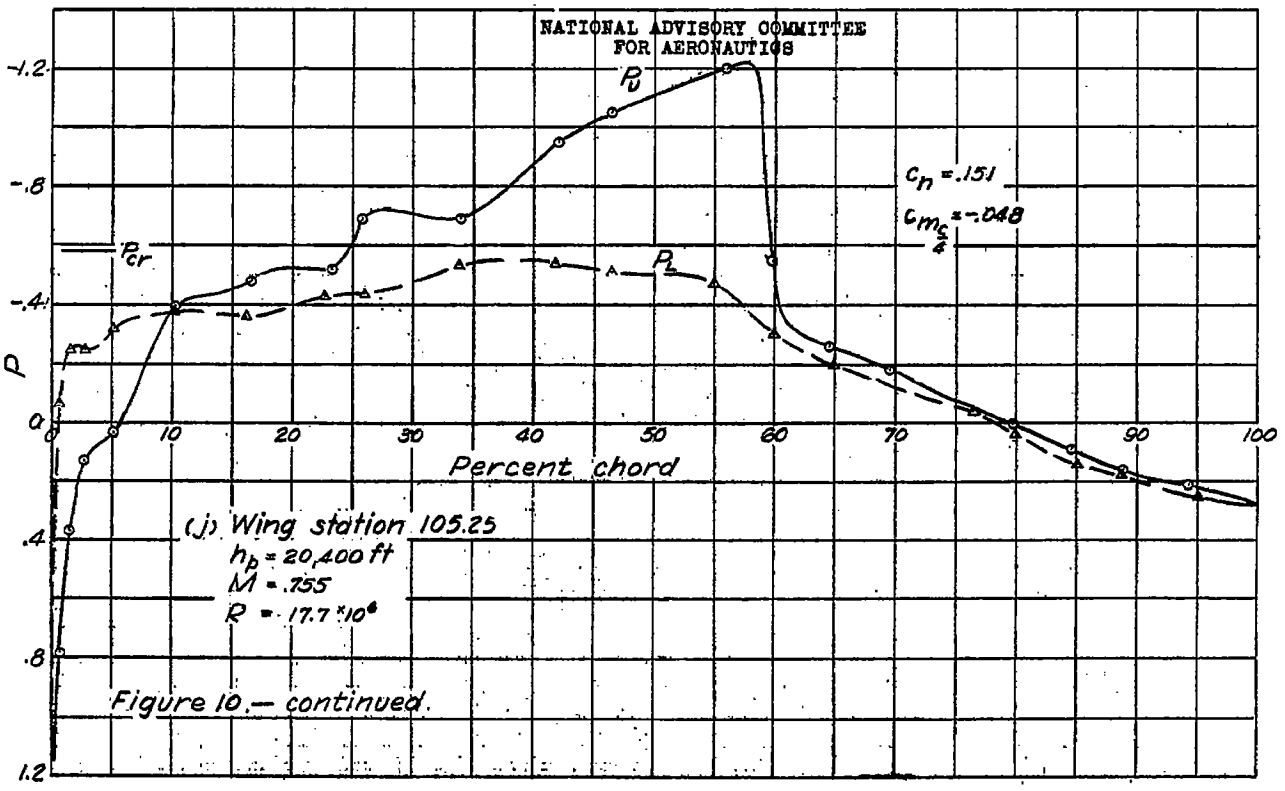

Figure 10.— continued.

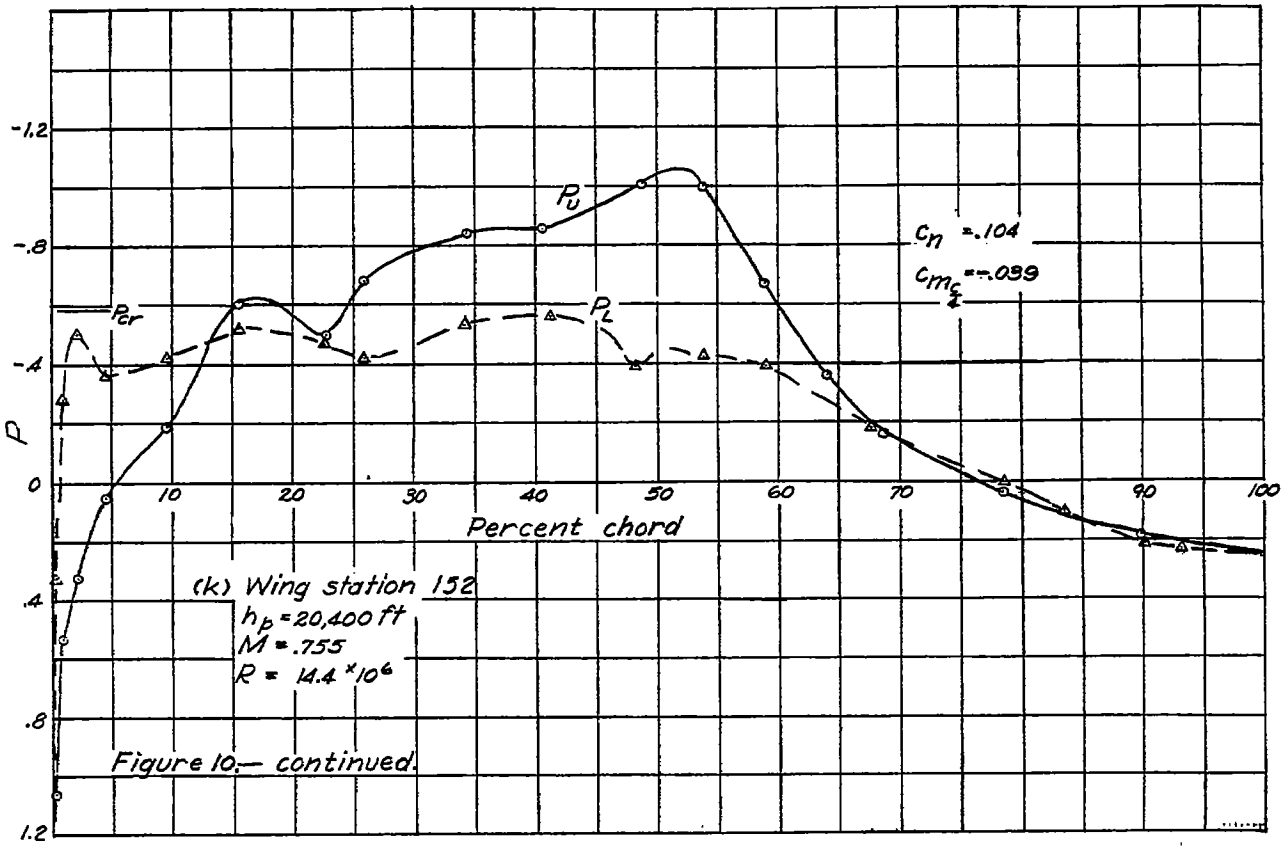

Figure 10.— continued.

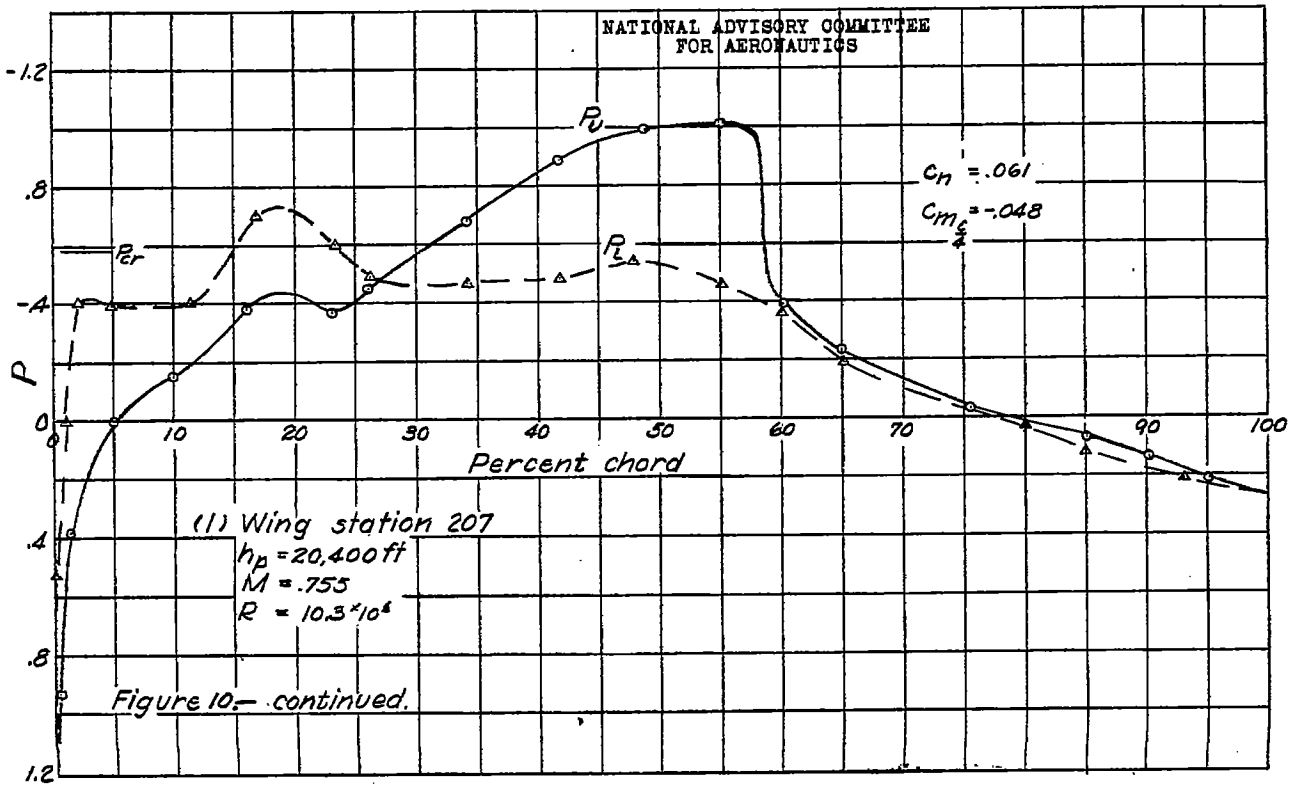

Figure 10.— continued.

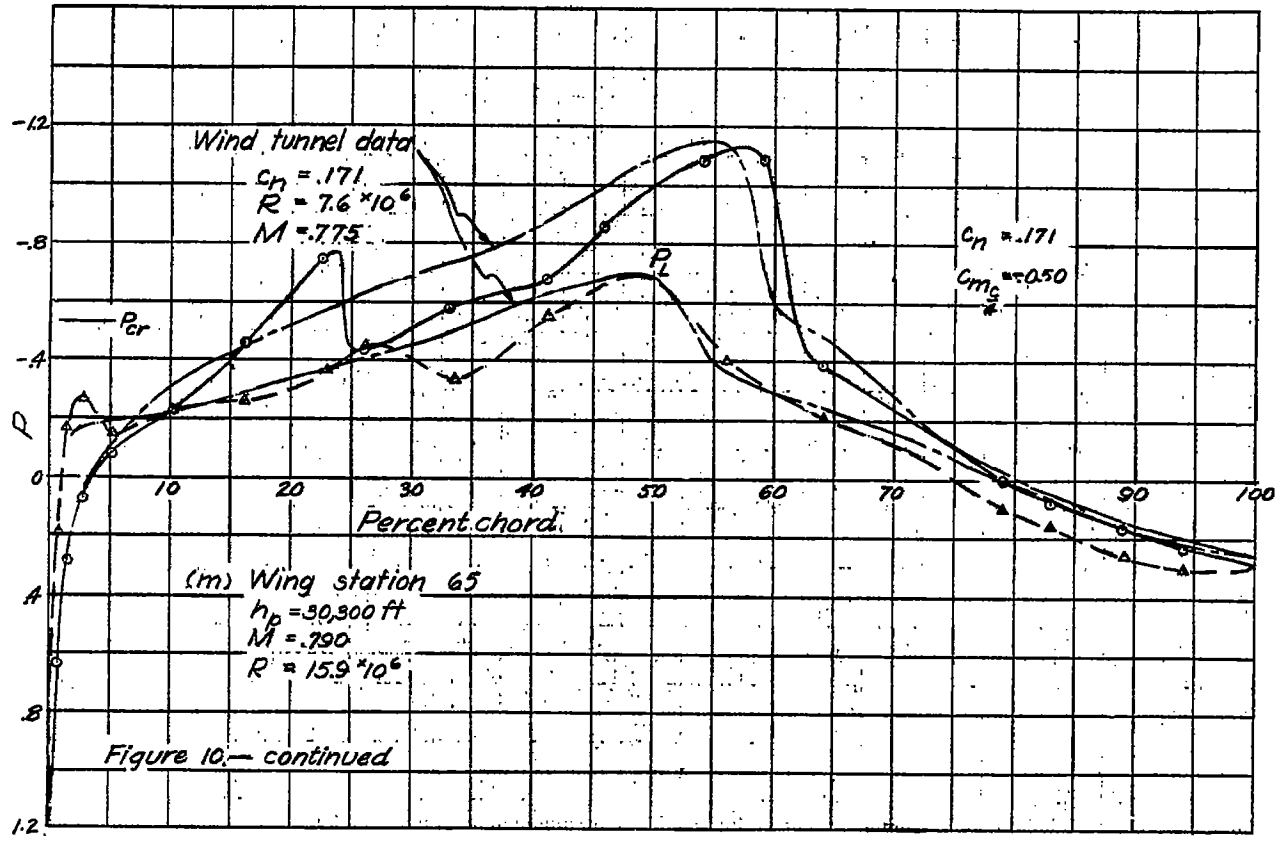

Figure 10.— continued

NATIONAL ADVISORY COMMITTEE
FOR AERONAUTICS

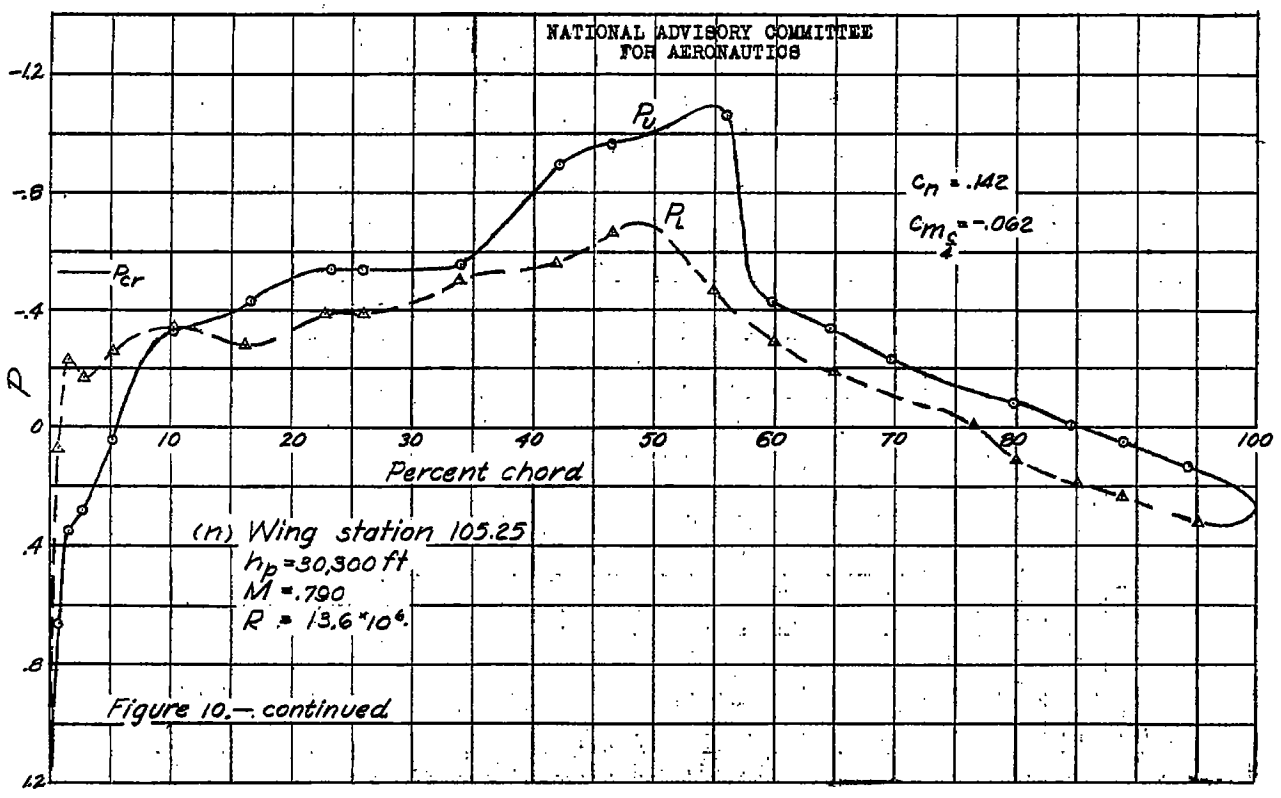

Figure 10.— continued

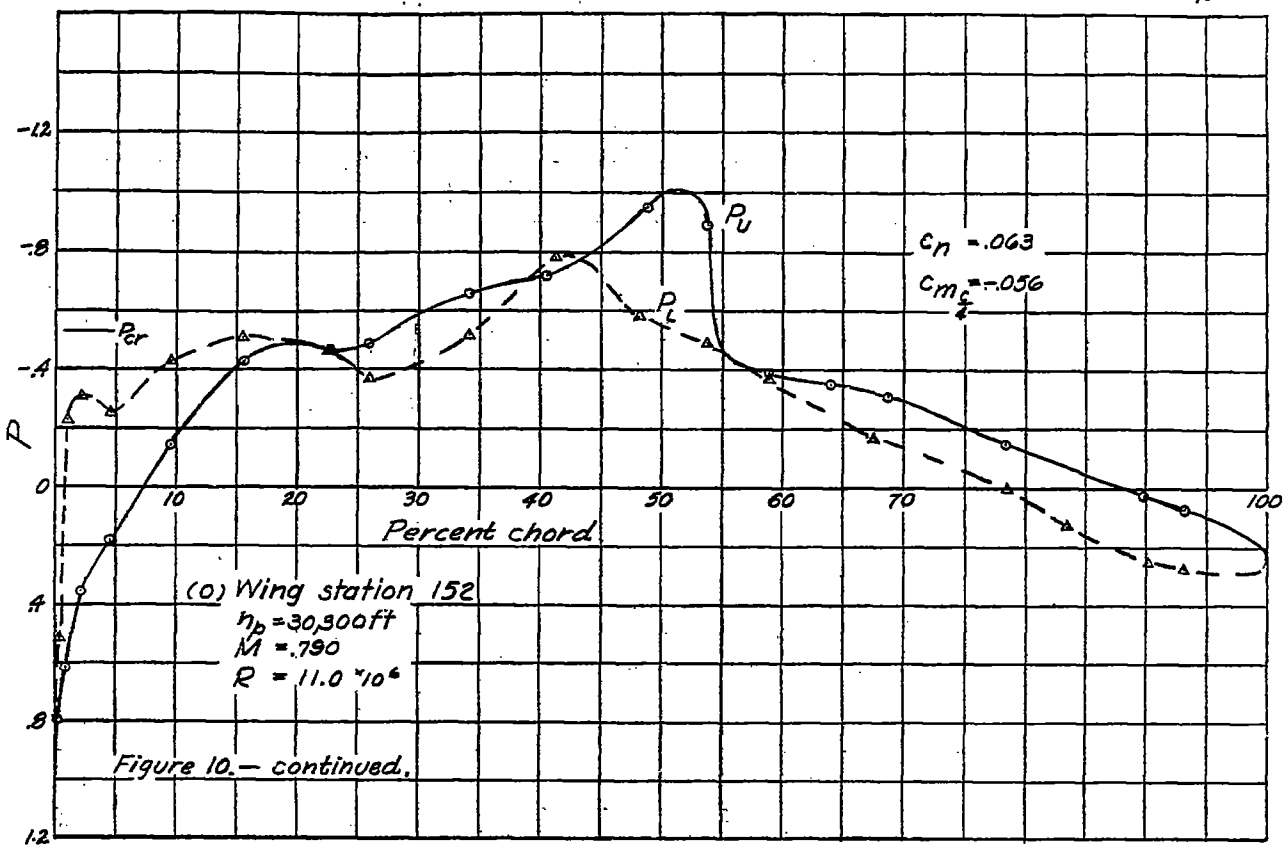

Figure 10.— continued.

NATIONAL ADVISORY COMMITTEE
FOR AERONAUTICS

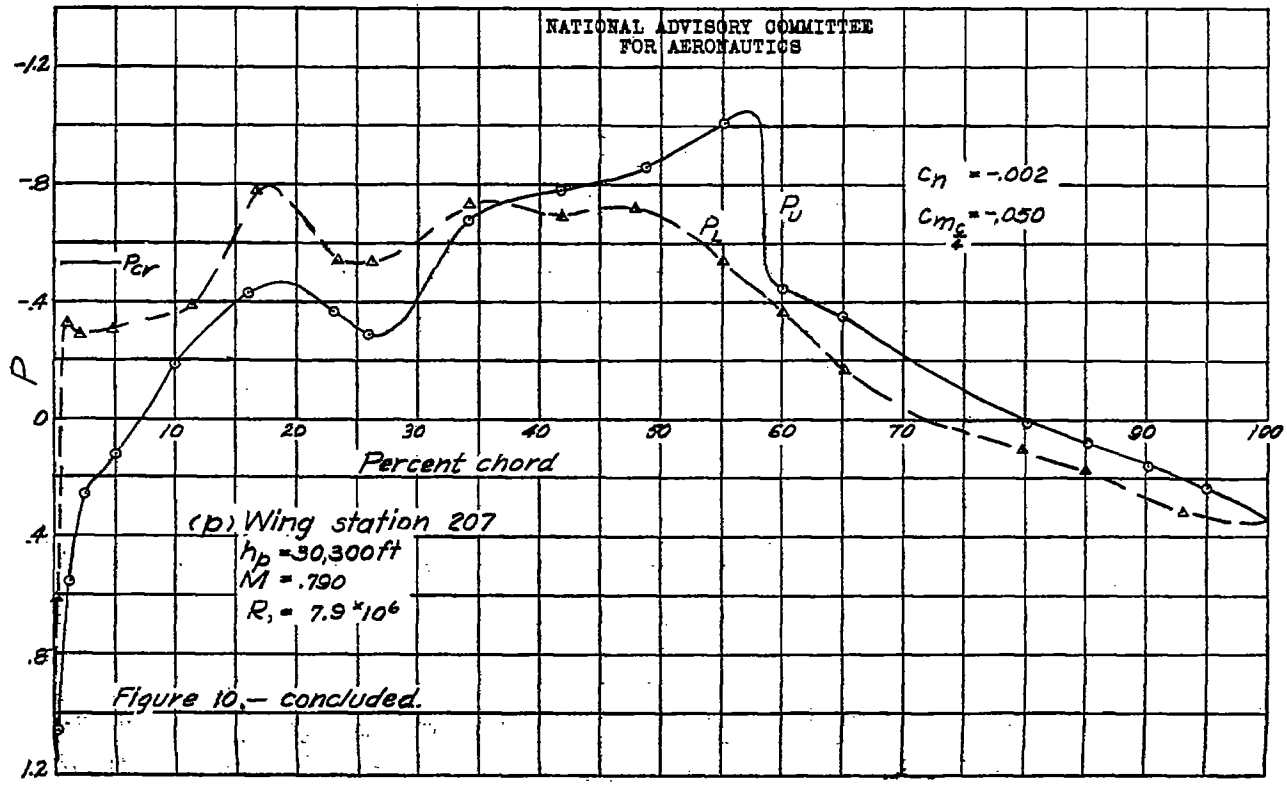

Figure 10.— concluded.

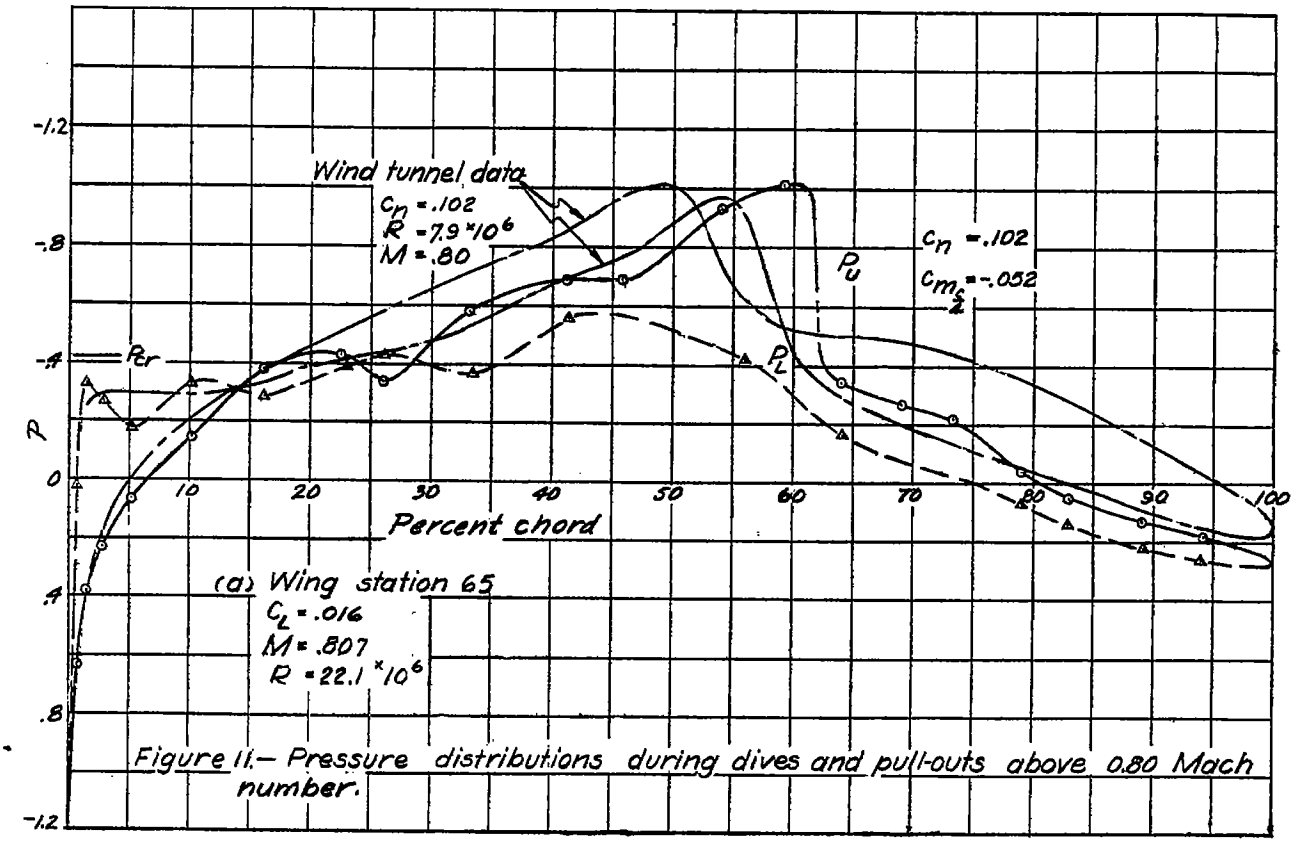

Figure 11.– Pressure distributions during dives and pull-outs above 0.80 Mach number.

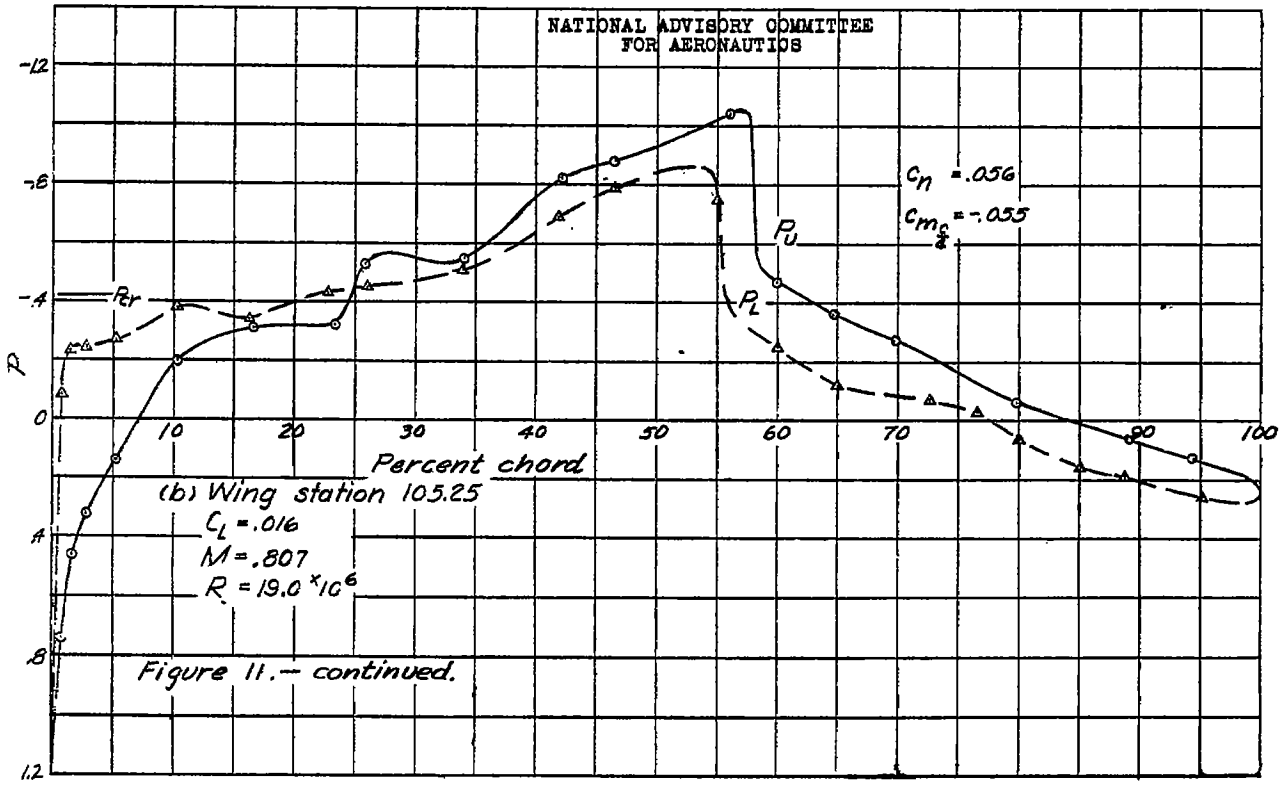

Figure 11.– continued.

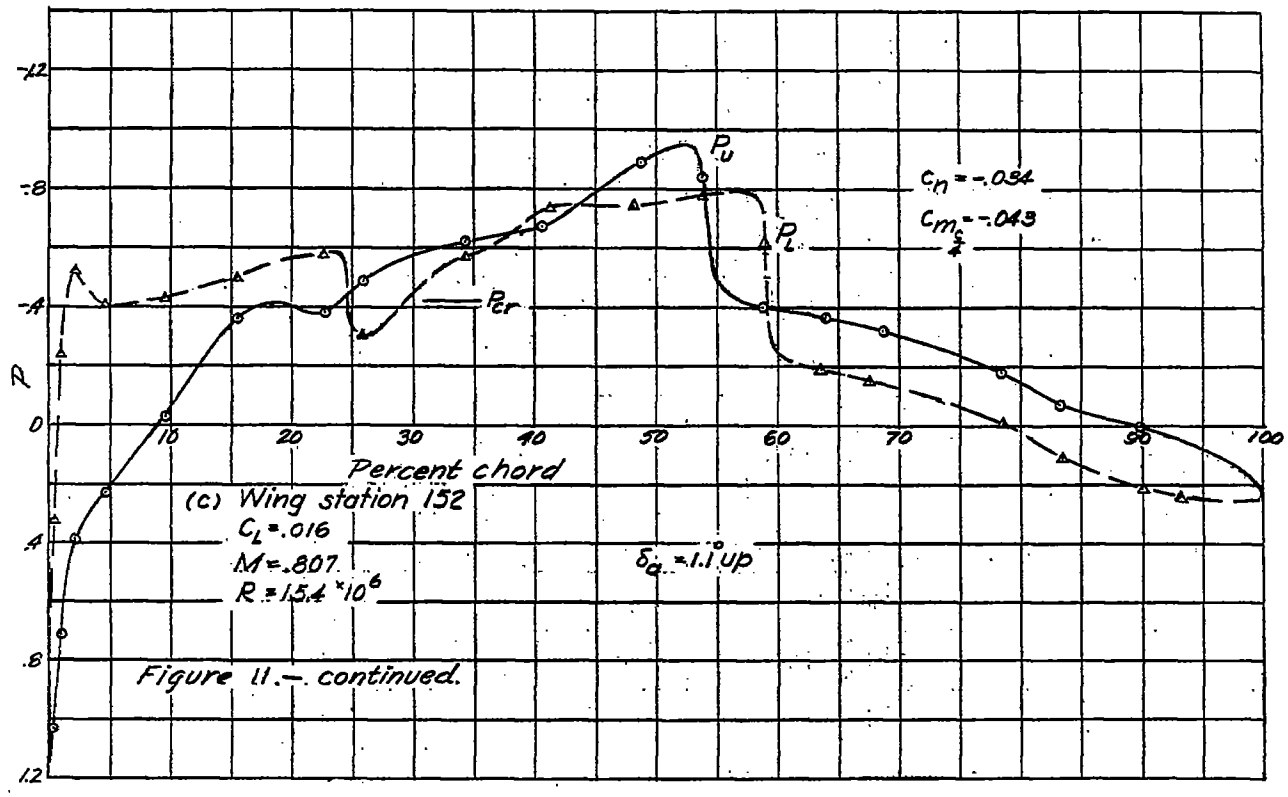

Figure 11.—continued.

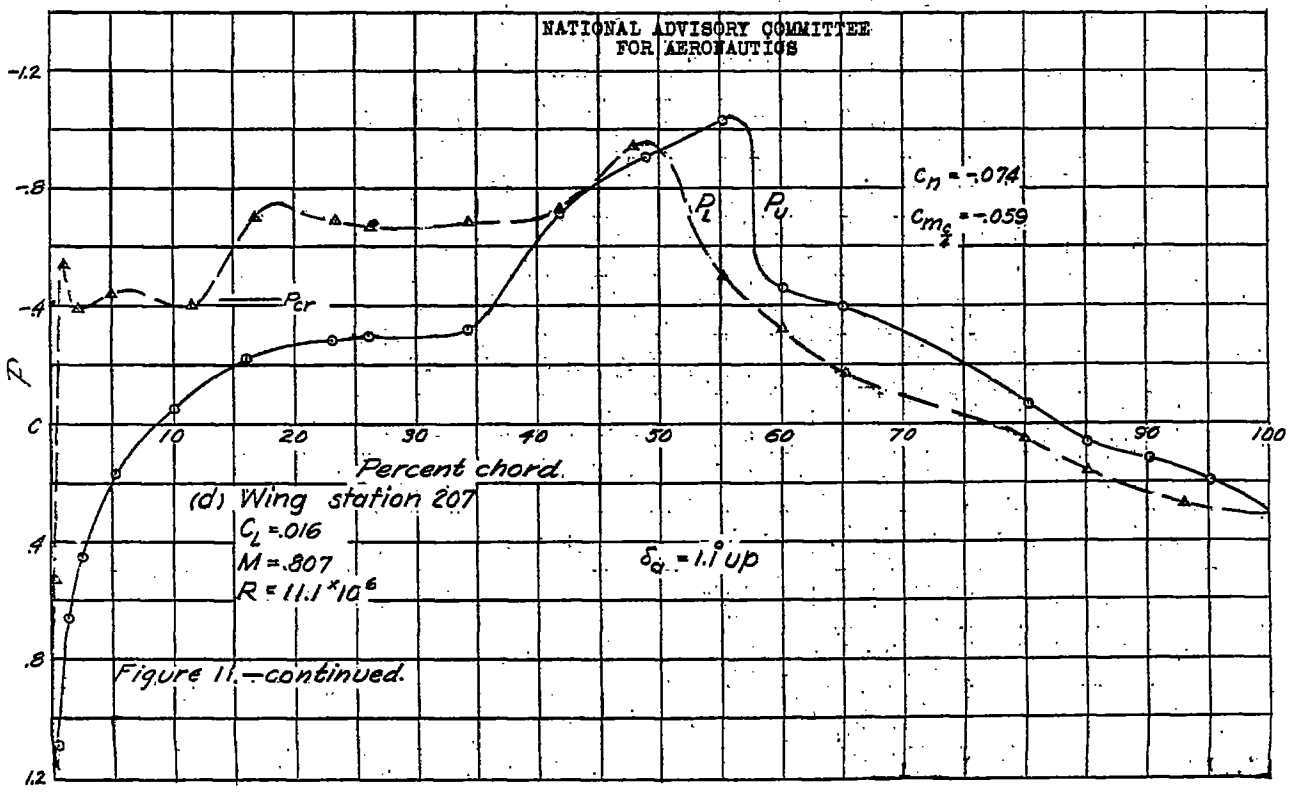

Figure 11.—continued.

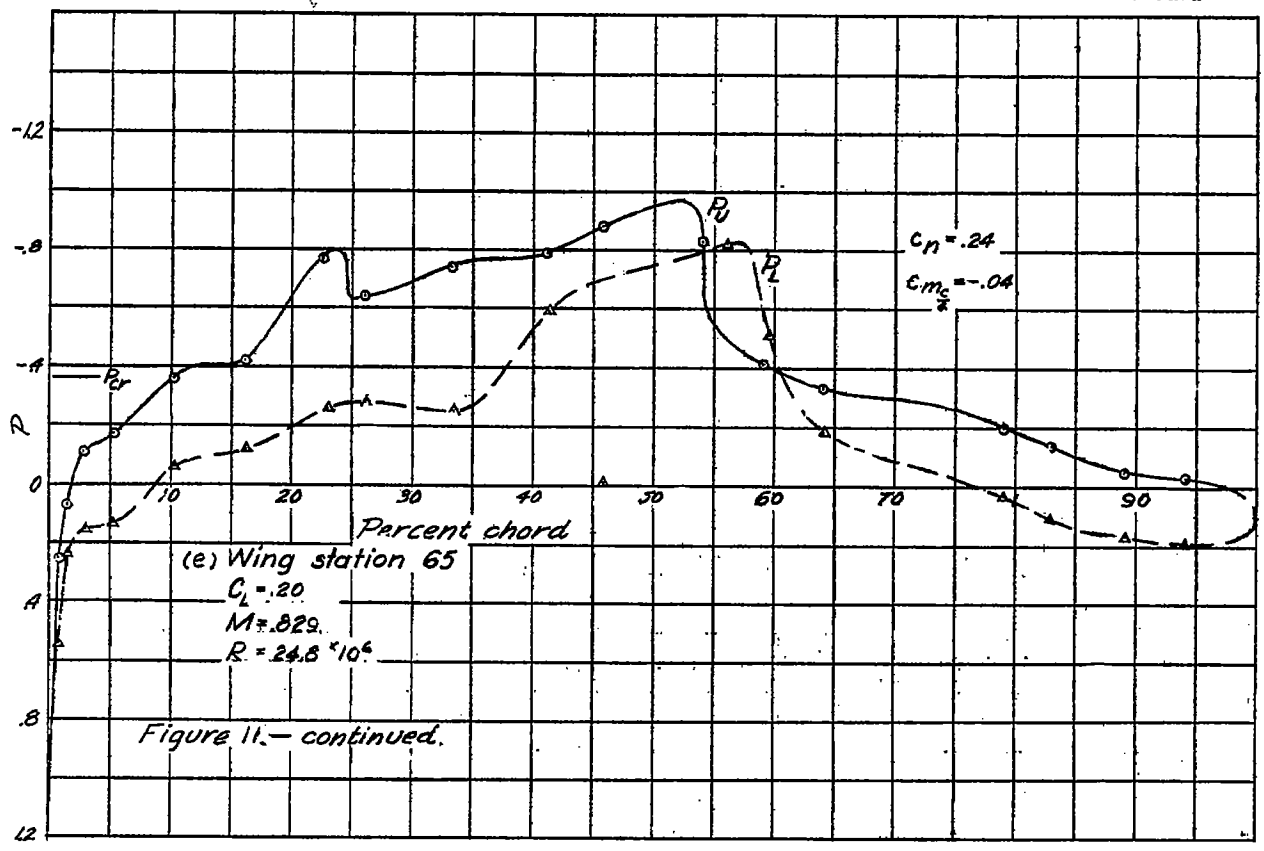

Figure 11.— continued.

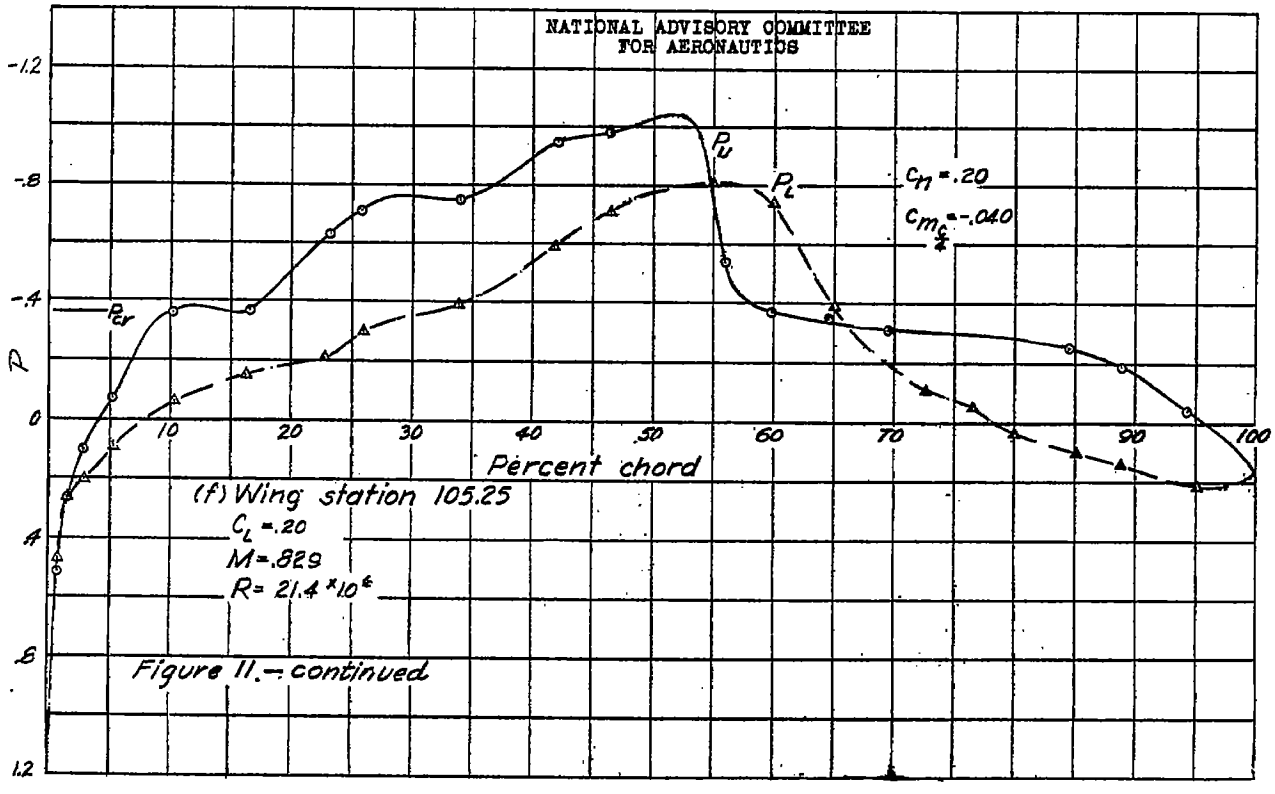

Figure 11.— continued.

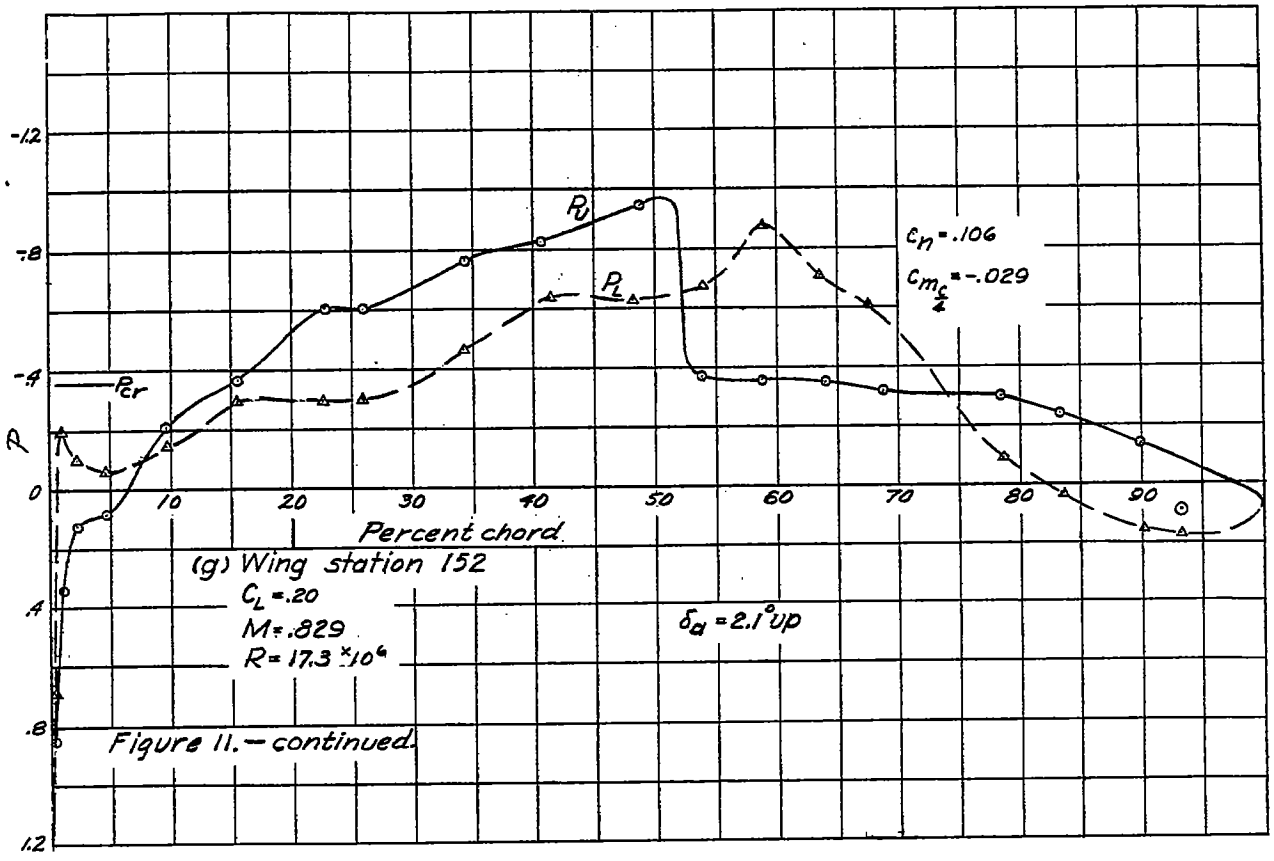

Figure 11.— continued.

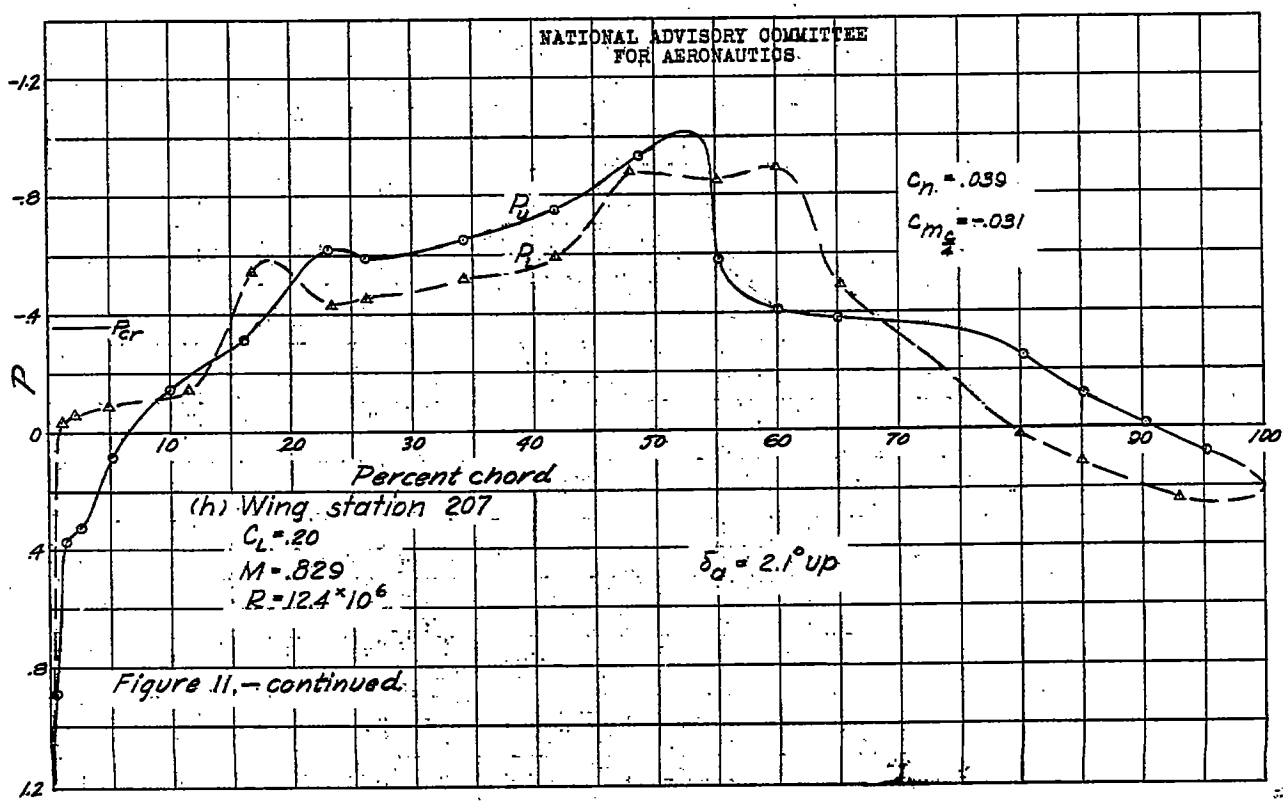

Figure 11.— continued.

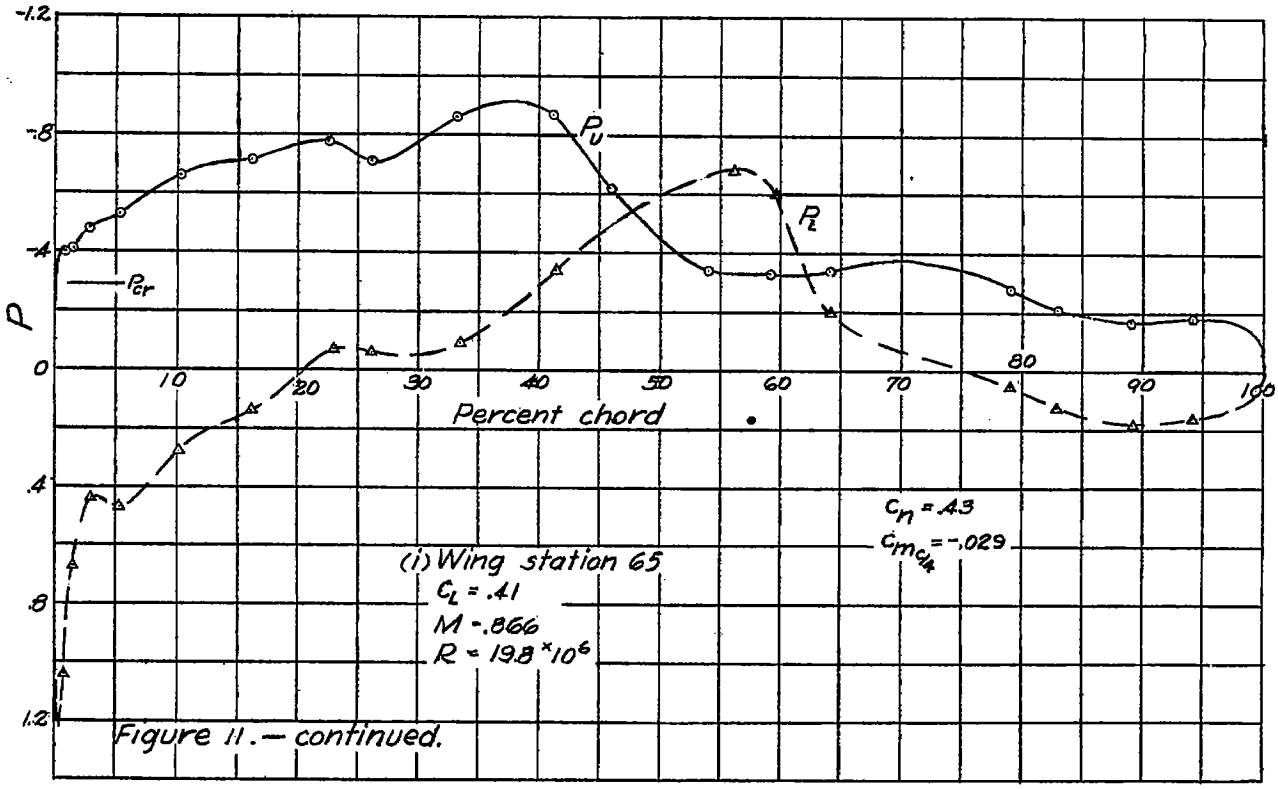

Figure 11.— continued.

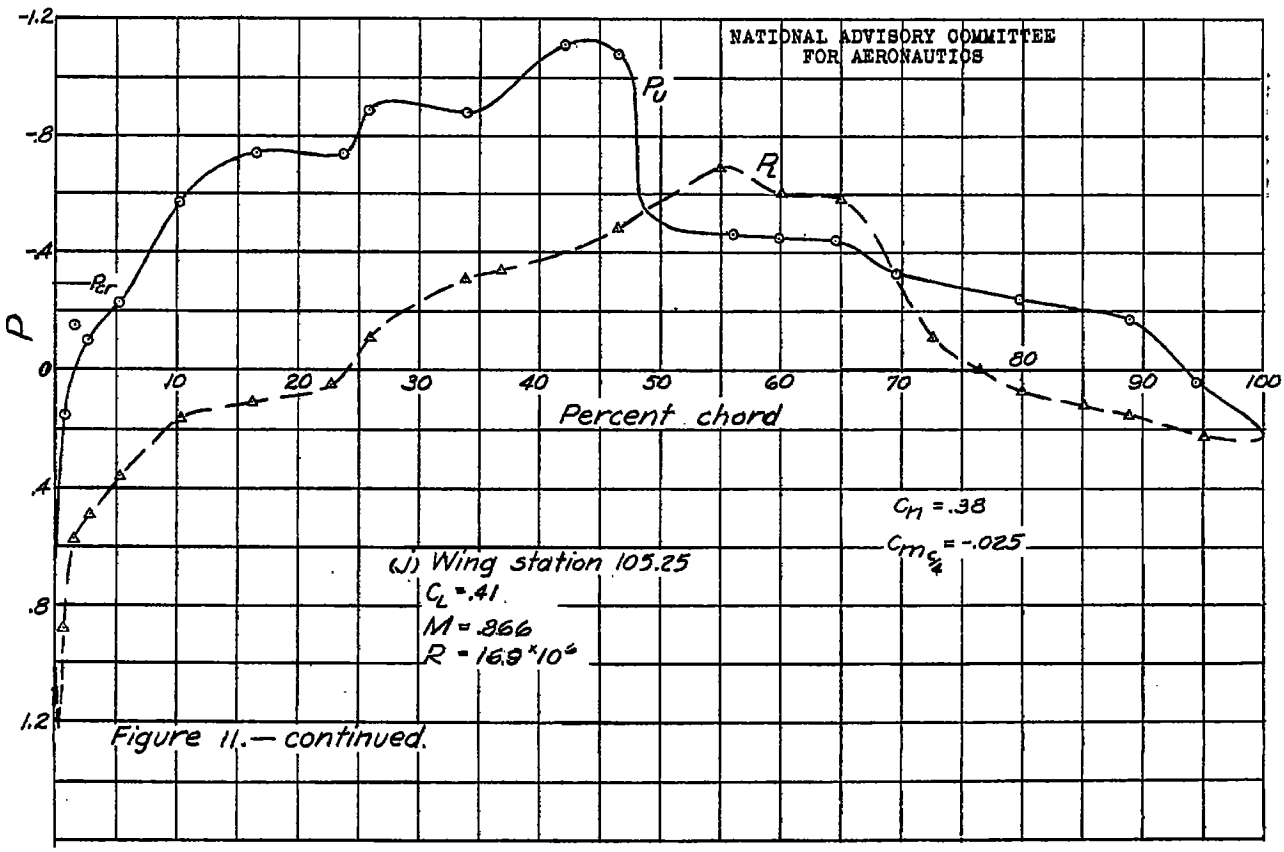

Figure 11.— continued.

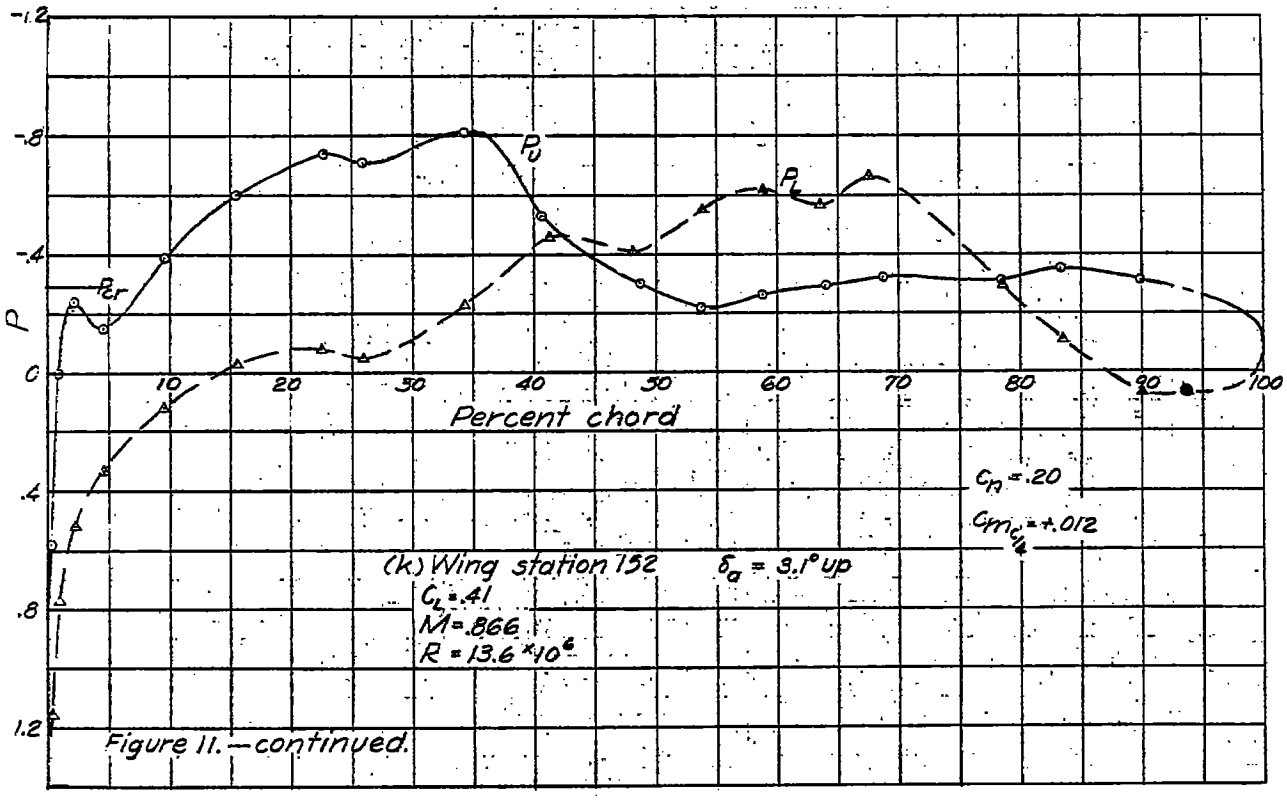

Figure 11.—continued.

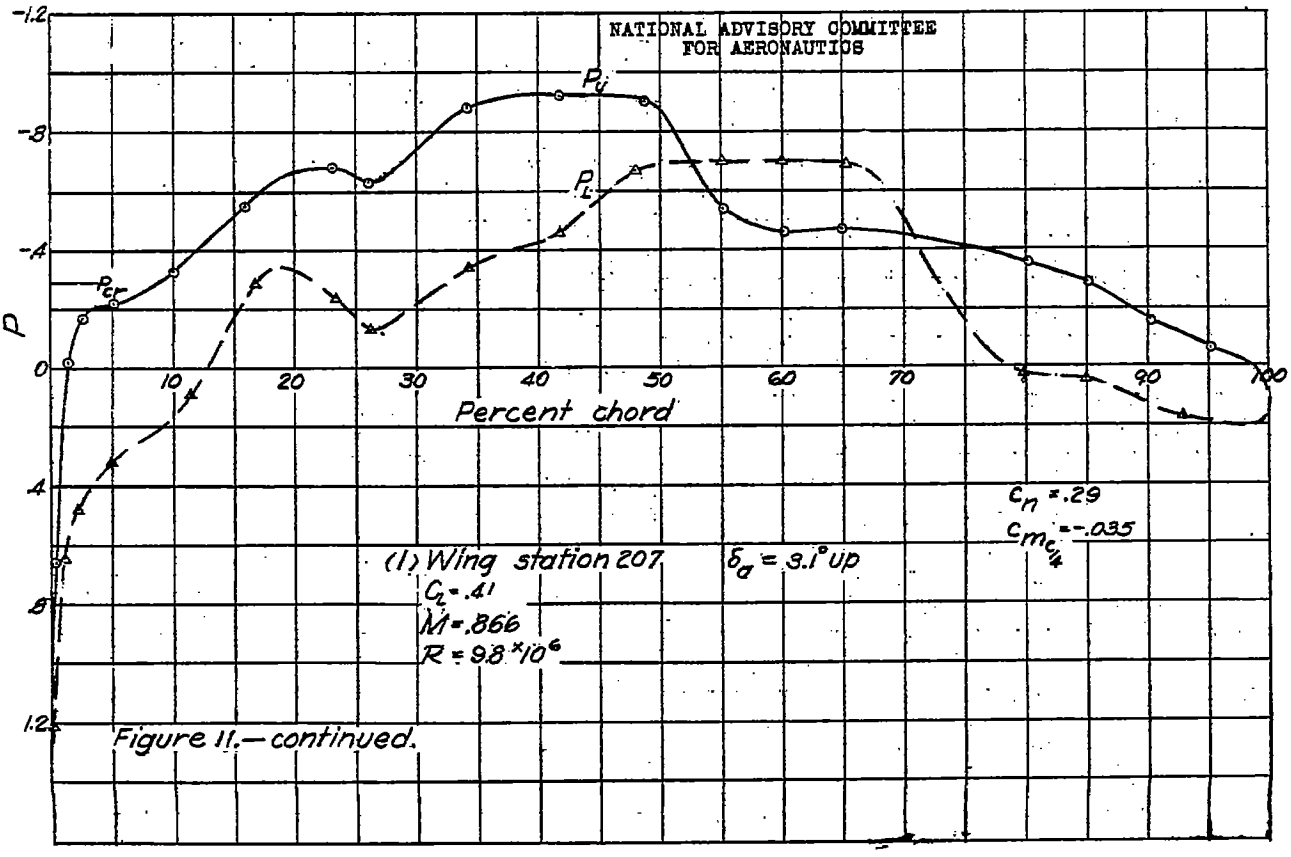

Figure 11.—continued.

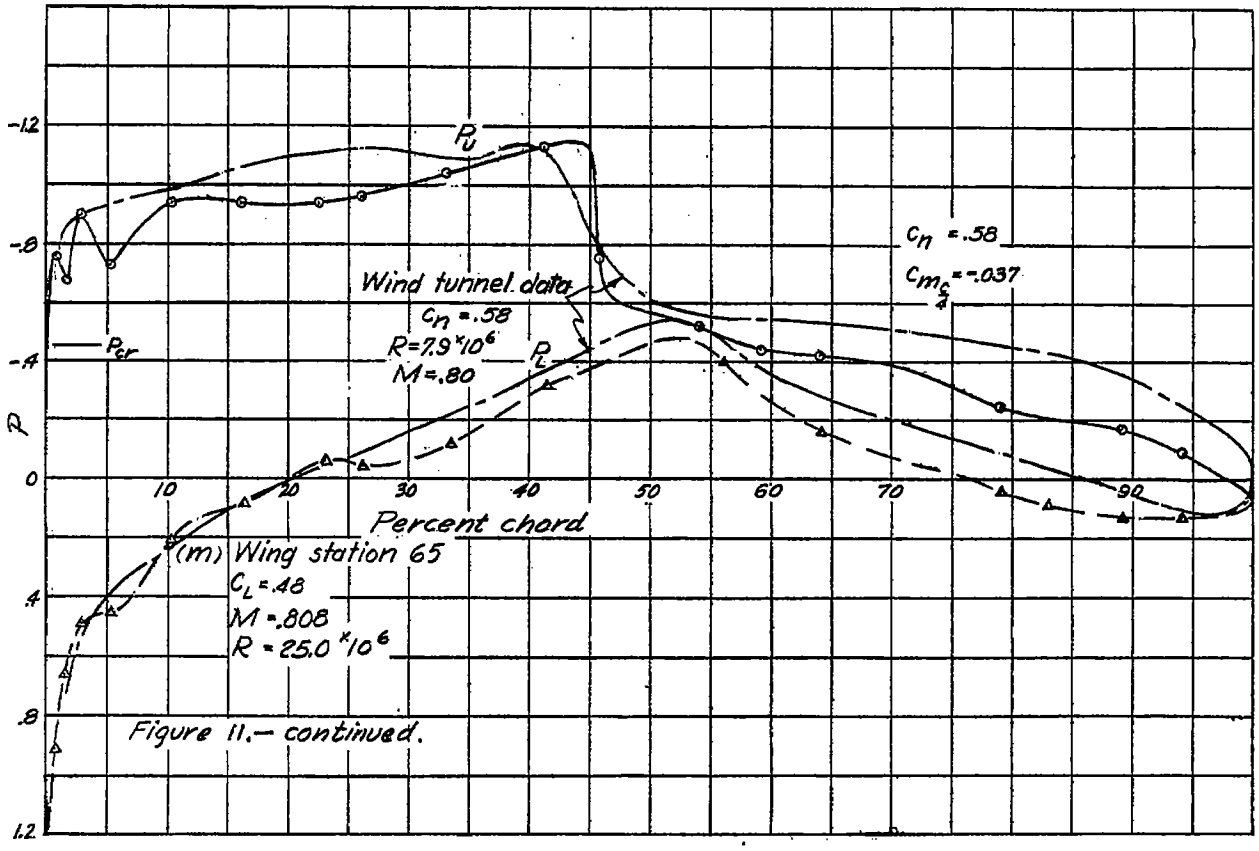

Figure 11.— continued.

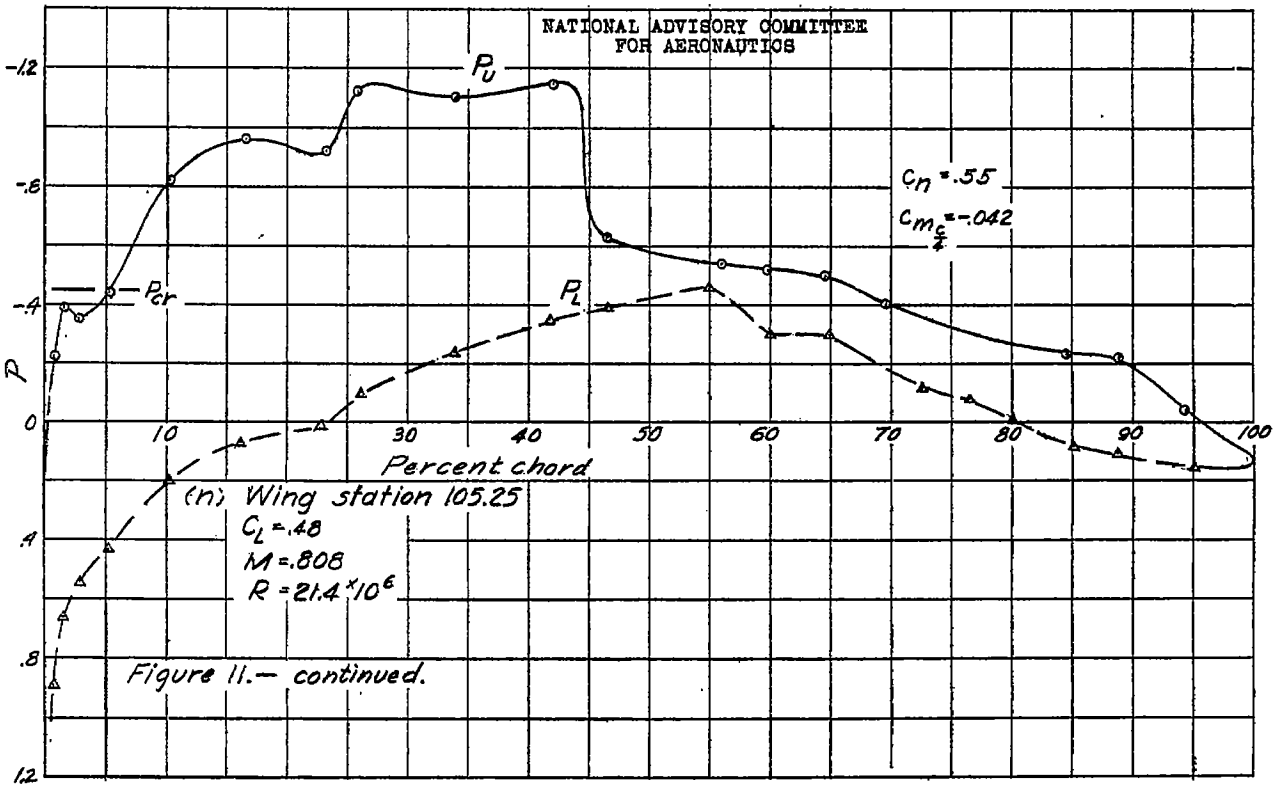

Figure 11.— continued.

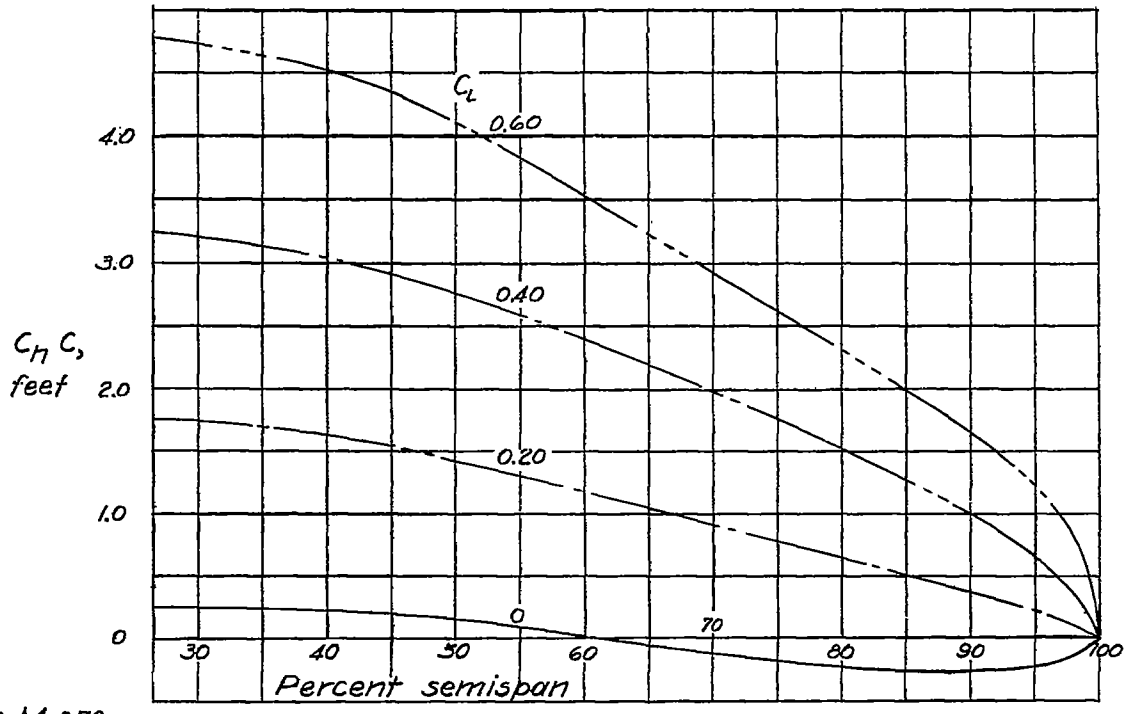

(b) M=0.70

Figure 13.— continued.

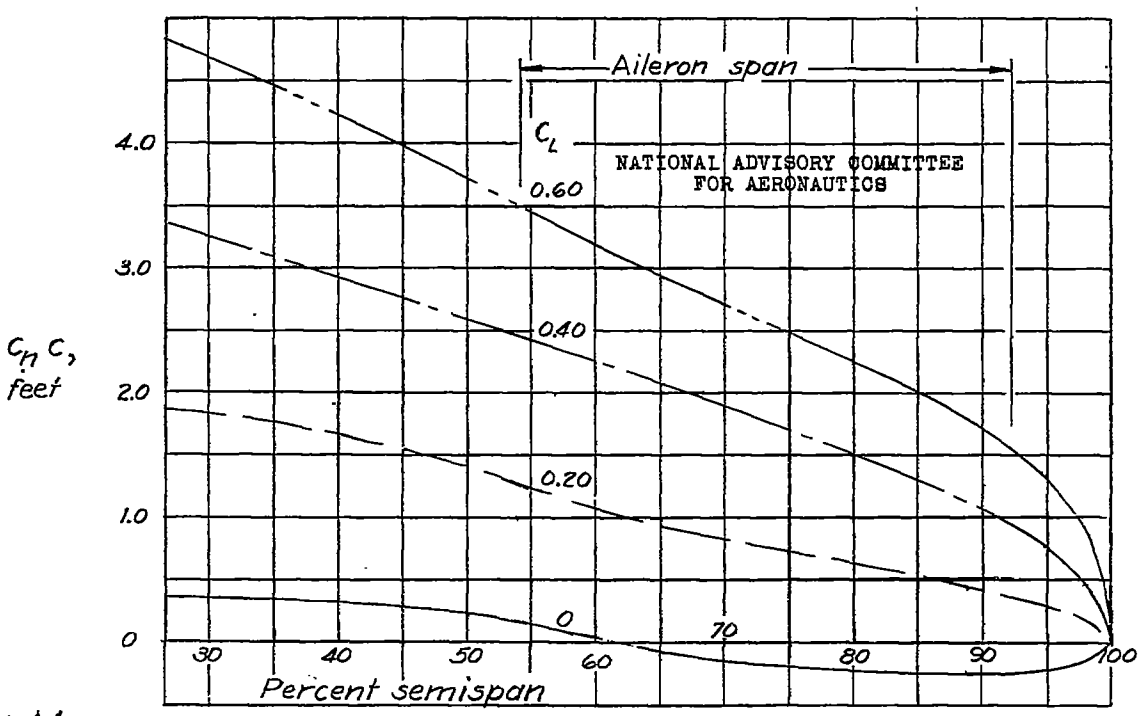

(c) M=0.75

Figure 13.— continued.

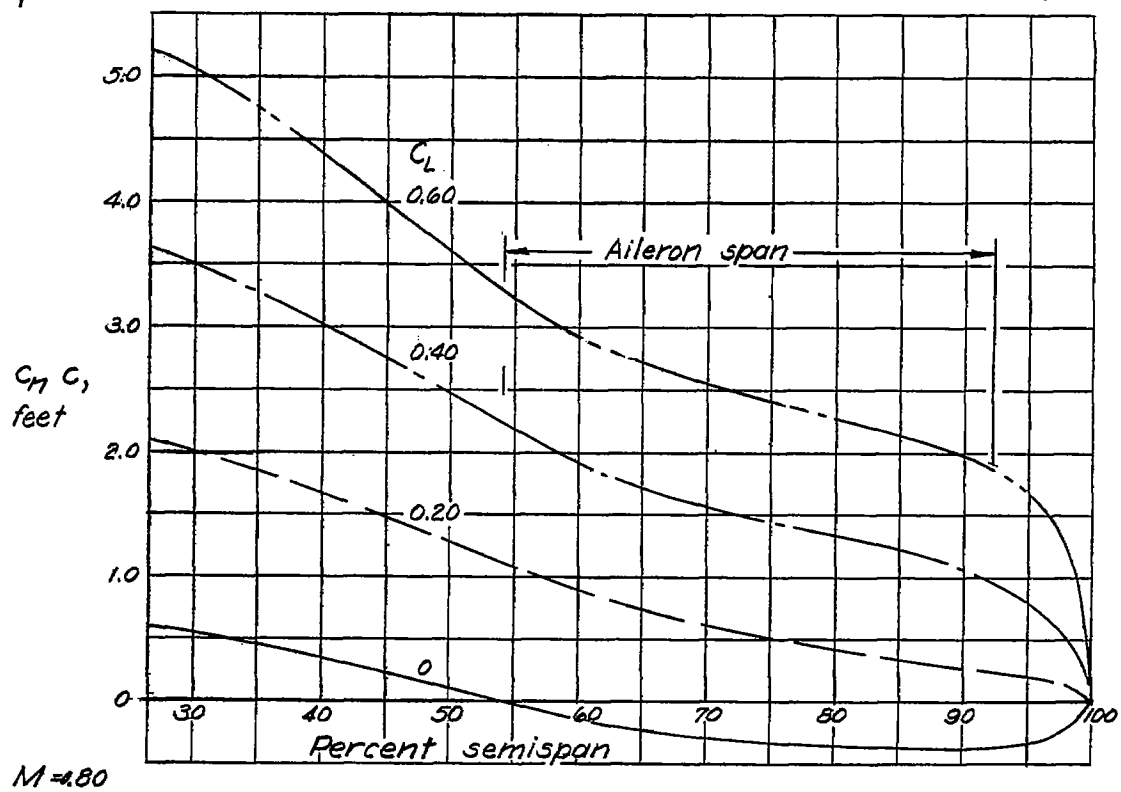

(d) M = 0.80

Figure 13.— continued.

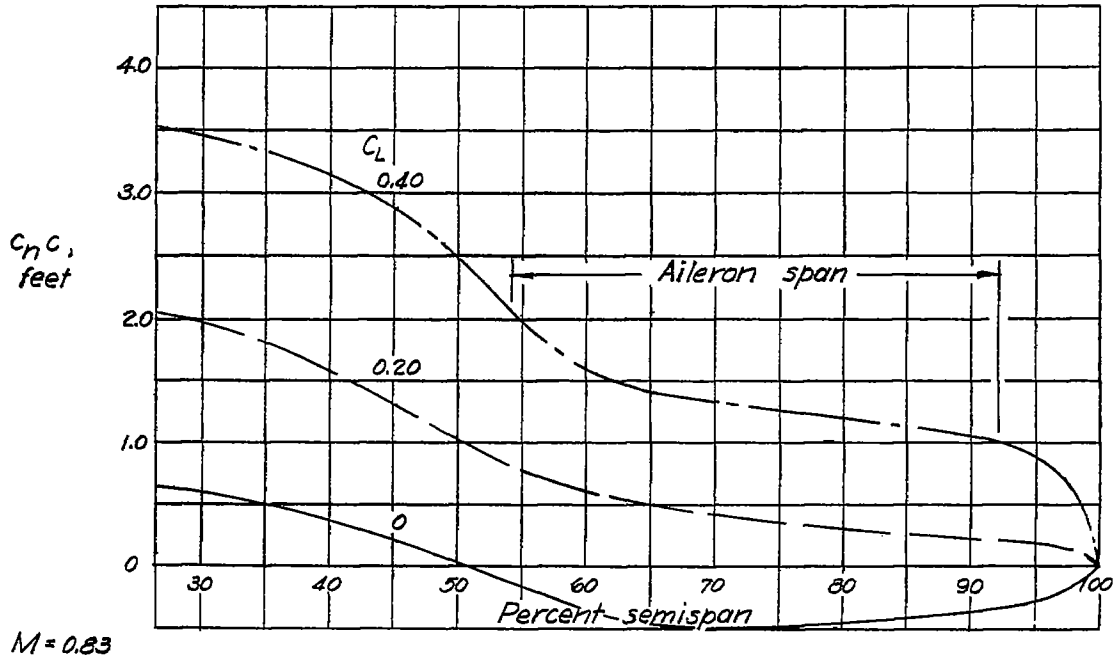

(e) M = 0.83

Figure 13.— continued

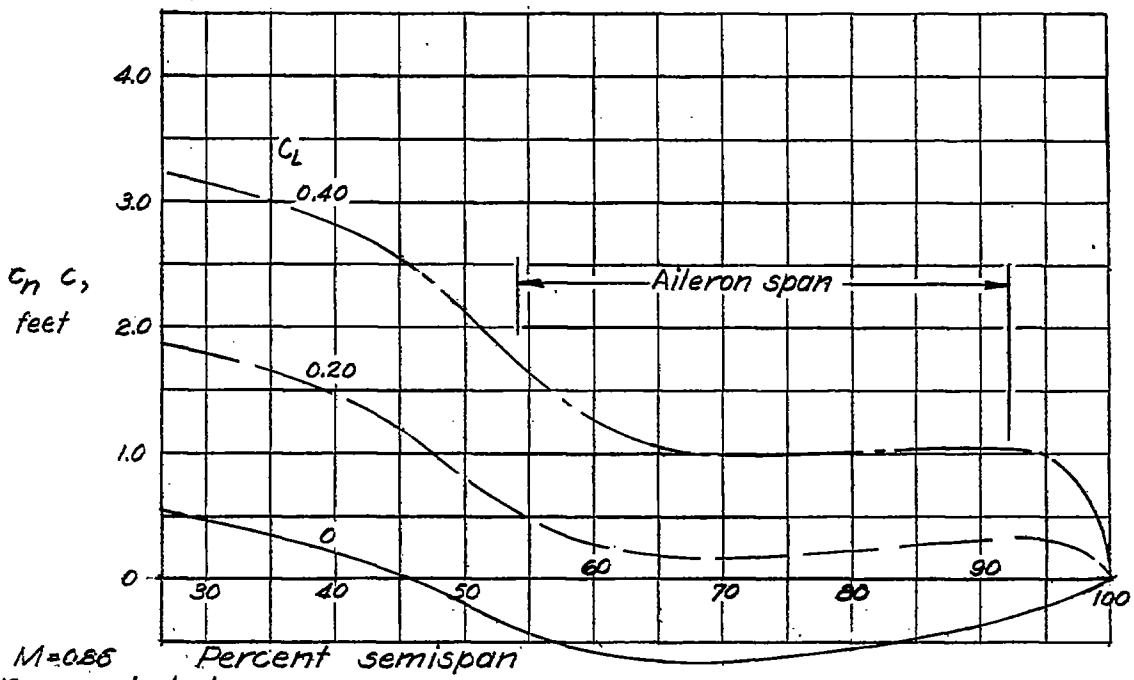

Figure 13.– concluded

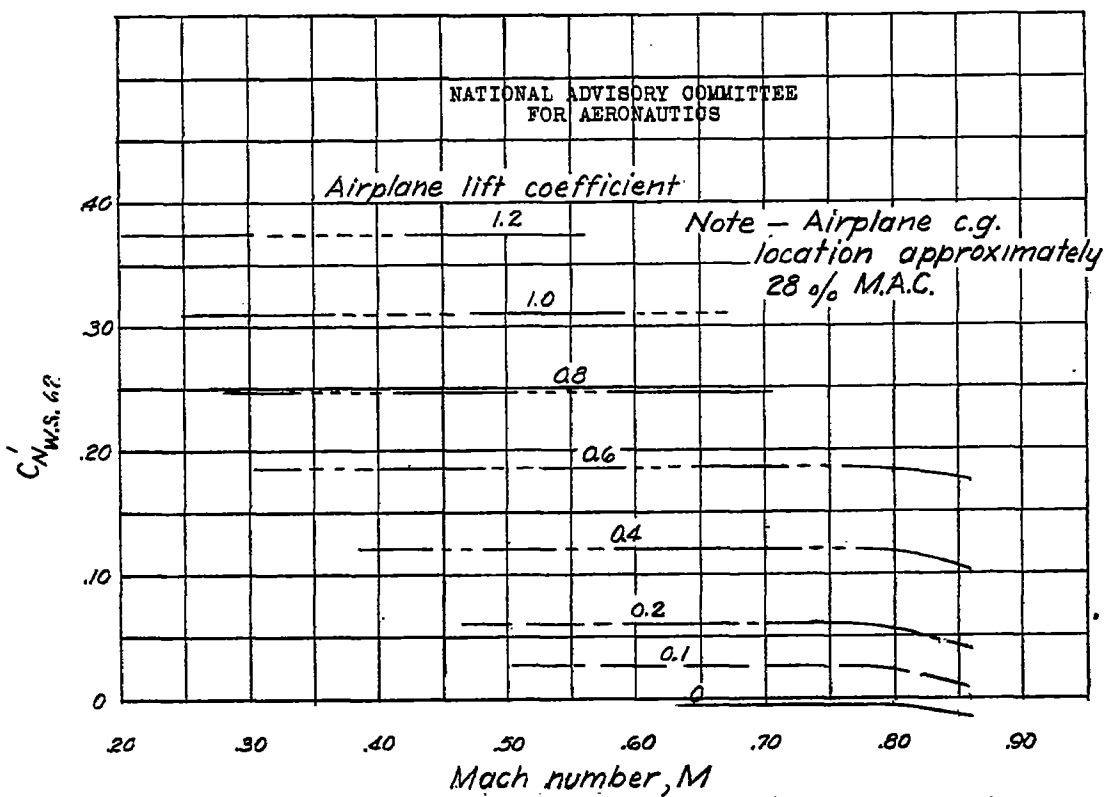

Figure 14.– Variation of the normal force coefficient with Mach number of that portion of the wing outboard of wing station 62 for several values of airplane lift coefficient.

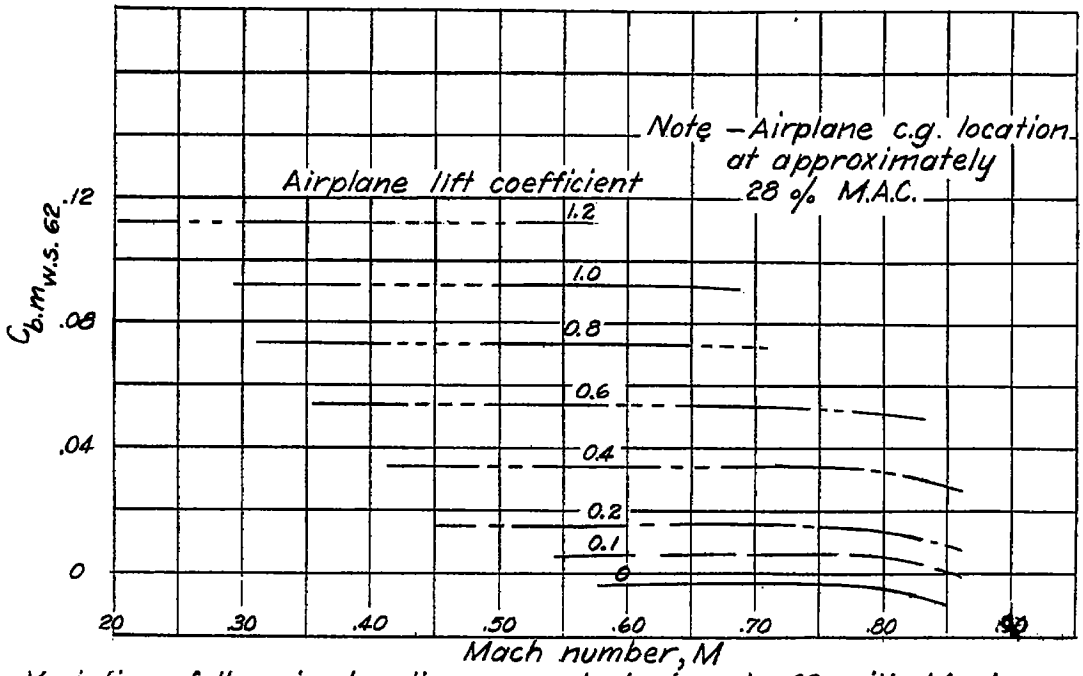

Figure 15– Variation of the wing bending moment at wing sta. 62 with Mach number for several values of airplane lift coefficient.

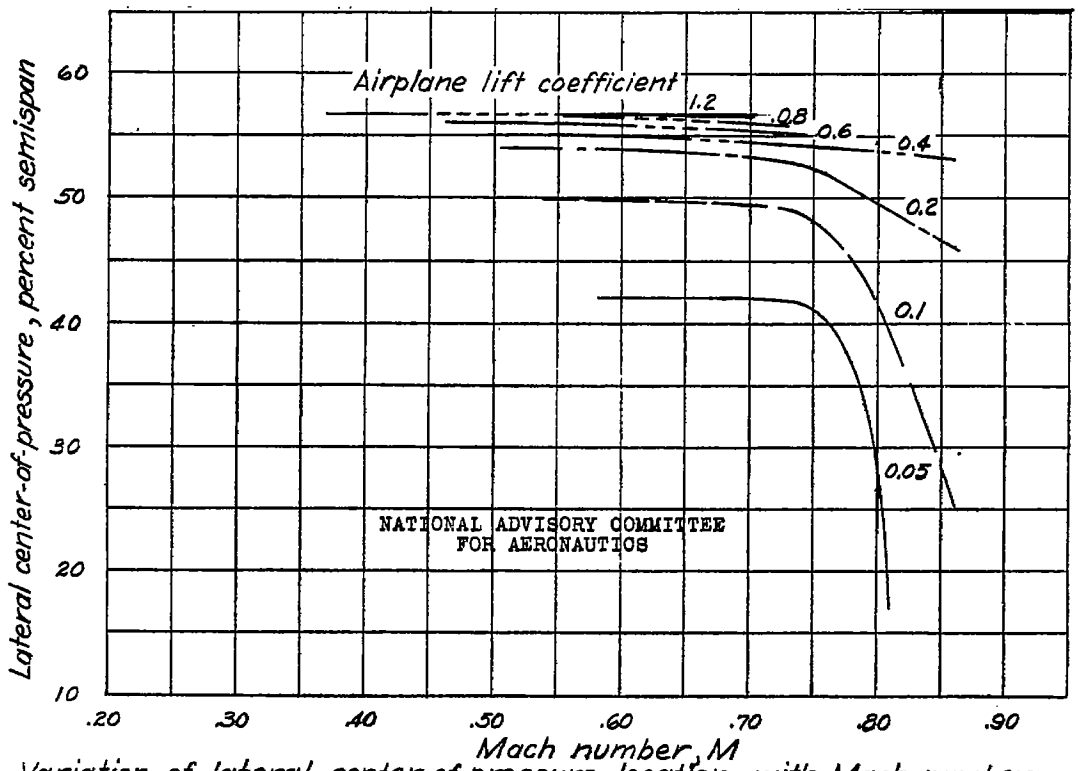

Figure 16– Variation of lateral center-of-pressure location with Mach number for that portion of wing outboard of wing station 62 for several values of airplane lift coefficient

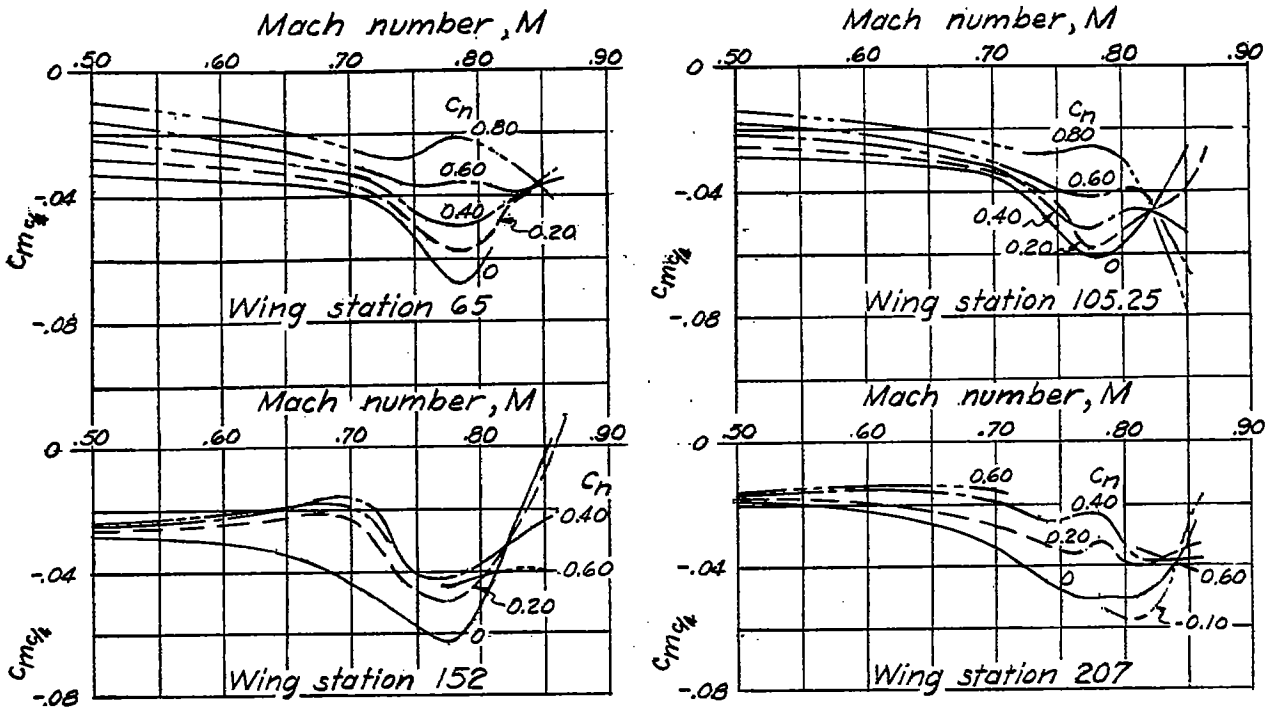

Figure 17.— Variation of section pitching-moment coefficient about the quarter chord with Mach number for several spanwise stations.

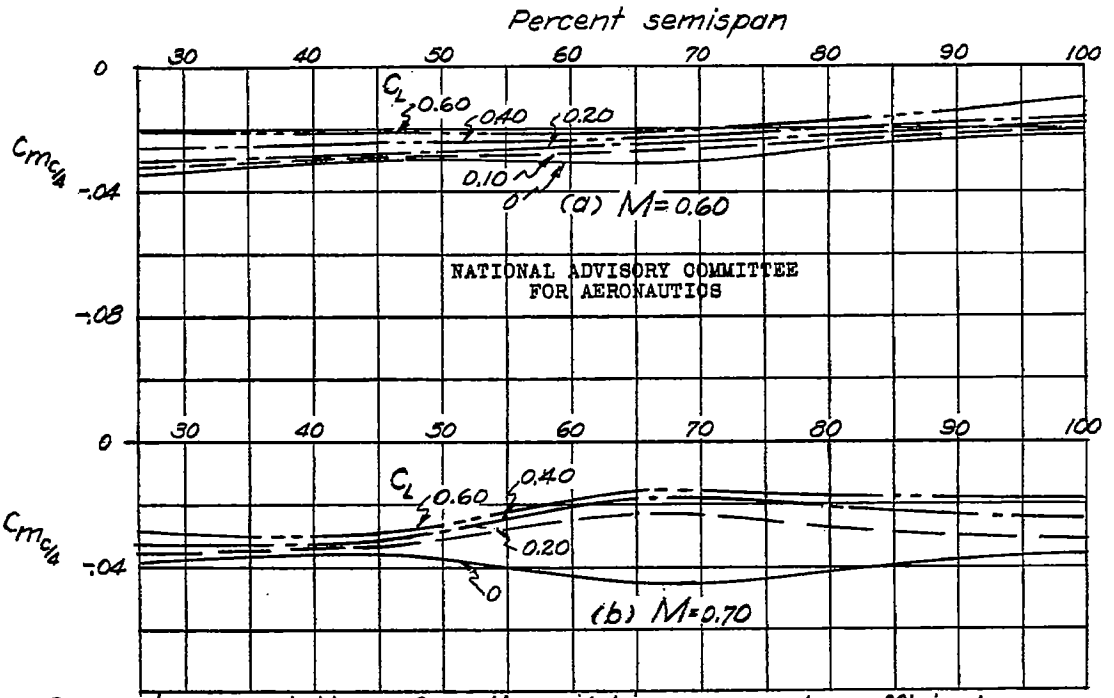

Figure 18.— Spanwise variation of section pitching-moment coefficient at various values of airplane lift coefficient for several values of Mach number.

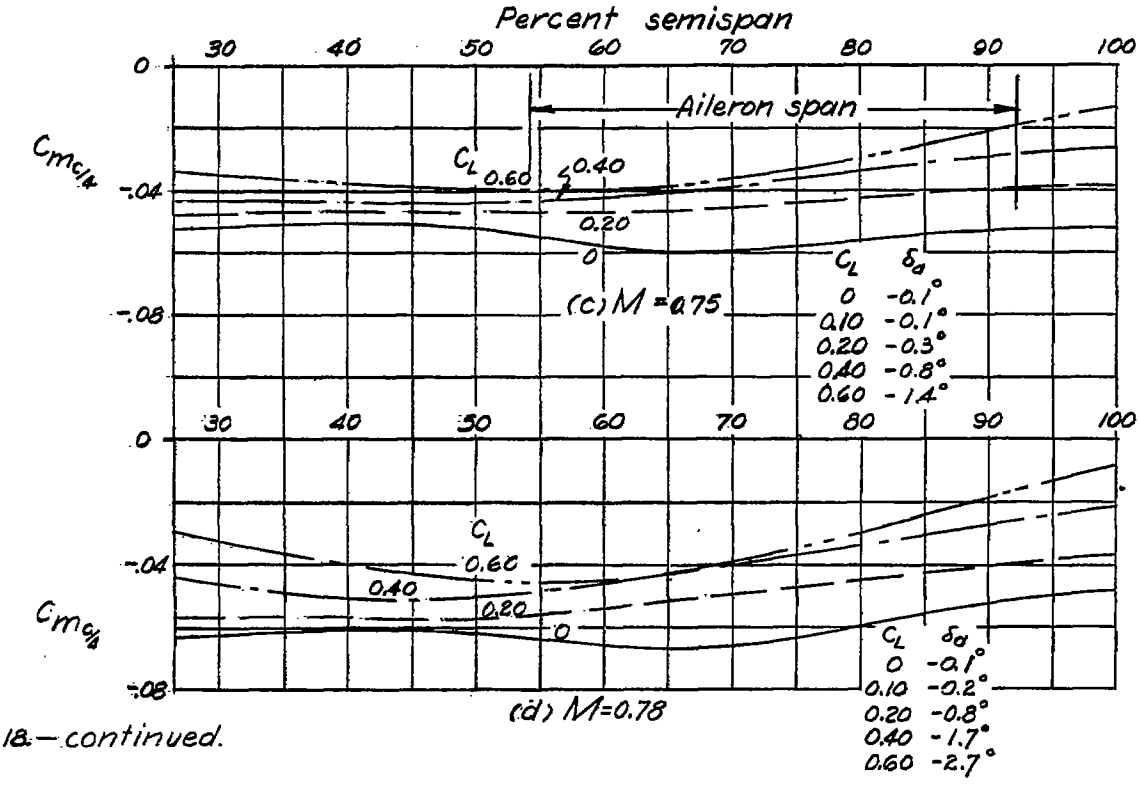

Figure 18.— continued.

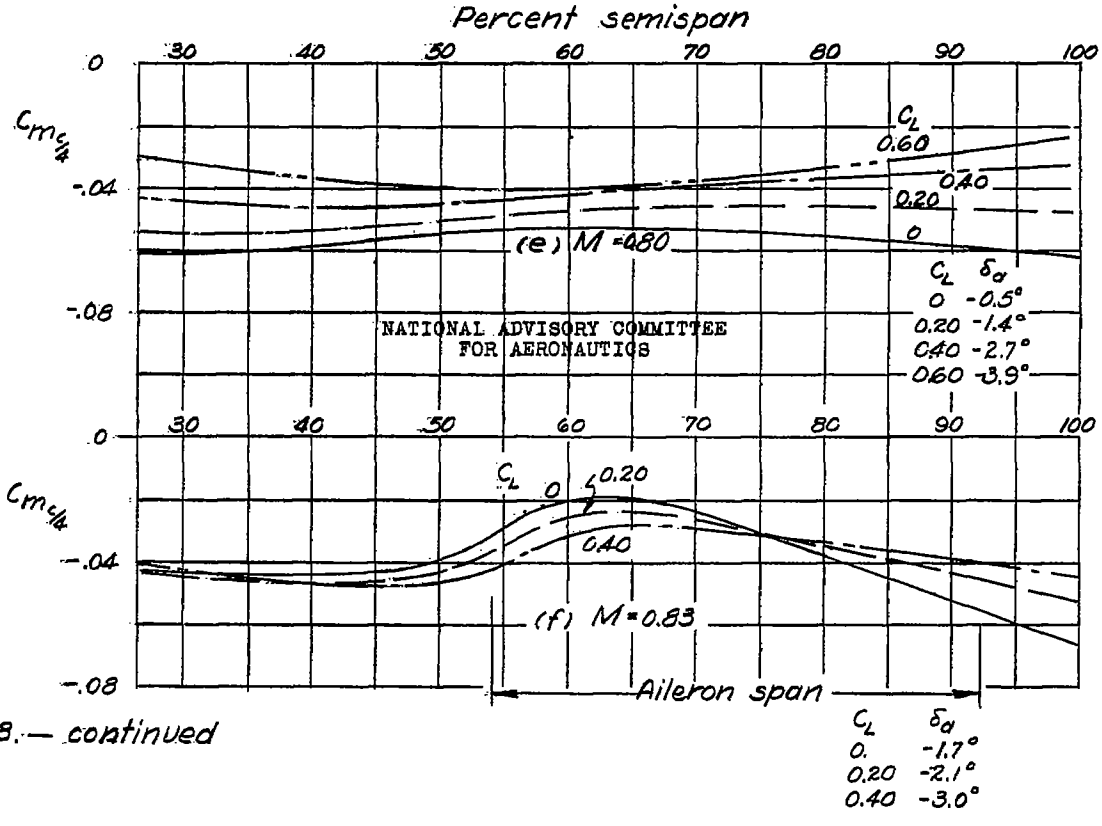

Figure 18.— continued

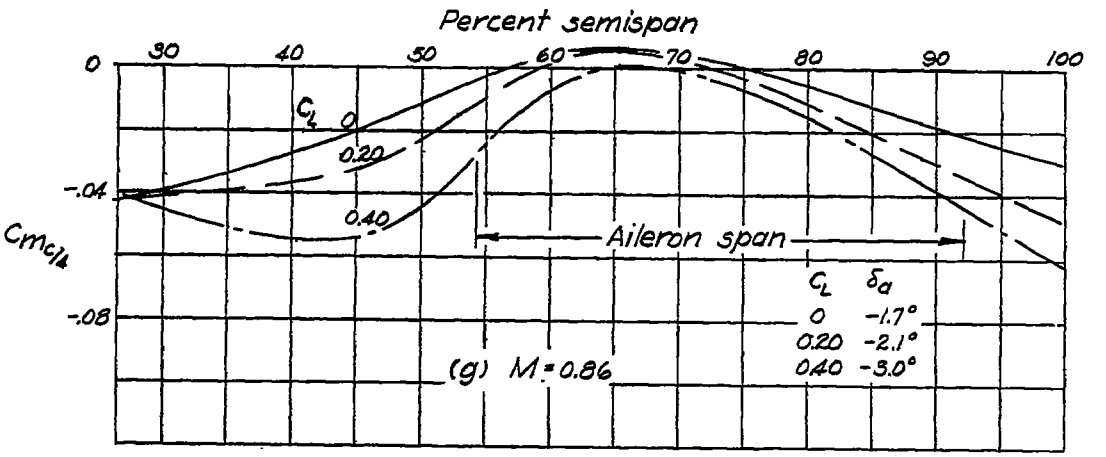

Figure 18.— concluded

NATIONAL ADVISORY COMMITTEE
FOR AERONAUTICS

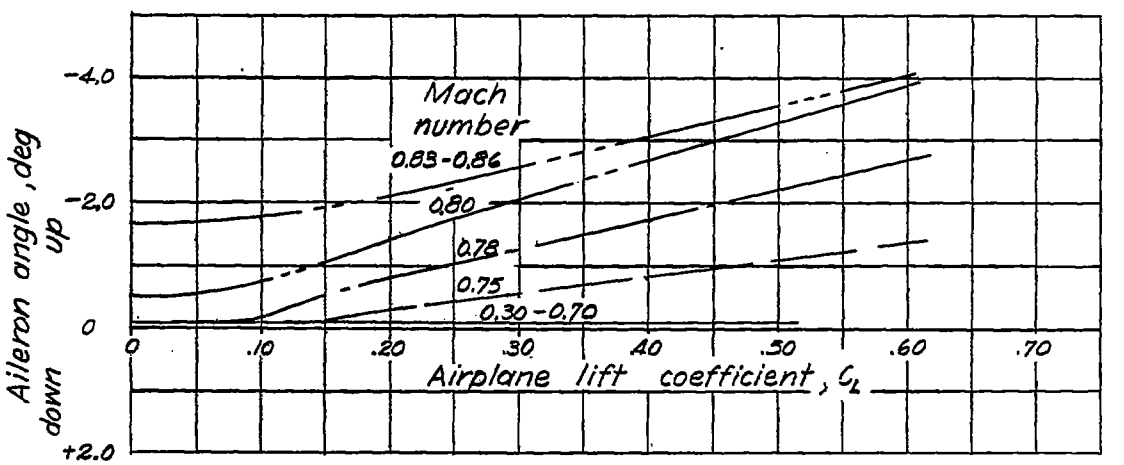

Figure 19.— Variation of right aileron angle with lift coefficient during dives and pull-outs.

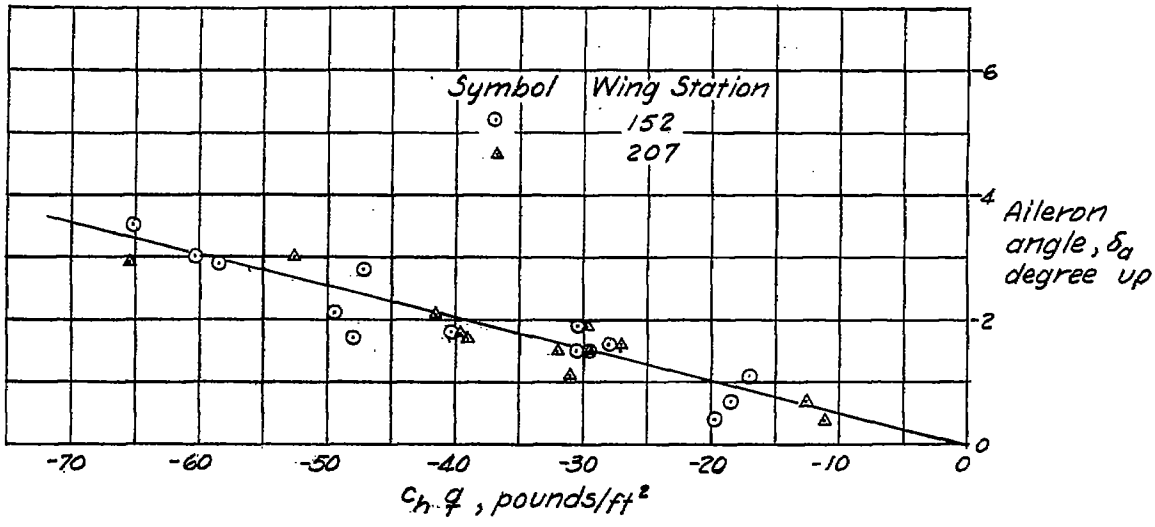

Figure 20.— Variation of aileron surface deflection due to cable stretch with $c_h q$.

NATIONAL ADVISORY COMMITTEE
FOR AERONAUTICS

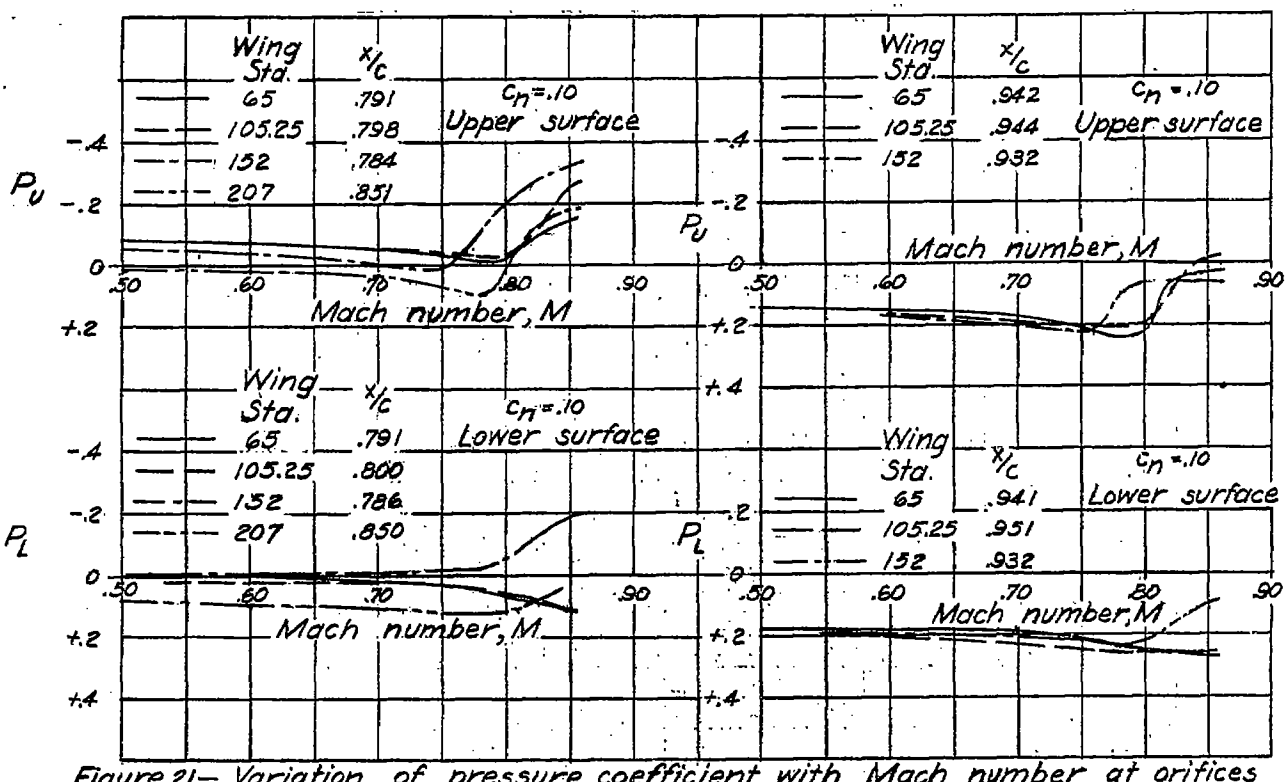

Figure 21.— Variation of pressure coefficient with Mach number at orifices near the trailing edge at several spanwise stations.

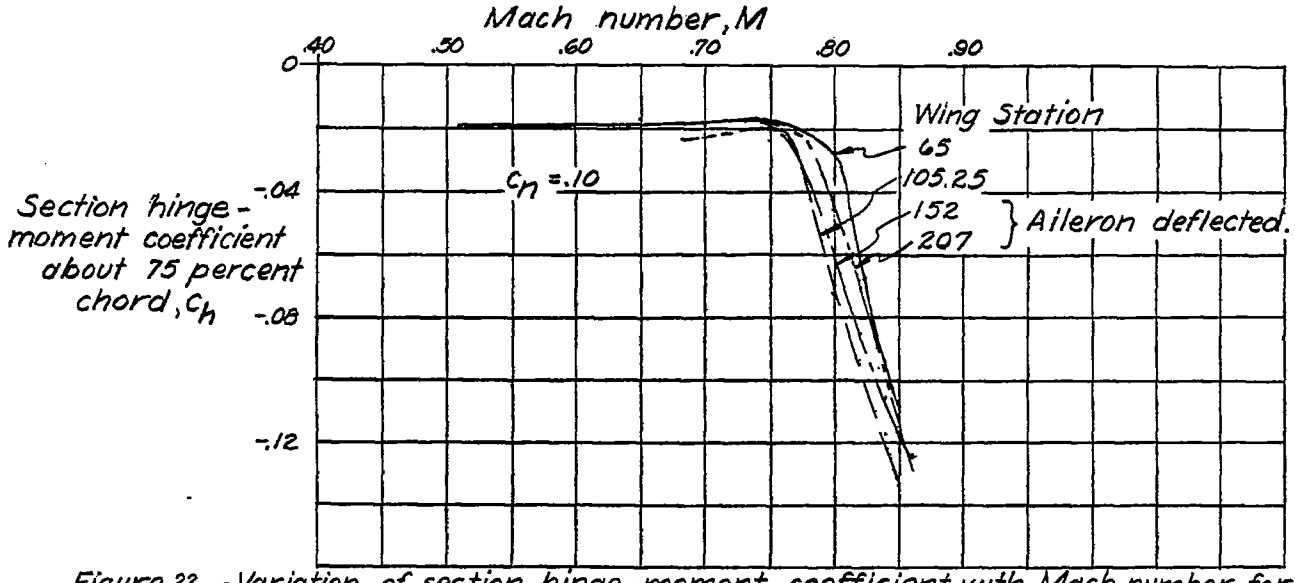

Figure 22.— Variation of section hinge-moment coefficient with Mach number for aft 25 percent chord at wing stations over aileron and inboard of aileron.

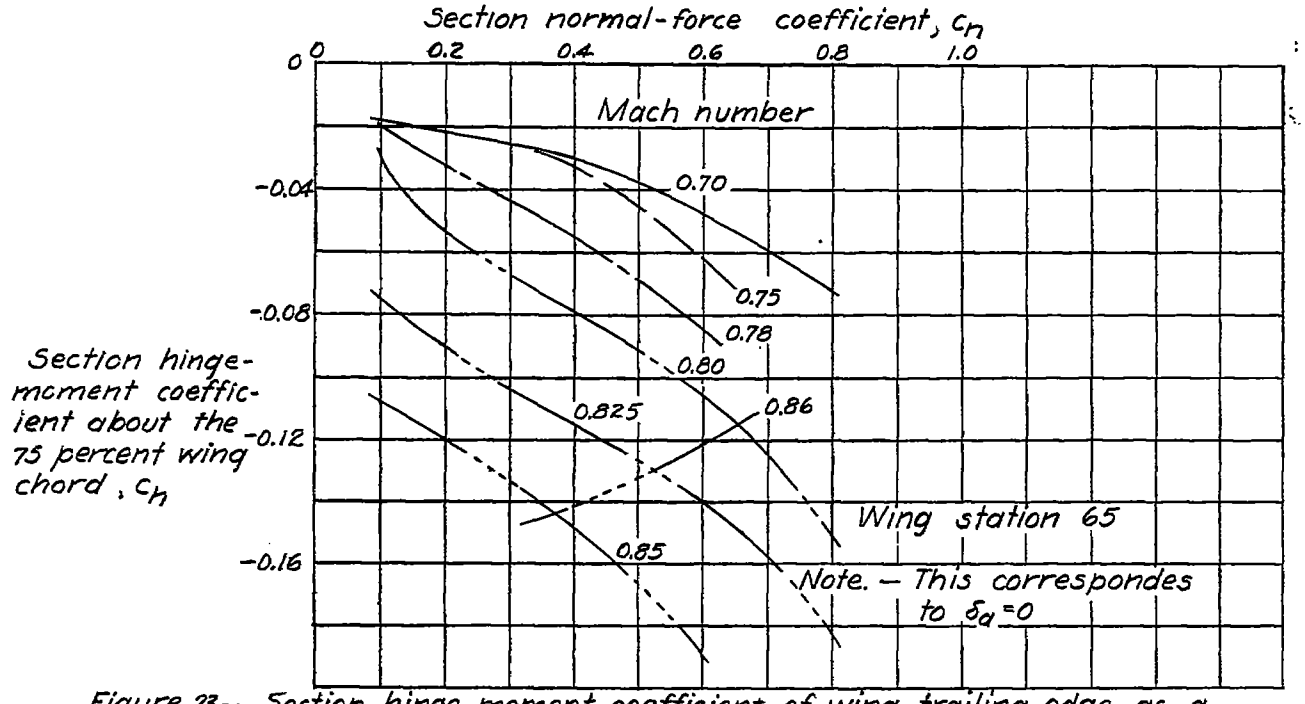

Figure 23— Section hinge-moment coefficient of wing trailing edge as a function of section normal-force coefficient and Mach number